mise en page : Patrick Kaye - k*f*x - Liège
impression : J. Chauveheid - Stavelot

Université Catholique de Louvain
Faculté de Médecine
Unité d'Imagerie Moléculaire et de Radiothérapie Expérimentale
(IMRE)

Multi-Modality Imaging in Planning Patients with Head and Neck Squamous Cell Carcinomas : Myths and Reality

Jean-François Daisne, M.D.

Thesis submitted in fulfilment of the requirements for the degree of
« Docteur en Sciences Médicales »
Orientation « Radiothérapie Oncologique »
2005

Promoter : Prof. Vincent Grégoire
Co-Promoter : Prof. Guy Cosnard

Members of the Jury

Promoter :
Prof. Vincent Grégoire
Radiation Oncology Department
Molecular Imaging and Experimental Radiotherapy
Université Catholique de Louvain

Co-Promoter :
Prof. Guy Cosnard
Radiology Department - MRI Unit
Université Catholique de Louvain

President of the Jury :
Prof. Jacques Melin
Internal Medicine Department
Université Catholique de Louvain

Members :
Prof. Anne Bol
PET Laboratory
Université Catholique de Louvain

Prof. Hervé Reychler
Oral and Maxillo-facial Surgery Department
Université Catholique de Louvain

Prof. Pierre Scalliet
Radiation Oncology Department
Université Catholique de Louvain

Invited Members :
Prof. Clifford Chao
Radiation Oncology Department
MD Anderson Cancer Center
Houston (Texas - USA)

Prof. Wilfried De Neve
Radiation Oncology Department
Ghent Universiteit

REMERCIEMENTS - *ACKNOWLEDEGEMENTS*

L'écriture de ces quelques mots de remerciements représente pour moi une occasion unique d'adresser ma gratitude à tous ceux qui, de près ou de loin, ont participé à l'élaboration de ce travail de thèse, mais également à tous ceux qui m'ont permis de devenir et d'être qui je suis. C'est également une phase délicate dans la mesure où l'angoisse d'oublier quelqu'un de manière individuelle ou au sein d'une équipe est permanente. Si par malheur, mon éternelle distraction devait me mener à oublier qui que ce soit au moment où je rédige ces lignes, j'ose espérer qu'il ne m'en tiendra pas (trop longtemps) rigueur.

Je tiens en premier lieu à exprimer ma plus profonde gratitude à mon promoteur, le Professeur Vincent Grégoire qui, en juillet 1999, m'a suffisamment fait confiance pour me proposer ce projet. Il est indéniable que sans sa science, sa clairvoyance et son opiniâtreté vous obligeant sans cesse à vous dépasser, ce projet n'en serait pas à sa conclusion. Je le remercie également de m'avoir initié aux mystères de la pathologie cancéreuse de la sphère cervico-maxillo-faciale. J'ai conscience de la chance qu'il m'a été donnée de pouvoir apprendre en sa compagnie.

Je remercie également mon co-promoteur, le Professeur Guy Cosnard qui m'a ouvert les portes de la radiologie, permettant de mener ce projet aux fondements radiologiques à son terme.

Ma gratitude va également au Professeur Pierre Scalliet qui, le premier -alors que j'étais en deuxième doctorat- m'a fait découvrir au travers de son cours la merveilleuse spécialité qu'est la radiothérapie. C'est à ce moment que j'ai compris que ce serait là que je finirais par trouver tout ce que j'avais cherché jusqu'alors : une pratique médicale avec des patients cancéreux, de la physique et un soupçon d'informatique. Si mon souvenir est exact, c'est également lui qui fut le premier à me suggérer de m'engager sur la voie de la recherche. Qu'il en soit également remercié.

Je remercie également les autres membres du jury, à savoir le Professeur Jacques Melin, président, qui n'a jamais manqué de gestes et de paroles d'encouragement, le Professeur Anne Bol de l'unité de tomographie par positrons (TOPO) à Louvain-la-Neuve qui a non seulement accepté de remplacer au pied levé le Professeur Christian Michel lors de son départ sous d'autres cieux professionnels, mais m'a également accompagné dans mon travail à la caméra

PET. Le Professeur Hervé Reychler pour ses remarques pertinentes, ses petits mots d'encouragement et la travail de relecture minutieux qu'il a effectué lors de la rédaction finale de cette thèse. C'est également un honneur que de pouvoir compter au sein du jury deux membres éminents de la scène radiothérapique, à savoir les Professeurs Clifford Chao (MD Anderson Cancer Center, Houston, Texas) et Wilfrid De Neve (Ghent Universiteit). Je les remercie d'avoir accepté de faire partie du jury et d'avoir libéré du temps dans leur agenda pour se consacrer au travail que cela implique.

It is a great honor for me and my department that Professors Clifford Chao (MD Anderson Cancer Center, Houston, TX, USA) and Wilfrid De Neve (Ghent University, Belgium) accepted to be members of the Jury. I should like to thank them for having finding time in their busy agenda to consciously do the work it implies.

Je tiens également à remercier le Président de l'école doctorale clinique, le Professeur Pierre Gianello. Ma plus profonde reconnaissance va également à Monsieur Gomes, secrétaire de l'école doctorale, dont l'amabilité, la précision et l'organisation sont à la base du bon fonctionnement de la dite école.

Derrière la réalisation de ce projet, multidisciplinaire par essence, se cachent de nombreuses personnes qui m'ont toujours accueilli à bras ouverts. Il m'est difficile de citer chacun jusqu'au dernier, ce pourquoi je préfère citer les équipes et leurs responsables, en soulignant le rôle prépondérant de certains en particulier : l'équipe d'imagerie par résonance magnétique du Professeur Cosnard, le Docteur Thierry Duprez en particulier pour son expertise et sa disponibilité dans l'aide à l'interprétation des images de résonance. L'équipe du scanner « Twin » et le Docteur Emmanuel Coche. L'équipe de la caméra à positrons, en particuliers le Professeur Anne Bol, le Docteur Max Lonneux, Monsieur Mérence Sibomana -qui a écrit et adapté les logiciels de corégistration et de contourage-, le Professeur Chritian Michel, Monsieur Raymond Bausart et le Professeur Daniel Labar. Les équipes de chirurgie ORL du Professeur Marc Hamoir et de stomatologie du Professeur Hervé Reychler. Un merci tout particulier au Docteur Pierre Mahy qui a plus d'une fois joué à Gütenberg pour mes posters. L'équipe d'anatomo-pathologie du Professeur Jacques Rahier, particulièrement les Docteurs Birgit Weynant (qui nous a apporté toute son expertise pour la délimitation des volumes tumoraux macroscopiques) et Pierre Moulin qui, grâce à ses connaissances informatiques, a permis l'alignement des coupes macroscopiques. L'équipe du laboratoire de télécommunications du

Professeur Benoît Macq. Le Professeur Annie Robert et Monsieur Eric Lecoutre de l'Institut des Statistiques pour leurs (patients) éclairages quant aux statistiques utilisées. Et bien entendu toute l'équipe (médecins, physiciens, infirmiers) du service de radiothérapie du Professeur Pierre Scalliet à laquelle j'adjoins bien entendu les membres du laboratoire IMRE : Mesdames Blanche De Coster et Myriam Goosse, le Dr John Gueulette et Monsieur Marc De Bast qui ont perpétuellement fait preuve de gentillesse, de disponibilité et de patience.

J'ai également une infinie reconnaissance pour les 29 patients qui ont accepté, bien qu'étant malades, de nous consacrer de leur temps pour réaliser des examens complémentaires non directement utiles à l'aboutissement de leur traitement. J'ai une affection particulière pour chacun d'eux car j'ai vécu à leur contact des moments privilégiés, parfois drôles, souvent émouvants. Les nombreuses acquisitions d'imagerie et les temps de préparation et d'attente (en particulier au PET) les ont souvent menés à sympathiser dans un premier temps, à se confier ensuite. Ils m'ont permis de ne pas oublier, dans ce temps de recherche un peu éloigné de la réalité clinique, ni pour qui, ni contre quoi j'avais décidé de m'engager.

On a beau avoir toute la bonne volonté du monde, aucun projet de cette envergure ne peut aboutir sans financement. Celui-ci a été apporté essentiellement par le Fonds National de la Recherche Scientifique par le truchement de l'argent rapporté par les opérations Télévie 1999 et 2001. Cette thèse est donc aussi le fruit du travail des médias et des milliers d'anonymes qui, chaque année, consacrent leur temps, leur énergie et leur foi à gonfler de manière conséquente le financement public de la recherche médicale en Communauté Francophone de Belgique. Citons également la Loterie Nationale de Belgique et l'Université Catholique de Louvain qui ont complété le financement. Un merci tout particulier à Madame Christiane Pasteels et à Messieurs Sprumont, Groutars et Janssens pour leur aide logistique lors de la conclusion du travail.

La conclusion de ce travail de recherche scientifique et de la thèse qui en découle va, à quelques mois près, de pair avec la fin de ma formation d'assistant spécialiste. Cela m'évoque la chance que j'ai eue de rencontrer des enseignants peu ordinaires m'ayant donné le goût d'apprendre, ce depuis ma petite école primaire du village de Soy (Mesdames Leboutte et Herman), en passant par l'Institut Saint-Remacle de Marche-en-Famenne (en particulier pour avoir cultivé mon goût pour les mathématiques Messieurs Van Belle

et Bouvy, et pour les sciences Messieurs Walckiers et Pigeon), pour terminer par l'Université Catholique de Louvain. Les stages effectués en doctorat ont tous été des plus fructueux. Je garde un souvenir particulièrement positif des stages de Médecine Interne effectués auprès du Docteur Guy Roche à Marche-en-Famenne et du Professeur Philippe Hainaut aux Cliniques Saint-Luc à Bruxelles. Finalement, j'ai pu bénéficier d'une excellente formation technique et clinique d'assistant spécialiste en radiothérapie dans les services du Professeur Scalliet à Bruxelles, du Docteur Emile Salamon à Namur et du Professeur Van den Bogaert à Leuven. Que ces maîtres de stage et leurs collaborateurs soient remerciés de leur implication dans l'enseignement de cette belle (mais combien méconnue) spécialité.

Je tiens à mentionner que des amitiés sincères se sont liées pendant toutes ces années de formation, en particulier durant ces dernières années de spécialisation. Je remercie mes amis Olivier, Xavier, Laurent et Lorraine de leur soutien et de leurs encouragements dans les moments plus difficiles.

Merci à Monsieur Bob Gruehn d'avoir relu par deux fois la thèse et de l'avoir mise aux normes de la langue anglo-américaine. Merci également à mon ami d'enfance Patrick Kaye qui a assuré la mise en page et l'impression de cette thèse.

I want to sincerely thank Mister Bob Gruehn who read the thesis two times and made it fit to English American language standards.

Dans une volonté de souligner leur rôle prépondérant dans ma vie, je tiens à terminer ces remerciements par tous ceux qui me sont proches de coeur. Je mentionnerai en premier lieu mes parents, André et Danielle, sans qui non seulement je ne serais pas là, mais ne serais pas qui je suis. Leur amour, leur confiance absolue et leur perpétuelle disponibilité ont été les plus grandes sources d'encouragement à atteindre les buts que je m'étais fixés. Je remercie mon épouse Sylvie et mes deux cadeaux du ciel, Pauline et Lisa, de leur amour et de leur patience face aux week-end entiers passés devant la littérature ou l'ordinateur. J'ai la chance d'avoir une (très) grande famille. Merci à mes frères Frédéric et Christophe, ma grand-mère, mes oncles, tantes, cousins et cousines qui ont toujours été présents lorsque j'avais besoin d'eux.

List of Abbreviations

3D	Three Dimension(al)
4D	Four Dimension(al)
AC	Anterior commissure
AEF	Aryepiglottic fold
b-IGRT	Biological Image Guided Radiation Therapy
BOLD	Blood oxygenation level-dependent
CDK	Cyclin-dependent kinase
Ci	Curie
CRT	Conformal Radiation Therapy
CT	Computer Assisted Tomography scanner
CTV	Clinical Target Volume
DNA	Desoxyribo-nucleic acid
dsbs	Double strand breaks
EBV	Epstein-Barr Virus
EGFR	Epidermal Growth Factor Receptor
EPI	Electronic portal imaging
f-MRI	Functional Magnetic Resonance Imaging
FBP	Filtered back projection
FDG	^{18}Fluoro-Deoxy-Glucose
FNAC	Fine Needle Aspiration Cytology
FORE	Fourier rebinning
FOV	Field of view
FWHM	Full width at half maximum
GTS	Glossotonsillar sulcus
GTV	Gross Tumor Volume
GTV-N	Gross Tumor Volume-Nodes
GTV-T	Gross Tumor Volume-primary Tumor
Gy	Gray
HU	Hounsfield Unit
HNSCC	Head and Neck Squamous Cell Carcinoma
ICRU	International Commission on Radiation Units and Measurements
IMRT	Intensity Modulated Radiation Therapy
IV	Intravenous
kV	Kilo voltage
LET	Linear Energy Transfer
LINAC	Linear accelerator
LOR	Line of Response
LSO	Lutetium oxyorthosilicate

mAs	Milli-amperes per second
MET	^{11}Carbon-Methionine
MI	Mutual information
MLC	Multi leaf collimator
MRI	Magnetic Resonance Imaging
NTCP	Normal Tissue Complication Probability
OAR	Organ at Risk
OSEM	Ordered subsets expectation-maximization
PCA	Principal Component Analysis
PD	Proton density
PES	Preepiglottic space
PET	Positron Emission Tomography
PGS	Paraglottic space
PPS	Parapharyngeal space
PPW	Posterior Pharyngeal Wall
PRV	Planning Organ at Risk Volume
PS	Piriform sinus
PSF	Point spread function
PTV	Planning Target Volume
QA	Quality Assurance
RC	Retrocricoid
RMT	Retromolar trigone
ROI	Region of interest
RX	X-rays
S/B	Source-to-Background ratio
SCC	Squamous Cell Carcinoma
ssbs	Single strand breaks
TCP	Tumor Control Probability
TGF-α	Tumor Growth Factor α
TK	Tyrosine Kinase
TKI	Tyrosine Kinase Inhibitor
TNM	Tumor, Node, Metastases
TPS	Treatment planning system
UICC	Union Internationale Contre le Cancer
US	Ultrasounds
VC	Vocal cord
WFS	Water-to-fat shift
XML	Extended markup language

1. INTRODUCTION

1.1. Anatomy of the Head & Neck area

The « Head and Neck » (HN) region is commonly defined as all anatomical structures enclosed in the space lying below the base of skull down to the sternal angle. The axis is constituted by the superior aerodigestive tract which, from an endoscopical or radiological descriptive standpoint rather than a purely anatomicophysiologycal standpoint, is divided into seven different regions : the nasal cavities, the paranasal sinuses, the oral cavity, the pharynx divided into naso-, oro- and hypopharyngeal regions, and the larynx. The exact limitations of these regions are fully described elsewhere [UICC 1997, 2002].

It must be mentioned that some descriptive subdivisions occur for some regions. For the good comprehension of present work, we only mention these subdivisions for the oropharynx, the larynx and the hypopharynx. The oropharynx is subdivided into the soft palate, the tonsils, the base of tongue and the posterior pharyngeal wall. The larynx is subdivided into the supraglottis, the glottis and the subglottis. The hypopharynx is subdivided into the piriform sinuses, the retrocricoid region and the posterior pharyngeal wall. For the readers interested into the descriptive anatomy of these regions, we advise them to consult *section* 10 and anatomy monographies [Rouvière 1972, Chevallier 1998].

The respiratory tract allows the air to reach the lung via the nasal cavities, then the nasopharynx which is directly communicating with the oropharynx, then the larynx and finally the trachea which by definition does not belong to the HN region. The digestive tract allows to taste, masticate and swallow the food via the oral cavity, the oropharynx and finally the hypopharynx which is continued in the mediastinum by the esophagus. Phonation is another function assumed by HN structures : the air coming from the lung makes vibrating vocal cords located in the larynx, generating vocal vibrations which are amplified and transformed into different sounds by geometric modifications of hypopharyngeal, oropharyngeal and oral cavity structures.

These different compartments are surrounded by other structures which are necessary to their physiology : numerous complex muscles allowing complex movements, blood vessels for nutriments deliverance and metabolic waste evacuation, lymphatic vessels and nodes for lymph drainage and filtration, sali-

vary glands for oral cavity lubrication, (mainly cranial) nerves for all these structures stimulation or inhibition, the cervical vertebrae and the spinal cord which are mainly in transit between the brain and the rest of the body and finally the skin which constitutes a barrier to out-of-body aggressions.

1.2. Epidemiology of Head & Neck tumors

1.2.1. Frequencies

In 1998 in Belgium [Registre du Cancer 1998], superior aerodigestive tract cancers were the sixth most frequent cancers (after breast, broncho-pulmonary, digestive, genitourinary and hematologic malignancies). They represented 4.3 % of the 40,997 cancers registered in the national database with a sex ratio of 3.8 and mortality rates of 15.72 and 3.66 for 100,000 males and females, respectively.

1.2.2. Pathology

Malignant tumors can virtually develop in all anatomical substructures, but the most frequent ones affect the surface squamous epithelium which is by definition more exposed to both physical and chemical aggressions. Repetitive aggressions lead first to squamous metaplasia, then to dysplasia and finally to Squamous Cell Carcinoma (SCC) which can be more or less differentiated (i.e. showing different degrees of squamous-like organization).

1.2.3. Risk factors and location

Environmental agents are at the origin of the vast majority of HNSCC, among which tobacco and/or alcohol consumption are the leading causal factors of oral, oropharyngeal, laryngeal and hypopharyngeal SCC. Nasopharyngeal cancers are most often caused by Epstein-Barr Virus (EBV) infection in predisposed ethnicities like Magrebian and South-Asian peoples. Finally, nasal and paranasal sinuses cancers are the hazard of carpenters chronically exposed to exotic wood dust inhalation.

1.3. Treatment strategies based on stage

HNSCC are commonly staged according to the 1997 or 2002 Union Internationale Contre le Cancer (UICC) Tumor, Nodes and Metastases (TNM) staging system [UICC 1997, 2002]. TNM staging is of the utmost importance for prognosis prediction and subsequent treatment aggressiveness according to local (T), regional (N) and distant (M) extension. Treatment strategies are being discussed for the most frequent HNSCC in Western countries, i.e. oral cavity, oropharyngeal, laryngeal and hypopharyngeal tumors. They are largely inspired from evidence-based guidelines used in our center [UCL Guidelines].

1.3.1. Early stage (T1N0 and T1N1)

Such small tumors are generally easily curable (5-year local control from 80 % for hypopharyngeal tumors to 95 % for laryngeal tumors). The use of a sole conservative treatment modality is often sufficient and the choice of it depends on available therapies on site, specialists skills and experience and -last but not least- patients prerogatives.

Considering the primary tumor, it can be cured either by limited surgical procedures (conventional or laser surgery) or by external RT, or brachytherapy for tumors selected for their small size and ideal location for needle implantation (such as base of tongue, the antinomian example being posterior pharyngeal wall). Conventional RT doses (66 to 70 Gy, two Gy a fraction, five days a week) are sufficient for such small tumor volumes. If indicated [Peters 1993], postoperative radiation total dose generally ranges from 60 to 64 Gy in conventional fractionation.

Treatment of neck nodes can be performed either by conventional surgery or by external RT. Regarding levels [Robbins 1991] to be treated, their selection is driven by the same criteria [Grégoire 2003] whatever treatment modality chosen. Selective neck treatment is generally the rule. Unilateral treatment can even be chosen for selected patients showing a lateral border of tongue, a tonsillar fossa or a vocal cord tumor.

RT dose for prophylactic treatment is 50 Gy in conventional fractionation. The dose for gross metastatic disease in a small (less than three cm) unique and homolateral node ranges from 66 to 70 Gy in conventional fractionation. If postoperative radiation is required, the dose to be administered also ranges from 60 to 64 Gy in conventional fractionation.

1.3.2. Moderately advanced stage (T2N0 and T2N1)

Regarding primary tumor, treatment options are either radical surgery or external RT. Brachytherapy only applies to small T2 tumors because of the limiting volume factor. If chosen, external RT should preferably be administered through an accelerated regimen during the last third of treatment time [Rosenthal 2004] or associated to concomitant chemotherapy at radiosensitizing doses [Gilbert 2004]. Both strategies allow to gain in significant local control rate (about five to 10 % at five years) [Fu 2000, Pignon 2000, Bourhis 2002] by increasing administered biological dose, which is needed by the increased amount of cancer cells to be killed. If postoperative RT is required, dose ranges from 60 to 64 Gy according to specific risk factors of relapse [Peters 1993]. Treatment options for the neck are the same as those exposed in § 1.3.1.

1.3.3. Locally advanced stage (all T3, T4, N2 and N3)

T3 and T4 tumor treatment options are discussed together because all these tumors show the common feature of local invasion, i.e. local transgression of centrifugal anatomic compartment barriers.

Basically, the choice will have to be determined between either radical surgery (nearly) always followed by postoperative RT or RT alone with modified fractionation regimen or in combination with chemotherapy, surgery being kept as rescue modality. The fact that postoperative RT is so often the rule is due to the stage factor in itself, being a risk factor for local relapse [Foote 1993, Peters 1993, Zelefsky 1993]. In some T4 tumors (like hypopharyngeal or laryngeal ones) surgery is often the first choice modality because the destruction of anatomical structures is so large it precludes functional recovery after organ preservation therapy. On the other hand, about one third of the patients presenting a laryngeal carcinoma and two thirds of those with an advanced hypopharyngeal cancer beneficing of organ preservation treatments will have to be rescued by surgery because of local failure [Veteran Affairs 1991, Kraus 1994, Forastiere 2003].

N2 and N3 diseases ideally require an aggressive treatment :

- bilaterally;

- extended to levels I to V (as well as level VI for tumors of the larynx, transglottic tumors, Killian triangle or thyroid cancers) and even in pharyngeal locations to the retropharyngeal ones;

- with surgical and radiation modalities in combination. Their timing is mostly driven by the modality which will be chosen for primary tumor cure but also by the uni- or bilateral pattern of gross metastatic disease and the degree of invasiveness of adjacent non nodal structures.

RT doses in conventional regimen are 50 Gy (or biologically equivalent dose in modified fractionation schedules) for prophylactic treatment of N0 levels and 70 Gy (but ideally higher doses which are achieved through the use of modified fractionation schedules) for nodal levels.

1.3.4. Recurrent (rT, rN) and metastatic (M1) disease

Recurrent disease (and by extension second primary tumor in previously treated HN area) is a challenging issue because of the difficulty of technical and functional outcome issues. Patients with recurrent disease are rarely fit for surgical procedures because of local consequences of previous treatments leading to exaggerated morbidity [*review by* Kao 2003]. Reirradiation combined with chemotherapy has proved to be useful for selected patients [Schaefer 2000, Spencer 2001, *review by* Kao 2003], giving equivalent results to systemic chemotherapy. It is thought that patients fit for potential reirradiation should be randomized in studies evaluating its usefulness.

For patients unfit for reirradiation and all those presenting distant metastatic disease, palliative treatment through most often platine- or taxane-based systemic chemotherapy regimen are the only alternative mainly allowing satisfying symptoms relief. Compared to monotherapies, multidrug regimen offer better response rates but do not improve survival. Lot of hope is put in new generation targeted therapies [*review by* Cohen 2004].

2. RADIOTHERAPY FOR HEAD AND NECK SQUAMOUS CELL CARCINOMA

2.1. Basic principles of radiotherapy : the selective effect of radiations

X-rays (RX) were discovered in 1895 by Wilhelm Roentgen. This discovery was immediately used for diagnostic assistance but also for a wide variety of medical as well as non medical applications. Not more than a year later RX began to be used to try to treat unoperable cancers with convincing evidence of efficacy. Mechanism of action was poorly understood and radiations were used up to the 40's on an empirical basis, total administered dose being driven by apparent skin reaction. Both radiobiological and physical knowledge began then to grow on an exponential manner, allowing for more and more accurate and tailored anti-neoplastic treatments.

Radiations mainly kill cells by inducing direct or indirect (through the production of toxic free radicals) genomic damages at the desoxyribo-nucleic acid (DNA) level, but gene mutation, chromosome aberration and membrane modification are other recognized lethal effects [*review by* Cohen-Jonathan 1999]. At the DNA level, radiations induce an array of molecular lesions, e.g. base damage, sugar damage, DNA-proteins cross links, single strand breaks (ssbs), double strand breaks (dsbs), ... Among these lesions, dsbs are typically recognized as the most lethal. Indeed, they can be unrepaired or misrepaired, potentially leading to cell misfunction. Due to both non lethal mutations and accelerated cell cycle, tumor cells are less proficient than normal cells for DNA integrity restoration. This makes it possible for a same dose to kill tumor cells while keeping the integrity of surrounding normal cells.

These capabilities of destruction as well as of restoration are far from being absolute rules. They depend on both biological factors (intrinsic radioresistance modulation, oxygenation status, use of radiosensitizers and/or cytoprotectors, fractionation schedules) and physical factors (inner or outer source, focusing technique, type of radiation used).

All these elements determine and eventually allow the modification of what is called the « therapeutic index ». It is defined for a given dose by the ratio between the Tumor Control Probability (TCP) and the Normal Tissue Complication Probability (NTCP) [Fig. 1]. Both TCP and NTCP curves are sigmoid shaped, indicating that (1) a minimal dose is necessary to both tumor cure

or normal tissue complications and (2) a tiny increase of the dose dramatically increases studied effects. By modulating either biological and/or physical factors described further, one can shift either TCP curve towards the left (radiosensitization), or NTCP cure towards the right (radioprotection), the aim being to gain in terms of radiocurability while maintaining an acceptable rate of complications.

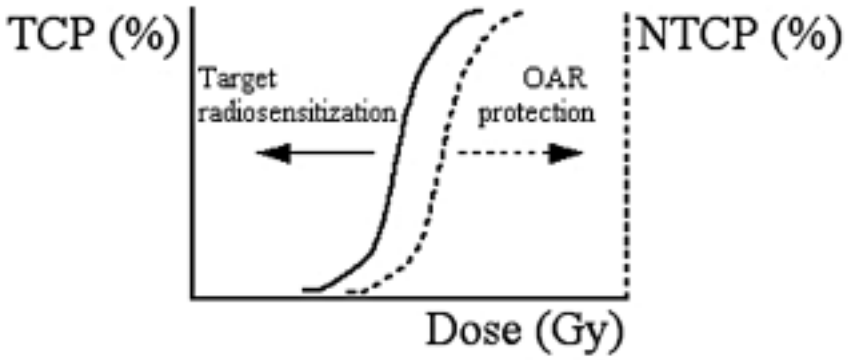

Figure 1 : Theoretical dose-effect curves showing the percentage of Tumor Control Probability (TCP) – on the left, continuous line- and the percentage of Normal Tissue Complication Probability (NTCP) – on the right, dotted line- as a function of the dose in Gray. As one can see, a small increase in the dose can lead to a higher cancer cure rate counterbalanced by unacceptable complications. Both chemical and physical tricks aiming at targeting the tumor conceptually lead to a shift on the left of the TCP curve. Both chemical and physical tricks aiming at protecting OARs lead to a shift on the right of the NTCP curve.

2.1.1. Biological selectivity

2.1.1.1. The mitotic cell cycle and the compartments of a tumor

A tumor is a burden of cells all aiming at mitosis. Before one can divide into two clones, it must first cycle through a well defined path with four successive phases corresponding to microscopic descriptions of chromosomes status [*reviews by* Rubin 2001 and Vermeulen 2003] : the G1-phase which can be considered as the premitotic phase corresponding to basal status of a living and active cell being not yet in the mitotic process. Then the S-phase which allows for DNA replication and finally the G2-M-phase which is the division phase in itself. All the cells involved in this process make part of virtual compartment called the « P » (for proliferating) compartment. Not all the cells are proliferating in a tumor, a large part of them being in a quiescent state (« Q » compartment) named the G0-phase because of oxygen and other nutriment deficiencies. These cells can be recruited to enter the mitotic process via the G1-phase.

All this cell cycle is regulated by a complex process of positive (mediated by protooncogenes like cyclins) and negative (by antioncogenes like retinoblastoma (pRB) or p53) stimuli. Any deregulation of this complex control process can potentially lead to carcinogenesis [Vermeulen 2003].

2.1.1.2. Increased radioresistance conditions

◆ Increased radioresistance is an **intrinsic** characteristic of some phases of the cycle. Indeed, not all the phases of the cycle are equivalently radiosensitive, the most radiosensitive one being G2-M where the cell does not have enough time to repair DNA. On the contrary, late S-phase and G0-phase are more radioresistant because cells still have the time to repair their DNA [Rubin 2001].

◆ But intrinsic radioresistance can also be the fact of various **genomic mutations** or **protein overexpressions** leading to more aggressive phenotypes [*review by* Smith 2001]. For example, some mutations lead to the inhibition of the « guardian of the genome » p53 gene which by consequence does not promote anymore the apoptosis process which is necessary to kill a cell damaged by radiations.

The second example concerns the uncontrolled overexpression of protooncogenes like cyclin D1 which production is stimulated by growth factors. If its concentration increases (either because of extrinsic growth factors stimulation, or because of intrinsic overexpression due to a translocation of its gene near a heavily produced protein as in mantle cell lymphoma), it binds to cyclin-dependent kinase (CDK) proteins. The CDK-cyclin D1 implies an entry of the cell in the G1-phase. Increased concentrations of cyclin D1 thus correlate with shortened G1 time and accelerated cell cycle.

Lastly, the overexpression of the HER-1 gene resulting in higher concentrations of Epidermal Growth Factor Receptors (EGFR) at the surface of the membrane is found in about 90 % of the HNSCC. This receptor is activated by autocrine ligands (like EGF or Tumor Growth Factor α – TGF-α) which are found in high concentrations in case of cancer. This leads to an increased stimulation of the Tyrosine Kinases (TK) and the subsequent mitotic cascade with accelerated cells repopulation as final effect. The overexpression of EGFR also has a negative effect on radiation induced apoptosis, leading to increased intrinsic radioresistance.

Those three examples of genome related increased radioresistance were chosen among all modes described up to now because they are the more deeply studied, both on the cellular but also clinical levels [Smith 2001].

◆ **Hypoxia** is long well known as being a negative prognostic factor for HN patients treated with radiotherapy. When performing low hemoglobin levels (< 13 to 14 g/dL for men and < 11 g/dL for women according to different studies) patients are known for having lower local control and survival probabilities [Harrison 2002]. At the cellular level, sufficient oxygen concentrations are needed to ensure the indirect effect of X-rays on DNA because it allows the stabilization of free radicals produced in the cytoplasm and thus to increase the probability for free radicals to encounter and damage DNA [Horsman 2002]. A complimentary explanation to the intrinsic radioresistant characteristic of hypoxic cells is related to the origin of hypoxia itself. Fast growing tumor tissues are characterized by poor structural organization, particularly regarding the blood supply. Cells situated too far from a neovessel receive not only too little oxygen, but also too little of other nutriments necessary to their development and proliferation. This leads them to enter into the quiescent (G0) phase which, as already mentioned, is by essence relatively more radioresistant.

2.1.1.3. Modulation of the radioresistance

◆ **Fractionation** is the administration of radiations by small doses on a repetitive manner. Standard fractionation is the administration of two Gy per fraction, one fraction a day, five days a week.

Fractionation allows to increase the therapeutic index by taking into account the fact that non tumor tissues have superior capabilities compared to tumor tissues to repair DNA. In other words, both TCP and NTCP curves are shifted towards the right, NTCP curve being however shifted faster than TCP one.

But this is not the only biological advantage of fractionation. The destruction of cells originating from the proliferative compartment makes room and frees nutriments and oxygen which may impact by :
–decreasing the proportion of hypoxia in the tumor;
–recruiting cells from radioresistant G0-phase to the radiosensitive proliferating compartment;
–supporting tumor cells repopulation which in turn could lead to reassortment between cell cycles, particularly towards more radiosensitive phases.
From a clinical point of view, the theoretical advantages of fractionation have

led to the design of altered fractionation schedules, among which accelerated (same dose given faster leading to a decrease in total treatment time) and hyperfractionated (smaller doses per fraction given twice or thrice a day leading to a small increase in total delivered dose) are most popular regimen. This is mainly because they were proved to bring a five percent increase of local control compared to standard fractionation in HNSCC patients treated with organ preservation protocols [Bourhis 2002].

◆ **Gene therapy.** p53 deficiency is the most documented and most often diagnosed gene mutation in HNSCC. This fact naturally opened the way to virus mediated gene therapy tentatives which were proved in phase I and II trials to be efficient, non toxic, highly specific of deficient cells and clinically efficient – but even more when chemotherapy or radiotherapy were added. For those who are interested in this early but very promising subject, above mentioned results together with others were reviewed and updated in depth by Moon et al. [Moon 2003]. These encouraging results open the way of other specific deficient gene repair or modulation, like the downregulation of cyclin D1 by antisense gene [Sauter 1999].

◆ **Biological modifiers.** Overexpression of EGFR and its ligands are proved to be deleterious to intrinsic radiosensitivity and hence to HN patients local control and overall survival [*review by* Sartor 2003 and Ang 2004].

Two main strategies aimed at thwarting EGFR activity have been developed. The first one relies on the use of small molecules given orally which bind to the intracellular portion of the EGFR, thus blocking downstream signaling. This class of molecules is called Tyrosine Kinase Inhibitors (TKI) among which gefitinib and erlotinib are most well known and clinically advanced, mainly in the lung cancer. For HNSCC, only one *in vitro* study to our knowledge showed evidence of a radiosensitizing effect of gefitinib [Shintani 2003].

The second strategy concerns the development of antibodies specifically targeting the extracellular portion of the EGFR, also resulting in a blockage of its activity. The most clinically advanced molecule in the field of HNSCC is the cetuximab or C225 which was proved to be an effective radiosensitizer in a randomized phase III trial comparing radiotherapy plus C225 to radiotherapy alone in locally advanced HNSCC. The arm using the combined treatment allowed the achievement of a three year overall survival of 57 % compared to the 44 % of the radiotherapy arm (P = 0.02) [Bonner 2004].

◆ **Oxygenation.** Blood transfusions in anemic patients have never been studied in thorough randomized study and are more and more unpopular because of lack of safety.

The use of recombinant erythropoietins allows for rapid hemoglobin level recovery, but clinical results of randomized studies are quite disappointing [Glaser 2001, Henke 2003] perhaps due to their potential angiogenic effect.

Encouraging results were observed in phase I and phase II trials of accelerated radiotherapy using carbogen (a hyperoxic gas allowing the increase of oxygen diffusion in tissues) and nicotinamide (a vasoplegic drug acting on perfusion related hypoxia). This promising method named ARCON [Kaanders 2002] is for the moment the purpose of a phase III investigation which should define its place in clinical practice.

Another studied approach is the use of nitroimidazole compounds which mimic the action of the oxygen by stabilizing free radicals. Main compounds studied are misonidazole, etanidazole and nimorazole. Nimorazole was used in a phase III study which proved its effectiveness in terms of both local control and overall survival in supraglottic laryngeal and pharyngeal carcinomas [Overgaard 1998]. This compound is available in Denmark only.

◆ **Bioreductives** are cytotoxic compounds which show a high affinity for hypoxic cells [*review by* Stratford 2003]. Most well known and studied one is mitomycin C. It was proved to be significantly beneficial for local control but not for overall survival when used in combination with radiotherapy compared to radiotherapy alone [Haffty 1993].

A promising new product named tirapazamine is currently under investigation in a phase III trial where a combination of concurrent radiotherapy and chemotherapy (cisplatine and 5-FU) is compared to the same regimen plus tirapazamine.

◆ **Concurrent chemotherapy.** Diverse common chemotherapy drugs have brought some evidence of radiation effectiveness enhancement (significant increase of local control of about five percent but no modification of overall survival) through different mechanisms of cell cycle modification, at least when used concomitantly to radiation [Pignon 2000]. Among them, cisplatine and 5-FU -which both decrease repair in tumor cells- are the most widely used drugs. A recent metaanalysis [Pignon 2000] even demonstrated that platine based

regimen were the most effective. Recent and well conducted phase III trials put more evidence about the gain which can be made from cisplatine used concomitantly to radiation, even in the postoperative settings [Forastiere 2003, Bernier 2004, Cooper 2004]. Among recent drugs, the most promising ones are the taxanes paclitaxel and docetaxel which synchronize tumor cells in a sensitive phase cycle. Only phase II results are available, showing effectiveness when used either alone or in combination with other drugs.

The main problem with concurrent radiochemotherapy is the significant increase of acute normal tissue reactions one has to face, mainly in terms of dermatitis and mucositis [Pignon 2000].

2.1.2. Physical selectivity

Physical selectivity accounts for all methods aimed at focusing the dose to the target (the tumor) while giving the lowest possible dose to surrounding normal tissue. The vast majority of today's HN radiotherapy is delivered by linear accelerators which provide mainly high energy γ-rays and electrons. High energy γ-rays roughly deliver, beyond an initial dose build-up zone, a log-linear decreasing dose with depth, leading thus to a substantial unwanted irradiation of non target tissues.

◆ Modern and mostly widespread method of radiotherapy aiming at substantially diminishing the dose delivered to non target volumes is **three-dimensional conformal radiotherapy (3D-CRT)**. The principle is to homogeneously concentrate the dose to the target volume while diluting the dose to surrounding tissues by multiplying the incidences used to hit the tumor. The shape of the field is also tailored to the shape of the target volume. All this work is performed on consecutive Computer Assisted Tomography scanner (CT) slices, allowing to visualize target as well as non target volumes in three dimension (3D). This method, and its evolution the Intensity Modulated beam Radiation Therapy (IMRT), will be developed in § 2.2.5.

◆ The smartest way to reach a target without collateral damage is to hit it from inside. In radiotherapy this can be done by inserting radioactive sources directly in the tumor. This is called **brachytherapy**. Implanted sources will continuously -at least during a time determined by their initial activity and intrinsic half-life- emit low energy γ- and/or β-radiations which will be highly concentrated at a small distance (few millimeters) from the source. Main limitations for

use of brachytherapy in HN area are :
–the close vicinity of vital anatomic structures (see § 1.1) which must be avoided by implants;
–the functional nuisance of implanted material into very mobile structures;
–the low availability of experienced physicians able to safely and correctly position radioactive sources.

Small tumors of the floor of the mouth, mobile tongue, tonsil, soft palate and lips are ideal ones for brachytherapy implantation, but require being performed by a skillful and experienced manipulator.

◆ **Charged particles** (e.g. protons, helium, carbon), to the contrary of photons, increase their energy deposit as they slow down. They abruptly release the majority of their energy when they stop (Bragg peak effect). For clinical use, the Bragg peak needs to be spread out by modulating the beam energy. From a dose distribution point of view, charged particle beams allow a better sparing of the surrounding normal tissues, especially when several coincident beams are used. From a radiobiological point of view, whereas proton beams are low LET radiation, heavy charged particle beams (e.g. carbon ions) are high LET radiation combining thus both a biological and a dose distribution advantage. Today, the greatest clinical experience was acquired with proton beams.

2.2. Modern radiotherapy delivery for Head & Neck tumors

HNSCC RT treatment is a quite complex technique which requires a proper logistic and trained and skilled personal for its completion. Main steps for accurate HNSCC RT planning are reviewed hereunder.

2.2.1. Immobilization

In order to minimize intra- as well as interfraction movements, patients must be planned in an as much as possible comfortable and above all reproducible position. This can be achieved through the use of customized thermoplastic masks that are firmly fixed to a table top in which a special neck cushion is adapted, which is specially designed to fit anatomical curves. Gilbeau et al. [2001] studied the accuracy of such a mask and concluded that patients were accurately setup in 90 % of the treatments within three mm for both the head and the neck and within four mm for the shoulders.

2.2.2. Imaging

In the early days of RT, fields were purely clinically defined. This was highly sufficient since only low energy beams were in use, making it unnecessary to visualize profound (unreachable) structures. This became a need with the birth of high energy beams and their capacity to deposit energy deeper in the body, making it mandatory to more precisely locate the different target volumes. This was done at first (from late 50's) by exclusive definition on simple radiography films where targets were indirectly located through their generally known position relative to bone and air structures. In the late 70's and early 80's, CT slices became available parallel to the exponential development of computer capabilities, making it possible to precisely locate the different anatomical structures on a three dimensional (3D) manner. In the early 90's, other anatomical (Magnetic Resonance Imaging [MRI], Ultrasounds [US], ...) as well as functional (functional MRI [f-MRI], Positron Emission Tomography [PET], ...) imaging modalities became available, making it possible to differently or complementary visualize a tumor. This will be developed in depth in § 3.

2.2.3. International Commission for Radiation Units (ICRU) concepts of target and non target volumes

Radiation oncologists can be considered as operating virtual surgery, scalpel being replaced by X-rays. Like a surgeon, they must first determine what needs to be irradiated or not. In an effort to standardize the way volumes are delineated, International Commission for Radiation Units (ICRU) has developed reports #50 and #62 [ICRU 1993, ICRU 1999] aiming at thorough and constant definition of what target as well as non target volumes must be made of [Fig. 2].

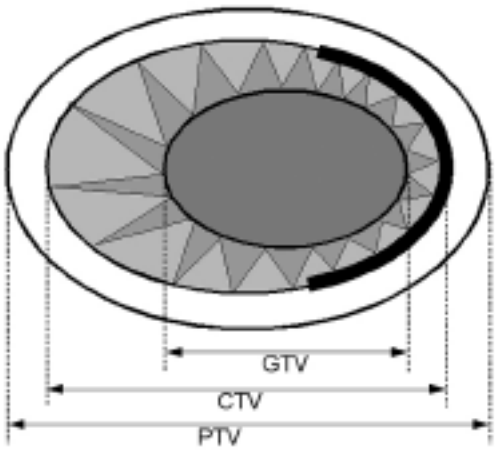

Figure 2 : « Schematic view of the target volumes defined by ICRU reports # 50 & 62. Gross Tumor Volume (GTV) relates to the macroscopically visible tumor. Clinical Target Volume (CTV) relates to the prediction of microscopic extension which can be limited by tough anatomical barriers (depicted here as a large line). Planning Target Volume (PTV) takes account of inter- and intrafraction movements. »

◆ **Gross Tumor Volume** (GTV) encompasses the whole primary tumor extension (GTV-T) as well as metastatic regional nodes (GTV-N) as it can be macroscopically evaluated.

Superficial extension is based on a complete description of the clinical examination : direct visualization of oral cavity and oropharynx tumors, indirect visualization of laryngopharyngeal tumors with a mirror or a fiberoptic endoscope and finally palpation of oral cavity, oropharynx (partly : base of tongue, tonsils and soft palate) and the neck to look either for an extralaryngeal extension in the prelaryngeal tissues or for metastatic nodes. Clinical examination is highly dependent on the operator's expertise which may give rise to a substantial degree of variability for the description of superficial extension of tumors. Moreover, neck palpation alone is a specific but poorly sensitive method to detect nodes and/or prelaryngeal tissues involvement.

Deep tumor extension is uneasily predicted from clinical examination [Zbären 1996] and thus needs to be evaluated with imaging methods such as CT and/or MRI. But differences in protocols used for images acquisition and display (slice thickness, injection of contrast or not, type of sequence used in MRI, gray scale window used for display,...) may also give rise to some variability in their interpretation. The evaluation of the nodal status is also best performed with imaging modalities such as CT, MRI or US with or without Fine Needle Aspiration Cytology (FNAC). They visualize deep seated nodes such as retropharyngeal ones. The use of US-FNAC gains in terms of sensitivity [van den Brekel 2000]. It appears from this presentation of the concept that, even if it is well defined, there remains potential "gray zones" on the best method(s) for its selection and delineation.

◆ The **Clinical Target Volume** (CTV) is a probabilistic volume which, based on the extension of the GTV, is aimed at taking account of the invisible or microscopic tumor extension. A good prediction is function of both a reliable delineation of the GTV and a good knowledge of local (micro)anatomy and subsequent weak points (facilitating tumor spread from one structure to another) or strong barriers (limiting tumor spread for a time). For example, supraglottic tumors of the larynx involving the laryngeal face of the epiglottis are reputed to easily invade the preepiglottic space (PES) through the fenestrations of the epiglottic cartilage. By consequence, the CTV-T selected for any tumor located in this subsite should totally encompass the PES because of its fatty nature, even if not clearly macroscopically invaded. On the other hand, both the hyoid

bone and the thyrohyoid membrane are very resistant structures precluding for a time the extension to prelaryngeal tissues. One thus should not encompass them in the CTV-T if the PES does not show clear evidence of complete repletion by the tumor.

Problems which give rise to a substantial degree of uncertainty when considering the concept of the CTV-T are the uncertainties listed in the previous paragraph about the delineation of the GTV-T, the absence of recognized guidelines for the selection of the CTV-T and the absence of pathological data about the possible maximum distance for tumor cells migration.

The selection and the delineation of the CTV-N according to the risk of presence of nodal involvement in the different neck levels are problems which are now solved thanks to the emergence of evidence based recommendations [Grégoire 2003].

◆ The **Planning Target Volume** (PTV) is a typical radiotherapy concept aimed at taking into account organ movement which may be intrinsic (due to breathing, swallowing, spontaneous movement) or extrinsic (fraction-to-fraction setup errors). Thanks to the use of predefined thermoplastic masks, we are able to predict that the use of a four mm margin around the CTV compensates for more than 90 % of the setup errors [Gilbeau 1999].

◆ **Organs At Risk** (OAR's) are defined by all those anatomical structures which show a relatively high sensitivity to radiations with subsequent functional impairment at therapeutic doses. Cellular organization of a given organ is important to know to correctly identify maximal critical dose which can be tolerated.
Parallel organization with independent substructures allows partial volume irradiation even at high doses. Remaining substructures will compensate, at least if they do not receive a critical dose. In the HN area, salivary glands are organized in substructures called "acini" which individually produce saliva collected in convergent tubules. It was well demonstrated that with a maximal mean dose of 20 Gy [Maes 2000] to 26 Gy [Eisbruch 1999] in conventional fractionation, the rate of significant (grades 3 and 4) xerostomia could be decreased down to 20 % and 0 %, respectively.

Serial organization is characterized by the fact that every cellular element is essential to whole organ function. If a lethal dose is given in only one point,

then all of the organ will misfunction. Spinal cord and brain stem are the two HN critical organs showing such an architecture. A maximal dose of 50 Gy in conventional fractionation is a reasonable dose avoiding permanent sectional myelopathy. In selected cases, higher doses can be tolerated at least in very limited volume because a certain degree of compensation can still be observed from surrounding tissues [Powers 1998].

The problem in HNSCC RT is that either primary tumor or more often nodal PTVs overlap with the parotid glands, leading to a compromise between PTV coverage and salivary glands sparing. Spinal cord and brain stem seldom overlap with PTV, but nodal PTV often shows a concave shape [Grégoire 2003] surrounding both structures which can be narrowed closer by posterior (typically Posterior Pharyngeal Wall) tumors giving a supplementary dimension to treatment complexity.

◆ A supplementary concept which was added to the ICRU report #62 is the **Planning Organ at Risk Volume** (PRV) which is for OAR like PTV is for CTV. In other words it takes account of setup and movement uncertainties for OARs delineation. Value of margins added are logically the same as those added from CTV to PTV.

2.2.4. Delineation of target and non target volumes

The gold standard imaging modality for volumes delineation (whatever location of the tumor) remains the CT. It however shows both inter- and intraobserver variability in both GTV and CTV delineation. This is a general problem documented for various anatomical locations like the cervix [Weiss 2003], the esophagus [Tai 1998], the brain [Leunens 1993], the lung [Giraud 2002] and Head & Neck tumors. Hermans et al. [1998] investigated the intra- and interobserver variability of CT based volume measurements of 13 laryngeal tumors by five different observers who repeated the delineation work four different times. They found that both the observer (interobserver variability) and -to a lesser extent- the session of delineation (intraobserver variability) had a statistically significant effect on volume measurement. They also found that experienced observers had stable results, leading them to conclude that variability for CT volumes measurements of laryngeal cancers can be substantially reduced if all the delineations are performed by one single, experienced observer. This is of potential problem since not all radiation oncologists are evenly talented in CT images interpretation.

It moreover may come from the facts that :
- purely clinical available data remain limited (particularly in the HN area where visualization and/or palpation of the lesions rarely predict in-depth infiltration);
- CT shows limited capabilities for soft tissues contrast;
- no clear rules exist for modified anatomy interpretation.

Evidence is growing that the use of better defined rules for delineation as well as complementary information coming from alternative imaging modalities could help in decreasing the variability encountered for the GTV delineation. In the Head & Neck, Rasch et al. [1997] studied the potential impact of the combined use of CT and MRI on the interobserver variability for the delineation of the GTV in six patients with a cancer of the base of skull (orbit, nasopharynx, ethmoid and parotid region). They demonstrated that MRI not only decreased interobserver variability but also the total volume by a factor of 25 %. In the lung, at least two correctly conducted studies [Vanuytsel 2000, Caldwell 2001] demonstrated that the combined use of CT and ^{18}Fluoro-Deoxy-Glucose (FDG)-PET led not only to a more consistent coverage of the GTV but also allowed to decrease the PTV and by consequence the volume of the lungs which receives a toxic dose of 20 Gy or higher by on average 27 %.

The determination of a GTV from functional imaging though is a critical step, which is usually performed by thresholding i.e. by segmenting a lesion of interest on the basis of a given level of radioactivity. Automatic thresholding method has been developed for SPECT studies and further extended and validated for FDG-PET in patients with lung tumors [Erdi 1995, Erdi 1997]. Studies on phantom were conducted to derive the relationship between the true volume and the threshold to be applied on the PET images. Such threshold varied according to the signal-to-background (S/B) ratios, being typically higher for less contrasted images. Such method however suffers from serious shortcomings, at least when functional imaging is to be used for radiotherapy treatment planning purpose. First, the automatic segmentation requires an *a priori* estimate of the volume of the lesion of interest from CT slices or other anatomical images. In absence of an *a priori* knowledge of the volume, it has been shown that a fixed threshold value between 36 % and 44 % of the maximal activity predicts well the true volume, but only for lesions larger than four cc. Second, for lesions smaller than four cc as usually observed in head and neck tumors, or for poorly contrasted lesions (S/B below 5.5), such thresholding method could lead to substantial overestimate of the true volume, even with the knowledge of the *a priori* volume. As the main challenge of introducing functional imaging in radio-

therapy treatment planning is to potentially resize the target volume or refine its shape relative to the anatomical information, the use of a CT volume as a gold standard from which a given threshold of activity will be selected, appears as a circular reasoning.

Delineation of OARs is generally performed on CT slices, but still remains possible on any anatomic imaging, *a fortiori* on MRI slices. The variability of this process has to our knowledge never been studied. It can be hypothesized that delineation on CT slices could give rise to a substantial degree of variability for reasons identical as those invoked for GTV and CTV. It should be though quite limited since the exact location of normal anatomical structures, extension and subject-to-subject variabilities are quite well documented in anatomy books.

2.2.5. Planning : Three-Dimensional Conformal Radiation Therapy, forward and inverse Intensity Modulated Radiation beam Therapy

In the early times, available photons were low energy ones only reaching quite superficial targets, eluding by itself the question of exact anatomical location. The birth in the 40's and 50's of megavoltage treatment and its possibility to reach more deeply seated tumors raised the question of their exact location. This was achieved through the definition of the fields on films based on the visualization of bony structures considered as indirect fiducial of common location of target as well as non target structures. However, both the interindividual variability and approximate knowledge of the exact extension of tumors led to the definition of generous borders which led itself to excessive irradiation of normal structures, limiting the total dose which could be achieved to the tumor unless accepting high risk of acute and long term side effects. Practitioners were quickly aware of the problem and rapidly tried to overcome it. At least as far as possible since a limited number of normal structures could be clearly identified on portals like rectum or bladder in the pelvis through the injection of contrast material. In the HN area, critical structures easy to identify were the spinal canal and the larynx which early benefited of shielding. Shielding was performed with simple predefined clinical lead blocks, or more complex tailored-« conformed »- lead moulds, or even in few centers with the ancestor of today's multileaf collimator (MLC) [Takahashi 1948]. One had to wait for the 80's and concomitant development of computer science and CT to see the emergence of 3D reconstructions of target as well as non target volumes. This allowed not only to more precisely define profound tumor extension, but also to develop powerful dedicated softwares called Treatment Planning Systems (TPS) which allow to tailor irradiation solutions through optimization of beams number,

angles and relative weights and customized field shaping based on the projection of structures viewed from beam source (Beams Eye View, BEV). This defines what is called 3D Conformal Radiation Therapy (3D-CRT).

Intensity Modulated beam Radiation Therapy (IMRT) is the ultimate evolution of 3D-CRT where one field is subdivided into numerous subfields through which the radiations are iteratively delivered. Resulting dose profile is not flat anymore but can adopt virtually any possible shape. It permits very steep dose gradients even in concave shaped targets surrounding or partially overlapping critical organs. Best example of such a situation is the bilateral irradiation of neck nodes whose PTV surrounds the spinal cord and overlaps with parotid glands. It explains why HN area rapidly became a focus of interest for IMRT development.

The most popular way to perform spatial modulation of beam intensity is through the use of a MLC, but other solutions exist (e.g. metal compensator or tomotherapy) which have been reviewed in details elsewhere [Webb 2000]. Each leaf is independent from each other. If leaves move when the beam is off and do not when it is on, one talks of static or segmented or “step and shoot” IMRT (s-IMRT). If leaves continuously move at various speed during irradiation, one talks of dynamic IMRT (d-IMRT).

Optimization of treatment plans is possible through evolutions of TPS which allow either forward or inverse planning. Forward planning is defined as “treatment planning in which the planner defines the beam directions and shapes, beam weights, wedges, blocks, margins, and so on, followed by the dose calculation and then the display of the dose distribution. Iteration through the process is performed manually to reach an acceptable plan” [Intensity Modulated Radiation Therapy Collaborative Working Group 2001]. The Inverse planning is “treatment planning in which the clinical objectives are specified mathematically and a computer optimization algorithm is used to automatically determine beam parameters that will lead to the desired dose distribution” [Intensity Modulated Radiation Therapy Collaborative Working Group 2001]. Whether forward or inverse, the iterative optimization process is driven either by intuitive analysis or mathematical algorithms which try to find the best compromise between optimal target coverage and minimal acceptable dose to a given percentage of an OAR (dose-volume constraints). One of the most intensive fields of research nowadays in IMRT is to translate the biological characteristics of the different tissues into mathematical functions (biological constraints) but the great biological

variability makes it quite difficult to use -at least for the moment- in routine [Webb 2000].

IMRT is really a hot topic with huge amounts of research work because it concentrates the dose to the target while decreasing the dose to normal tissues through the achievement of steep dose gradients. This points out the urgent need for an exact definition of tumor extent, either from macroscopic (GTV) as well as from microscopic (CTV) points of view. Indeed, a too restrictive definition of tumor extension would lead to geographical misses [Eisbruch 2002, Glatstein 2002] which would impair IMRT in achieving its goal to improve the therapeutic index of RT through diminishing side effects frequencies and/or intensities but also through dose escalation theoretically leading to improved local control probabilities.

2.2.6. Treatment delivery and Quality Assurance

Conventional treatments are nowadays delivered by megavoltage linear accelerators (LINACs). Complexity of machinery and treatments design imply a mandatory permanent control which is performed by computers. But this is still not enough, since any small error can have deleterious repercussions on treatment quality. Technical integrity of LINACs and MLCs are regularly checked and their dosimetric characteristics, being prone to day-to-day variations, are daily checked. But one must not forget that before a patient comes to the treatment bed, numerous preliminary steps have led to the design of the treatment (simulation, images acquisition, transfer in TPS, volumes contouring, dose calculation algorithms, block molding or MLC designs), each of which will have to be clearly checked through well defined Quality Assurance (QA) programs [Fraass 1998, Ferreira 2000, Intensity Modulated Radiation Therapy Collaborative Working Group 2001, Low 2002, Marcie 2003]. Moreover, the quality of the treatment provided will have to be checked during the whole treatment time for two essential parameters :

- setup reproducibility by recurrent portal films or Electronic Portal Imaging (EPI);
- effectively delivered dose through dosimetry (either *in vivo* or EPI based).

As can be seen, the refinement of radiotherapy techniques is possible only by increasing manpower, material (hardware and software) and subsequent costs. As physicians using the money of the community, it is our responsibility to identify when and how it is safe and efficient -or not- to use these new techniques.

3. IMAGING MODALITIES FOR TARGET VOLUME DELINEATION IN HEAD & NECK TUMORS

3.1. Requirements from a radiotherapy prospective

Considering the use of images in radiotherapy, they need to show specific qualities which meet both the physician's and physicist's requirements.

3.1.1. Physician's requirements

◆ An important requirement for an image is its **contrast**, which roughly means its capacity of showing differences between two different structures or functional compartments. One should first of all be able to easily define the limits of the body containing both target as well as non target volumes. This means one needs a good contrast between external contours (reliable depiction of the skin) and surrounding air as well as between internal air cavities (good distinction of mucosal interface) and air too.

Contrast for bony structures compared to surrounding soft tissues is also essential not only for possible bone involvement depiction but also because part of the planning and treatment verification are based on the exact definition of bony structures. Last but not least excellent contrast between soft tissues is needed to define GTV, CTV and OARs.

◆ A second important requirement of a "good image" lies in its ability to show the smaller possible details. This performance is reflected by what is called the **spatial resolution**. From the mathematical point of view it can be measured by imaging a point source [Fig. 3] which gives a more or less blurred image.

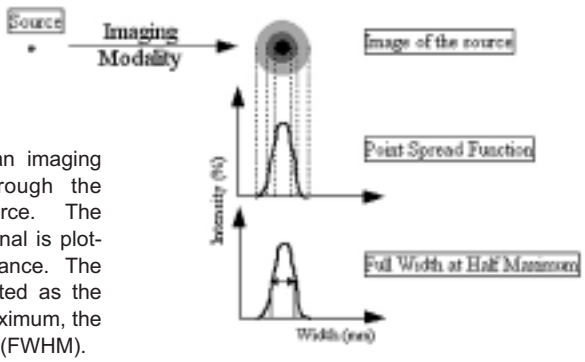

Figure 3 : Resolution of an imaging modality is estimated through the acquisition of a point source. The intensity of the acquired signal is plotted as a function of the distance. The spatial resolution is calculated as the width of the curve at half maximum, the Full Width at Half Maximum (FWHM).

The plot of recorded signal intensity as a function of distance is called the Point Spread Function (PSF). Spatial resolution is obtained by measuring the Full Width at Half Maximum (FWHM), i.e. the width of the signal at half maximum intensity. The lower the FWHM, the higher the spatial resolution.

◆ Finally, the ideal imaging modality should be able to provide not only the map of all volumes of interest (**anatomical** images), but also some specific information on the biology of a tumor (**functional** images) like differentiation, hypoxic zones, vascular pattern, specific metabolic pathways, oncogenes expression, ... in order to appropriately tailor the treatment to the physiological heterogeneous pattern of a given tumor [Ling 2000].

3.1.2. Physicist's requirements

Two physical characteristics are of the utmost importance to allow for accurate planning and dose distribution calculation : geometric accuracy and electronic density mapping.

Geometric accuracy is needed to locate external contours and all types of target as well as non target volumes to be able to propose optimal beam orientation and geometry leading to accurate treatments. Electronic density mapping of the different structures encountered during beam travel is necessary to determine energy deposit and subsequent dose calculation.

3.2. Anatomical images

3.2.1. Computer Assisted Tomography scanner

Computer Assisted Tomography scanner (CT) is nowadays the most popular and most convenient support for 3D-CRT planning.

The CT imaging modality is the tomographic evolution of the conventional planar radiology modality. Both are based on the attenuation through the imaged object of an incidental RX beam of initial intensity I_0. At the exit, the attenuated intensity (I) is an exponential function of I_0, the attenuation power of the irradiated object depending itself of the electronic density (μ) and of the depth of the object (x). Its formal mathematical notation is $I = I_0 e^{-\mu x}$. For display purpose, the images are expressed in Hounsfield Units (HU) which value is a direct function of the value of μ. The density of water was arbitrarily set to zero HU,

the one of the calcium (bone) at + 1,000 HU and the one of air at – 1,000 HU. The CT scanner [Fig. 4] is composed of (1) an RX emitter (the tube) from which a collimated beam is emitted and, opposed to it on a ring surrounding the imaged object, (2) a receptor composed of one or multiple detector(s). The ring determines the acquisition plane or xy plane. During the examination, density profiles are obtained at each discrete position on the detectors and digitized. These signals are stored and filtered by a computer. The resulting image is obtained after this treatment.

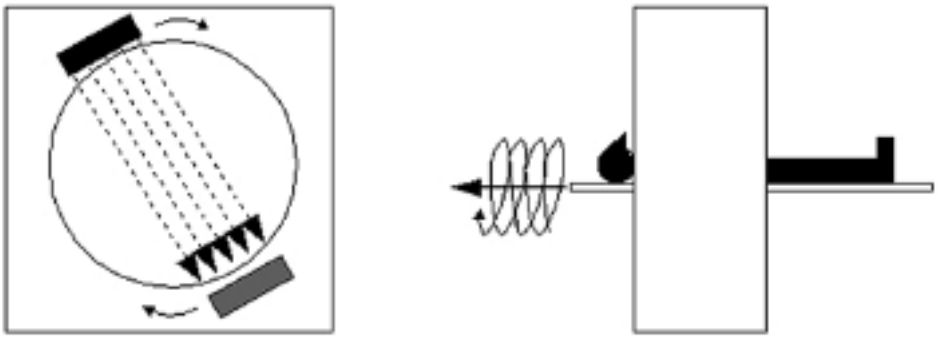

Figure 4 : Principle of spiral CT : patient progresses constantly in the ring while both the X-rays tube and its opposed detector continuously turn around him, allowing the acquisition of a whole volume.

A volume can be acquired by producing a stack of contiguous slices. This stack can be acquired either in a sequential mode by an iterative or step-by-step movement of the table top, or in a spiral mode by a continuous and constant movement of the table top on which the object is placed.

The different important parameters for image acquisition are the kilovoltage (kV) and the milli-amperes per second (mAs).

The different parameters for image reconstruction are the slice thickness, the acquisition matrix, the field of view (FOV) and the filter of reconstruction. The choice of the filter of reconstruction favors either the spatial or the contrast resolutions in the image.

Images are finally visualized on screens with software allowing a second treatment of the image by modifying the level and the width of the contrast window. During the acquisition, contrast material (generally iodinated products) can be administered either intravenously (IV), orally or rectally. This produces a modification of the contrast of the targeted compartment. In case of IV injection, different “times” can be imaged : vascular (arterial or venous) or parenchymatous.

Main **advantages** of CT for use in HN 3D-CRT are [Table1] :
- good contrast between air, fat and bone;
- high spatial resolution, down to less than one mm;
- no geometric distortion allowing the reconstruction of geometrically reliable volumes;
- electronic density mapping availability.

Table 1 : qualitative comparison of the three imaging modalities CT, MRI and PET for four characteristics particularly important to radiotherapy.

	CT	MRI	PET
ANATOMY			
External Contours	+	-	(+)
Bone / Air contrast	+	(+)	-
Soft Tissues contrast	(+)	+	-
FUNCTIONAL	(+)	(+)	+
ARTIFACTS			
Distortion	-	+	(+)
Movement	-	+	(+)
Metallic	+	+	-
RT PLANNING			
GTV Delineation	(+)	+	?
Spatial Resolution	+	+	-
Dose Calculation	+	-	(+)

Imaging modalities are quoted as + : good results, (+) : mild results and - : poor results considering the different items examined.

But it also suffers some important **limitations** :
- intrinsically limited contrast between soft tissues (i.e. between tumor and surrounding muscular structures) which may be, but not always, improved by the use of contrast agents;
- altered contrast in very dense regions due to the important absorption of the incident energy, like in the very osseous base of skull region or when there are teeth fillings inducing stellar artifacts.

3.2.2. Magnetic Resonance Imaging

While CT is based on X-rays absorption, MRI is based on proton density (PD) measurement. The positive proton rotating on itself (« precessing ») creates a very small local magnetic field which direction is called « spin ». All spins of a given volume are oriented haphazardly creating a resultant « magnetic moment » (M_0) equal to zero. When put in a strong magnetic field (called B_0) in a superconductive magnet, all the spins are suddenly oriented parallel to B_0, either in the

same direction (for a small majority of them) or opposed to it with non null resulting M_0. Precession frequency is function of B_0 and is called « Larmor frequency ». M_0 is what one wants to measure, but this is not directly possible, being too tiny to be measurable. A radiofrequenced magnetic field (called B_1), is applied perpendicular to B_0 with a frequency equal to Larmor frequency. All protons precessing at this frequency (resonance phenomenon) will be transitory flipped towards a direction perpendicular to their original one. Duration of B_1 application will determine total flip angle. Resultant perpendicular magnetic moment is called M_{xy} which can be indirectly measured thanks to the radio wave which is created by precession. M_{xy} being measured and flip angle being deduced, M_0 can be calculated (proton density imaging) by simple geometric calculation [Fig. 5]. Return to native direction takes time and is a function of two time constants called T1 and T2. T1 is the time needed by M_0 to recover 63 % of its native value. T2 is the time needed by M_{xy} to reach 37 % of its native value. T1 and T2 are not equal to each other because being a function of different physical factors. So, by saturating either T1 or T2, one can create images which specifically show T2 and T1 tissues, respectively.

Spatial location of the signal is made possible by introducing gradients in magnetic fields, provoking small differences in resulting protons frequencies and thus small differences in subsequent measured radio waves. Gradients knowledge allows to precisely locate where the radio wave comes from.

The MRI signal (function of M_0) is acquired thanks to a receiver coil and stored to computer. After Fourier transformation an image can be built. All images are dependent on Proton Density (PD), T1 and T2. By using different sequences, it is possible to create PD-, T1- or T2-weighted images. Main sequences used are gradient echo or spin echo sequences.

As with CT, IV administration of a gadolinium chelate can modify the image contrast of vessels and vascularized tissues.
Main **advantages** of MRI for potential use in HN 3D-CRT are [Table 1] :
- good contrast between soft tissues;
- high spatial resolution, down to less than one mm;
- possibility of performing functional acquisitions (see § 3.3.2).

But it also suffers some important **limitations** precluding its use as sole imaging modality for treatment planning :
- the complex nature of MRI is responsible for a lot of artifacts which can mimic pathology or cause mispositioning of signals : distortion artifact due to

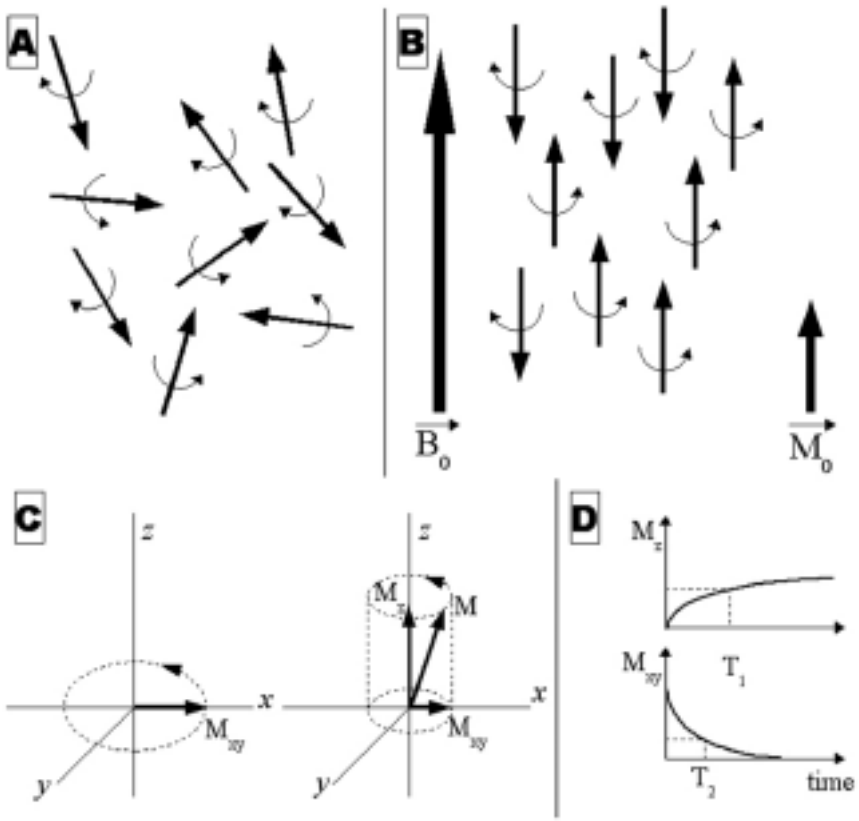

Figure 5 : Schematic representation of Magnetic Resonance principle. (A) Positively charged protons turn on themselves creating small magnetic fields (« spin ») which are haphazardly oriented, creating a null resultant magnetic moment. (B) When put in a strong magnetic field (B_0), they become oriented parallel to it, either in the same direction for a small majority of them or opposed to it. The resultant magnetic moment is small but non null (M_0). (C) If a transitory perpendicular magnetic field (B_1) is applied, all the spins tend to rock away from B_0 with an angle θ which is function of B_1 duration. M_0 then have two components : M_{xy} and M_Z. M_{xy} can be measured and, since θ is known, M_0 can be calculated. When B_1 stops, they go back to their native position, i.e. parallel to B_0, while still turning on themselves thus creating a radiowave which is what is really measured in MRI. (D) Restoration of M_Z and disappearance of M_{xy} are function of the time and can be measured. T1 time is the time necessary for 63 % M_Z restoration and T2 time is the time necessary for M_{xy} to reach 37 % of its native value.

inhomogeneous gradients, particularly at field of view edges; chemical artifact at water-fat interfaces provoking a spatial shift of this interface location; high susceptibility to paramagnetic substances, particularly paramagnetic metals causing local distortions in the magnetic field; high susceptibility to movement (blurring effect);

- absence of electronic density mapping;
- lack of contrast between contours and air, and with cortical bone which contains virtually no protons since it does not contain any water.

3.3. Functional images

3.3.1. Positron Emission Tomography

Positron Emission Tomography (PET) brings another dimension to the imaging of living creatures by providing targeted information on biological functions [Delbeke 2001], i.e. functional instead of anatomical imaging. Multiple metabolic pathways can be imaged by specific tracers : deoxy-glucose for glucose consumption, methionine and tyrosine for proteins synthesis, nitromidazole for hypoxia, … Mostly used tracers in HNSCC are by far FDG followed by ^{11}Carbon-Methionine (MET).

Deoxy-glucose enters the cells by the same transporter as glucose (called « GLUT », especially subtypes I and III that are overexpressed in tumors). It is then phosphorylated by a hexokinase (also overexpressed in tumors) and, to the contrary of glucose, remains trapped into the cell with no further metabolization. A high glucose consumption is not solely observed in tumors, but also in normal tissue such as brain cortex and in inflammatory cells. This means that ^{18}F-labelled deoxy-glucose is not a specific tracer.

Methionine is an amino-acid essential to protein synthesis. Its uptake was shown to reflect amino acid increased transport, transmethylation rate and protein synthesis within malignant tissues [Weber Wolfgang 1999]. It also lacks specificity since normal mucosa and salivary glands physiologically accumulate methionine.

Radiotracers used in PET imaging are labeled with positron emitter isotopes, the most commonly used being ^{18}F, ^{11}C and ^{15}0. Positron emitters have two major characteristics : (1) a short physical halflife (from two minutes for ^{15}0 to 120 minutes for ^{18}F, which means that some of them can not be used unless a cyclotron is running on site); (2) their scheme of disintegration : once emitted, the positron travels a few millimeters within matter and then encounters an electron, resulting in an annihilation reaction. Indeed, the positron, which is the antiparticle of the electron, is not directly detected by the camera. Annihilation gives birth to two strictly opposed - « coincident » - photons of 511 keV each [Fig. 6] which are detected by the camera.

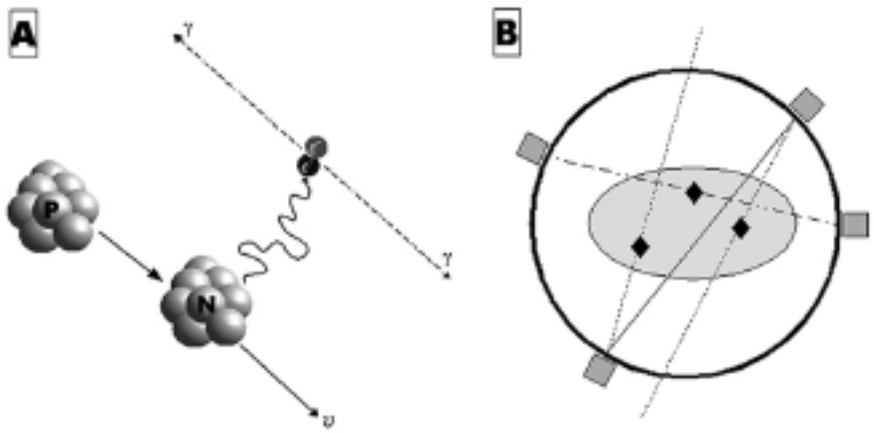

Figure 6 : (A) PET physicochemical principle. The nucleus is unstable because of the presence of a proton which will transform into a neutron, rejecting a neutrino and a positron. After short travel in the matter (« positron range »), it will annihilate with an electron, giving birth to two opposed photons of 511 keV each. These photons are indeed detected by the PET camera. (B) Two coincident photons are detected by opposed detectors allowing the location of the event along the true Line of Response (LOR) (dashed line). Random coincidences are due to the concomitant detection of two photons not originating from the same annihilation (dotted lines) leading to the recording of false event along a false LOR (plain line).

The PET camera detectors are arranged in multiple rings around the patient (or bed). For example, the CTI-ECAT EXACT HR camera which was used for the present studies is composed of 24 rings of 784 crystals each. Coincident photons have to hit a pair of detectors within a given time window (typically six to 12 nanoseconds) to be recorded (i.e. « true » coincidences). Each recorded pair of events determines what is called a Line of Response (LOR) and all recorded LORs allow the spatial localization of the emission event, i.e. where the annihilation reaction took place. The acquired « emission » data are stored on a computer as files called « sinograms » for further image reconstruction.

One of the main problems with PET is a limited spatial resolution which causes are multiple and mainly intrinsic, but reconstruction algorithms also play a role :

–the size of the detector (few millimeters) leads to uncertainty on the exact location of the event and thus affects the spatial resolution;

–as already mentioned, an emitted positron does not immediately annihilate with an electron. It first travels in a random direction before annihilation, which results in a direct travel range of few millimeters -depending on the positron energy- between the point of emission and the point of annihilation : on average 0.6 mm for ^{18}F and 1.1 mm for ^{11}C;

–the two emitted photons are not always strictly opposed, the angle between their directions being 180.0° +/- 0.5°. For coincident photons emitted at the center of the FOV, this 0.5° variation represents an incertitude of approximately

three mm at the level of the detector of a whole body tomograph;
–the interaction depth, due to the depth of the detector of two to three cm leading to an apparent larger dimension of the detector;
–the filter used in the reconstruction algorithm.

The final spatial resolution of an acquisition is a quadratic mix of all individual causes listed :

$$FWHM_{tot} = \sqrt{\Sigma\, FWHM_i^2}$$

resulting in a total FWHM of four to eight mm in the center of the FOV (without filtering).
Other physical problems may affect the image quality, producing loss of contrast and eventually decreased signal-to-noise ratio :
–the deadtime during which no event is recorded. This is related to the time needed by the computer to process incoming signal;
–the random coincidences which are due to the concomitant detection of two photons not originating from the same annihilation. If these two photons are simultaneously (i.e. within the range of the time window) detected by a pair of detectors, the event is recorded as a « true » coincidence, and thus a false LOR is drawn between [Fig. 6];
–the photons down-scatter due to Compton diffusion of photons interacting with the matter. The deviation of the photons leads to a mispositioning of the event [Fig. 6]. Both random coincidences and down-scatter can be reduced by the use of tungsten collimators. This acquisition mode is called the 2D mode in opposition to the 3D mode where no collimation is used. The drawback of using collimators is a reduced sensitivity leading to reduced signal-to-noise ratios;
–the attenuation of the photons originating from the deepest parts of the body which have less probability to reach the detector. This phenomenon is directly influenced by the density of the tissue the photons have to travel through. For example, photons traveling through the lungs will be far less attenuated than those coming from the center of the abdomen. It is possible to correct for this by measuring the attenuation factors. This is obtained by rotating an external source (^{68}Ge) around the patient. The attenuation map is then used to correct the emission data;
–the partial volume effect of small sources for which the recorded activity is distributed on a larger surface than the physical size of the source. The partial volume effect disappears when the size of the source is at least equal to two times the spatial resolution of the camera.
Behind all possible corrections, reconstruction filters can also improve contrast resolution with a price to pay in terms of spatial resolution.

Main potential **advantages** of PET for potential use in HN 3D-CRT are [Table 1] :
–potential help for delineation of tumor based on the higher metabolism of tumor cells compared to surrounding ones;
–possibility to map specific biologic clusters in the tumor (hypoxia, neoangiogenesis, …).

But it also suffers some important **limitations** precluding its use as sole imaging modality for treatment planning :
–lack of anatomical information;
–very poor spatial resolution (between five to ten mm according to position in the FOV –better in the center- and reconstruction algorithm used) and potentially low contrast resolution.

3.3.2. Functional Magnetic Resonance Imaging

Functional MRI (f-MRI) is a generic word encompassing at least three different techniques of non anatomical MRI.

First one is dynamic contrast enhanced MRI where distribution of a contrast agent bolus (generally gadolinium) is monitored as a function of time after injection. Such type of study allows the analyzation of tumor microvasculature. It could be potentially useful in HN RT by allowing a more accurate distinction between tumor and surrounding edematous tissues or by differentiating hypoxic subvolumes from well oxygenated ones in a given tumor [*review by* Baba 1999].

Second type of f-MRI image is based on the paramagnetic effect of deoxyhemoglobin which leads to a decrease of the T2 signal. This is widely known as the Blood Oxygenation Level-Dependent (BOLD) effect. Considering hypoxic regions containing high concentrations of deoxyhemoglobin, this technique could be of potential use not only to depict subvolumes in a tumor [Landuyt 2001], but also to predict which tumors would be eligible for targeting hypoxia and vasculature [Rijpkema 2002].

The last type of f-MRI study called diffusion-weighted MRI is based on the capacity of MRI to track the direction of diffusion of water molecules. A direct potential implication in HN RT could be through the distinction between tumor where diffusion of water is theoretically restricted and peritumoral edematous tissues where diffusion is more important by nature [Rowley 1999].

The main limitations with these techniques are related to the need for fast acquisitions leading to both poor spatial resolution by signal loss and image distortions due to magnetic field inhomogeneities, particularly at the air-tissue interface. This last point is by itself the most limiting one in HN area, making it an exciting field for research but still difficult to implement in clinical routine.

3.4. Image coregistration

Coregistration refers to every technique allowing direct spatial correlation between at least two images (2D) or volumes (3D). It can be used in virtually all science fields and is very trendy in medical science where complementary information (anatomical or functional) images can be acquired but for which direct comparison is difficult because of differences in slicing, slice width, spatial resolution, type of information provided, field of view (FOV), …

Different types of comparison can be performed according to the type of information of interest [*review by* Hutton 2002].
- Intrasubject, intramodality : for a given lesion evaluation as a time function.
- Intrasubject, intermodalities : for different types of evaluations of a given lesion.
- Intersubjects, intramodality : when group comparisons are needed, e.g. for the elaboration of an atlas of a given structure or region.
- Intersubjects, intermodalities. Technically feasible but no impact for clinical practice.

To reach this goal, many dedicated softwares were developed, they all show different features extensively presented and discussed elsewhere [*review by* Hawkes 1998]. Here follows a practical summary.

3.4.1. Rigid transformation

Rigid coregistration refers to all techniques by which the shape of all coregistered images is not altered during the process. Seven factors are necessary to define the coregistration process : three translations (in the three directions of the space), three rotations (around the three axis of the space) and one scaling factor to give all objects the same dimensions. These seven factors constitute a set called « transformation matrix ».

3.4.1.1. Manual

The definition by the operator of three or more identical –more or less- well defined anatomical points on each image to be coregistered as well as on the reference one is sufficient for a computer to calculate a transformation matrix. Main problem with such an algorithm is accuracy which can on average be as low as 10 mm [West 1997] mainly due to uncertainties in reference point definition, but also to the low number of reference points used.

One trick which can be used to overcome these two problems is to multiply the number of reference points used by (either manual or automatic) segmentation of reference image [Pietzryk 1994, Sibomana 1995, Habboush 1996]. The operator can thus try to find the transformation matrix to be applied by translating and rotating the to-be-coregistered objects. Accuracy of such a method is a bit better (around four to five mm on average) but is still operator dependent and the whole process takes quite a long time (around 20 minutes on average in our experience for a complete and satisfying coregistration).

3.4.1.2. Automatic

Two different methods are presently available for automatic definition of transformation matrix.

Chamfer-matching [van Herk 1994] segmentates both images. Segmentation is the base for calculation of transformation matrix. It is fast and robust, mainly because it is not sensitive to small deformations of the volume (i.e. pelvic images coregistration) if the operator takes care to erase useless structures susceptible to false calculations.

Mutual Information (MI) [Collignon 1995, Viola 1995] is perhaps the most popular algorithm, at least in the field of radiotherapy. The algorithm analyzes both volumes in terms of voxel characteristics and defines transformation matrix by minimizing the mean distance between similar voxels. It is fast and accurate but relatively less robust than chamfer matching because of requiring strictly identical shapes, though this can be overcome by optimizing function parameters. A complete review of MI algorithms was performed earlier [Pluim 2003].

3.4.2. Non rigid transformation

The estimation of soft tissue deformations has been largely studied in the last years. It is applied to compute the deformation due to a patient or organs movement between acquisitions. It is also used to automatically segment images from presegmented data sets by coregistering both together, allowing the generation of atlases. Some coregistration methods have been presented and applied between the same modalities (i.e. optical flow methods), between different modalities (i.e. splines based methods) or between segmented surfaces to find the best displacement to apply to every voxel of the image. Once this displacement field has been estimated, the deformation can be calculated.

4. OBJECTIVES OF THE STUDY

In modern radiation oncology, the development of new algorithms for 3-dimensional (3D) dose calculation and the use of computer driven linear accelerators able to deliver intensity modulated radiation beams have made it possible to precisely sculpt the radiation dose to target volumes of almost any shape. Improvement in the physical dose distribution obtained by such procedure (referred to as 3D-CRT and IMRT), has raised the issue of the accuracy of target volumes selection and delineation on a 3D-basis. The progressive introduction of IMRT in routine clinical practice has led to a major change in the radiation oncology community. Indeed, Radiation oncologists had to progressively move from the 2D to the 3D approach of the patient, thereby requiring the use of various imaging modalities to adequately identify and delineate the anatomical structures.

In this framework, Computer Assisted Tomography scanner (CT) has become the reference imaging modality for treatment planning purposes. It is widely available, does not suffer from geometric distortion and has intrinsic information on the electronic density of the various tissues, which is used by the dose calculation algorithms. CT however, lacks intrinsic contrast between soft tissues structures and tumor extensions. In laryngeal tumors, this has led to significant inter- and intraobserver variations for the delineation of the gross tumor volumes (GTV) [Hermans 1998]. Furthermore, CT images are degraded by the presence of dental filling, which significantly limits the performance of the modality in the assessment of oral and oropharyngeal tumors.

Magnetic resonance imaging (MRI) using various sequences (e.g. unenhanced T1-weighted, contrast enhanced T1-weighted and T2-weighted sequences with or without the fat suppression option) has been shown to be more accurate than CT in evaluating soft tissue or bone extension of head and neck tumors. In a limited series of tumors close to the base of skull, such advantage translated into a smaller interobserver variation in the GTV delineation compared to CT [Rasch 1997]. Furthermore, MRI images can be acquired in sagittal and coronal planes, resulting in easier and more accurate assessment of the cranio-caudal tumor extension. MRI however suffers from geometric distortion at the edges of the field of view and from susceptibility artifacts at bone/air interfaces. Furthermore, it does not carry any intrinsic information on the electronic density mapping, thereby precluding its use as a sole imaging modality for head and neck treatment planning purpose.

In addition to anatomic imaging, functional imaging with ^{18}F-deoxy-glucose (FDG) and ^{11}C-Methionine (MET) Positron Emission Tomography (PET) scan has been progressively incorporated into the management of cancer patients. Clinical studies using FDG-PET have demonstrated its value in the diagnosis, staging and evaluation of various tumor sites. For treatment planning, it has been shown in lung tumors, that the combined use of CT and FDG-PET resulted in an improved delineation of the GTV compared to CT alone leading, in selected patients, to a substantial reduction in the irradiated lung volume.

The uptake of MET has been shown to reflect amino-acid increased transport, transmethylation rate and protein synthesis within malignant tissues. Sensitivity and specificity of MET-PET for HNSCC staging are similar to FDG. A relationship between MET uptake and cell proliferation of HNSCC has been shown *in vitro* and *in vivo*, suggesting that MET could be more specific than FDG for measuring tumor aggressiveness. In addition, the early response to chemotherapy could be successfully assessed by MET in hypopharyngeal tumors, allowing to adapt the treatment scheme.

In the management of head and neck tumors, however, the added value of FDG- or MET-PET over CT or MRI appears limited and still deserves further clinical evaluation. Particularly, the value of FDG-PET in GTV delineation is unknown. PET however does not give any accurate information on the external and internal contours, which precludes its use as a single imaging modality for head and neck treatment planning purpose.

In this framework, it appears that combining different modalities could therefore result in a more accurate delineation of the GTV, while retaining the necessary information on patient anatomy. When multiple imaging studies of a same object are to be used, they must be spatially coregistered so that every voxel of one modality can have its counterpart in the other modalities. Several methods have been described for image coregistration ranging from interactive to fully automated, based on landmarks, surface or voxel coregistration, and using rigid or warping algorithms. We have developed an interactive rigid coregistration method based on semiautomated surface segmentation for coregistration of CT, MRI and PET images from patients with head and neck tumors. This method was used to evaluate the gain of MRI and PET on CT in the delineation of the GTV in patients with pharyngolaryngeal squamous cell carcinomas. A few teams already reported the feasibility of the technique. But, before one could demonstrate any additional value of one imaging modality over the others,

it was of utmost importance to perform a comprehensive quality assurance (QA) evaluation of the whole coregistration procedure. Indeed, the objective of combining multimodality imaging being to potentially improve the accuracy of the GTV delineation, it is essential to verify that the whole coregistration procedure does not introduce errors by far larger than the additional expected accuracy, i.e. in the order of a few millimeters. As a **first preliminary endpoint**, we reported **data on the accuracy, variability and consistency of an interactive coregistration procedure** using a dedicated phantom and a set of patients with primary head and neck squamous cell carcinoma (section 6).

Once coregistered, GTVs need to be determined on the different imaging modalities. If this step is relatively clear and natural on anatomic imaging, the determination of a volume from functional imaging is a critical step, which is usually performed by thresholding i.e. by segmenting a lesion of interest on the basis of a given level of radioactivity. Automatic thresholding method has been developed for SPECT studies and further extended and validated for FDG-PET in patients with lung tumors. This technique though shows intrinsic limitations for small and less contrasted tumors, which is often the case in Head and Neck. As a **second preliminary endpoint**, we elaborated an **automatic segmentation method for functional images** based on automatic thresholding of isoactivity independent of the *a priori* knowledge of the lesion of interest and valid for small and/or poorly contrasted lesions (section 7).

In view of the foregoing and after having completed the two preliminary endpoints, **the main purpose of our study was to compare CT, MRI, FDG- and MET-PET for the delineation of the GTV in pharyngolaryngeal squamous cell carcinoma, and to validate these imaging modalities with, whenever available, the macroscopic surgical specimen** (sections 8 & 9).

RT planning is not directly performed on GTVs. It is first needed to define the CTV according to the extension of the GTV. Such an extension is not simply geometrical but must take account of the different anatomical compartments encountered which either facilitate the diffusion of cancer cells (like fatty spaces) or on the other hand limit their spread because being intrinsically resistant like fascias or bones. Since it was mandatory to produce consistant CTVs for proper comparisons, we identified main pharyngolaryngeal SCCs spread pathways and derived **guidelines and recommendations for both the selection and delineation of primary pharyngolaryngeal SCC CTV** (CTV-T) (section 10).

These guidelines were used to produce and c**ompare CTVs and subsequent PTVs** derived from drawn GTVs. 3D-CRT planning calculations were performed for **comparison of subsequent dose distribution to both PTVs and OARs** (section 11).

5. GENERAL MATERIALS AND METHODS

5.1. Patient population

Twenty nine consecutive patients were included in the study from February 2000 to July 2002. Inclusion criteria were : 1) stage II-IV squamous cell carcinoma of the oropharynx, hypopharynx or larynx; 2) nonsurgical treatment by moderately accelerated radiotherapy (concomitant boost) or concomitant chemoradiotherapy, or total laryngectomy; 3) adequate general condition to sustain additional imaging modalities; and 4) informed consent. Twenty-five males (mean age 63 years, range from 44 to 82 years) and four females (mean age 59 years, range from 53 to 66 years) were included in the study. The mean age of the entire patient population was 63 years, ranging from 44 to 82 years. There was no statistical difference between the age of these two groups (Mann-Whitney test, $P = 0.57$), which matched the sex ratio for head and neck squamous cell carcinoma. Ten patients (nine males and one female) presented an oropharyngeal tumor (mean age 62 year, ranging from 44 to 81 year), 13 (11 males and two females) a laryngeal tumor (mean age 68 year ranging from 53 to 82 years), and six (five males and one female) a hypopharyngeal tumor (mean age 53 years ranging from 44 to 60 years). Patients in the hypopharyngeal group were significantly younger than those in the laryngeal group ($P < 0.001$, Mann-Whitney test). Sex ratios were evenly distributed among the three subsites ($P = 0.2$, Fisher's exact test). Twenty of these patients were treated by moderately accelerated radiotherapy (concomitant boost) or concomitant chemoradiotherapy. Eight patients who presented extended T4 laryngeal tumor (massive thyroid cartilage invasion with or without extralaryngeal infiltration) and one patient with a T2 subglottic laryngeal tumor were treated by total laryngectomy, bilateral neck node dissection and postoperative radiotherapy. Our study was approved by the local Ethical Committee, and informed consent was obtained from all patients.

5.2. Image acquisition

For acquisition of all images, patients were immobilized with a customized thermoplastic mask (Sinmed, The Netherlands) fixed to a flat tabletop. All patients were imaged with a CT, an MRI and a PET without predefined order. On average, for each patient, these examinations were performed within four days. For patients scheduled for total laryngectomy, surgery was performed on average five days after the first imaging study.

5.2.1. Computer Assisted Tomography scanner

CT acquisitions were performed on a dual-detector spiral CT (Elscint Twin, Haifa, Israel) using a slice thickness of 2.7 mm, an interval reconstruction of 2.5 mm and a pitch of 0.7. Images were acquired using a matrix of 512 x 512 pixels, and reconstructed with a final resolution at FWHM of 1.2 x 1.2 x 2.5 mm^3 (values provided by the manufacturer). Sixty ml of iodine contrast were injected IV at a rate of 2.5 ml/s, followed, after a three min rest period, by a bolus injection of 50 ml at 1.5 ml/s. Biphasic protocol combines the benefits of sufficient impregnation by the initial phase of the contrast medium perfusion resulting in optimal total body opacification, and of bolus opacification of the lumen of the patent vessels during the second phase, which is synchronized to the initiation of image acquisition. Image acquisition started immediately after the end of the bolus injection and the field of view started from the sternoclavicular joint to the frontal sinuses.

5.2.2. Magnetic Resonance Imaging

Axial MRI images were all acquired on a 1.5 Tesla superconducting system (Intera 1.5, Philips Medical Systems, Best, The Netherlands). As the immobilization device precluded the use of any dedicated head and neck coils, the body coil was utilized as receiver. Similar pulse sequence data were used in all patients including a 300 mm FOV, 256 x 256 matrix and either a 3.5 mm slice thickness without interslice gap, or a 3.1 mm slice thickness and a 0.4 mm interslice gap. The FWHM was 1.4 x 1.4 x 3.5 mm^3 in « x », « y », and « z » directions, respectively. These values of FWHM were calculated from the pixel size using the previously described method [Haacke 1999]. Only 2D acquisitions were performed to limit acquisition time. Pre- and postcontrast spin-echo T1-weighted images (TR 770 ms, TE 10 ms) and T2-weighted fast spin-echo images (TR 5000 ms, TE 100 ms) were obtained. Patients were asked to avoid swallowing or coughing during the acquisitions (each of approximately five min in time).

5.2.3. Positron Emission Tomography

PET scan acquisitions were performed on a Siemens Exact HR camera (CTI, Knoxville, USA) using an axial field of view of 275 mm (two bed positions, with a 25 mm overlap between the two bed positions).

Images were acquired using a matrix of 128 x 128 pixels. A 2D transmission scan of 10 min was first performed over each bed position. Thirty minutes after IV injection of 333–518 Mbq (9–14 mCi) MET, a 20 min 3D emission scan was obtained for each bed position. After the completion of the MET-PET, 185–370 mBq (5–10 mCi) FDG were injected. A 20 min 3D emission scan was obtained 60 min later. It must be noted that six patients (five with laryngeal tumor treated by surgery and one with hypopharyngeal tumor) could not be imaged in MET-PET for technical reasons.

Four different algorithms were used for image reconstruction :
1) a 3-D Filtered Back Projection (FBP) algorithm with decay, random, scatter and attenuation corrections using a 0.3 Hann filter [Kinahan 1989]. At a 10 cm distance from the center of the FOV, the FWHM reached 7.7 x 6.9 x 7.9 mm^3 in « x », « y » and « z » directions, respectively;
2) a Fourier rebinning (FORE) algorithm combined with an Ordered Subsets Expectation-Maximisation (OSEM) reconstruction [Hudson 1994] without Gaussian postsmoothing (termed OSEM) resulting in a FWHM at a 10 cm distance from the center of the FOV of 6.7 x 5.2 x 5.5 mm^3 in « x », « y » and « z » directions, respectively;
3) a FORE rebinning algorithm with an OSEM reconstruction using a six mm Gaussian postsmoothing (termed OSEM 6) resulting in a FWHM at a 10 cm distance from the center of the FOV of 9.2 x 8.1 x 8.5 mm^3 in « x », « y » and « z » directions, respectively;
4) a FORE rebinning algorithm with an OSEM reconstruction using an eight mm Gaussian postsmoothing (termed OSEM 8) resulting in a FWHM at a 10 cm distance from the center of the FOV of 10.6 x 9.7 x 10.1 mm^3 in « x », « y » and « z » directions, respectively. The values of FWHM were calculated from measurements performed in our PET camera using a method previously described [Wienhard 1997].

5.3. Coregistration software

CT, MRI and PET images were transferred to the coregistration workstation and the files were converted into the native Computer Technology and Imaging Emission Computer Assisted Tomography (ECAT-CTI) format. Volumes were coregistered using an interactive rigid coregistration method based on surface segmentation [Fig. 7], following the method previously described [Pietzryk 1994, Sibomana 1995, Habboush 1996]. Briefly, each volume was resliced to a com-

mon voxel size and simultaneously displayed as axial, coronal and sagittal planes. An automatic segmentation of the contours was performed on the reference volume (e.g. the CT) and overlaid on the other modalities. Using a transformer with real time visualization, the 'to-be-coregistered' volume was translated and rotated in x (axial plane, left to right), y (axial plane, posterior to anterior) and z (sagittal plane, feet to head) directions until visual matching of the volumes was found to be adequate by the observer. If required, the pairs of volumes could be fused to fine tune the coregistration. The transformation parameters were saved in extended markup language (XML) format for future display of the coregistered volumes.

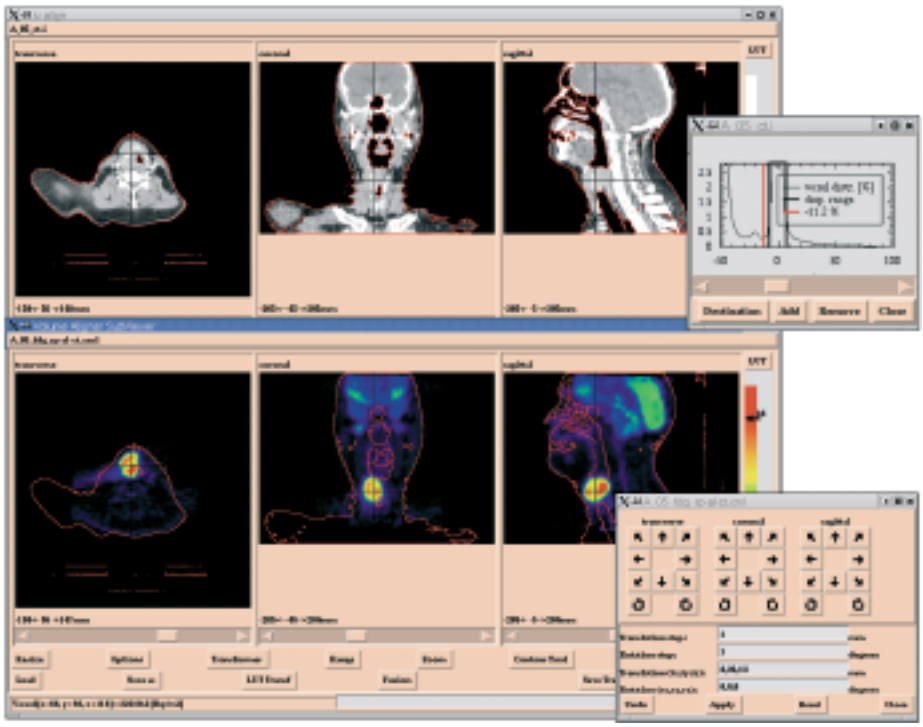

Figure 7 : Screen dump of the coregistration window. In this example, automatic segmentation of the CT volume (upper three slices) was performed based on selection of a particular threshold (upper right window) and overlay on the PET volume (bottom three slices). Interactive translations and rotations (lower right window) allow visual matching between the two modalities.

6. ACCURACY OF THE COREGISTRATION PROCEDURE

[Published as : Daisne, et al. Radiother Oncol 2003;69:237-245]

6.1. Specific introduction

Few teams [Wong 1996, Sercarz 1998, Uematsu 1998] already reported the feasibility of the technique. But, before one could demonstrate any additional value of one imaging modality over the others, it is of utmost importance to perform a comprehensive quality assurance (QA) evaluation of the whole coregistration procedure. Indeed, the objective of combining multimodality imaging being to potentially improve the accuracy of the GTV delineation, it is essential to verify that the whole coregistration procedure does not introduce errors by far larger than the additional expected accuracy, i.e. in the order of a few millimeters. To date, such an evaluation has not been reported in the head and neck area, as opposed to the brain area where several studies have already been published [Kapouleas 1991, Turkington 1993, Pietzryk 1994, van Herk 1994, Habboush 1996, West 1997, Woods 1998, Mutic 2001]. In this section, we report data on the validation of an interactive coregistration procedure using a dedicated phantom and a set of patients with primary head and neck squamous cell carcinoma.

6.2. Specific materials and methods

6.2.1. Phantom object : design and imaging

A phantom object was specifically designed for the purpose of the QA procedure. It consisted of an empty plexiglas cylinder with plastic objects figuring the neck structures : a 295 cc cylinder filled with plaster for the spine, one 55 cc cylinder filled with air mimicking the larynx and trachea, two 55 cc cylinders mimicking primary tumors and six cylinders of two cc mimicking invaded nodes [Fig. 8]. For CT and MRI, the phantom and the objects mimicking the tumor and nodes were filled with water and copper sulfate ($CuSO_4$), respectively. Three acquisitions were performed in CT, according to the protocol described earlier (§ 5.2.1) : (1) the phantom in a reference position (CT_{ref}) with its axes parallel to the table axes; (2) the phantom rotated through an angle of 30° on a axial plane; and (3) the phantom tilted by 14° on a sagittal plane. In MRI, 48 2D T1-weighed axial images (TR, 66.5 ms; TE, 10 ms) were acquired. For PET, a 20 min 2D-transmission scan was performed using external rotating rods of ^{68}Germanium sources. The phantom was then filled with 5.7 kBq/ml of ^{18}F, and the objects

mimicking the tumor and nodes were filled with ^{18}F at activities ranging from 24.4 to 490 kBq/ml. Data acquired in PET were reconstructed with two of the four reconstruction algorithms previously described : OSEM and OSEM6.

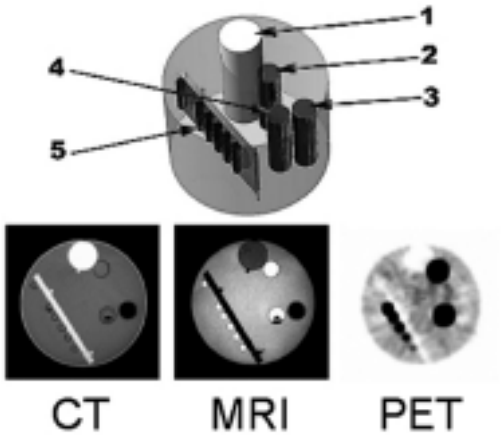

Figure 8 : Schematic view and axial CT, MRI and PET slices of the phantom with the plastic objects inside. Objects were filled with plaster (1), air (3), and $CuSO_4$ (CT and MRI acquisitions) or ^{18}Fluor (PET acquisitions) (2, 4, 5).

6.2.2. Patients imaging

Four patients with moderate to advanced squamous cell carcinoma (T4N2b; T3N0; T2N0; T2N0 - UICC 1997) of the pharyngolarynx were prospectively selected among the 20 patients referred for primary locoregional treatment with radiotherapy. For image acquisition, patients were immobilized with the thermoplastic mask used for treatment. All images were acquired before the start of radiotherapy using protocols described earlier (§ 5.2). Both transmission and FDG emission images were reconstructed with OSEM and OSEM6 algorithms. A second CT (CT_{boost}) was also performed after four weeks of treatment, just before the planning of the radiotherapy boost.

6.2.3. Coregistration procedure

Coregistration of the different volumes was performed blindly by naive observers (radiation oncologists or medical physicists).

For the phantom object, eight observers were asked to perform one coregistration of the different CT, MRI and PET volumes relative to the CT_{ref} volume [Fig. 9]. For CT, to test the coregistration algorithm without any other variable, the CT_{ref}

was randomly resliced to generate five new CT volumes. In total, 88 different coregistrations were performed.

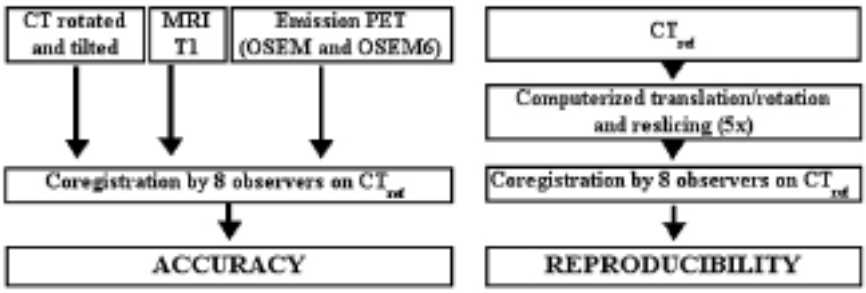

Figure 9 : Flow chart of the coregistration procedure for the phantom object. CT, MRI and PET volumes were coregistered relative to the CT_{ref} volume by eight different observers. Displacements (translations and rotations) were determined to calculate the coregistration accuracy and reproducibility. Reproducibility was only calculated from the coregistration of the resliced CT volumes.

For the four patients, four observers, all physicians were asked to perform four times (with at least three days between each session), the coregistration of the different CT, MRI and PET volumes relative to the pretreatment CT volume [Fig.10]. In total, 448 different coregistrations were performed.

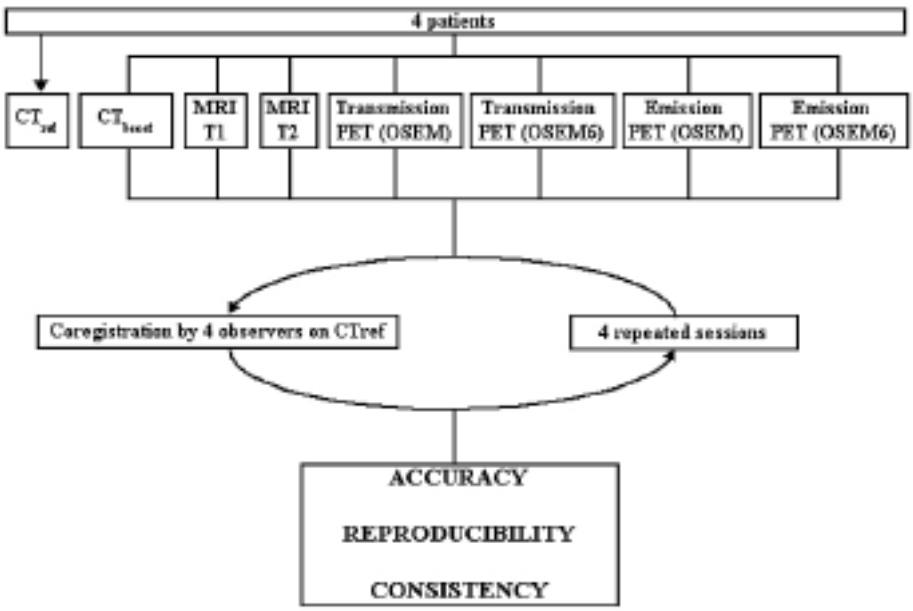

Figure 10 : Flow chart of the coregistration procedure for the four patients. CT, MRI and PET volumes were coregistered relative to the CT_{ref} volume by four different observers. Each coregistration was repeated four times by each observer. Displacements (translations) were determined to calculate the coregistration accuracy and reproducibility. Consistency was also calculated from the coregistration of MRI volumes.

6.2.4. Data analysis

The transformation matrix for the translation and the rotation (both in x, y and z directions) required to get a perfect matching with the reference image (CT_{ref}) was used to assess the accuracy, the reproducibility and the consistency of the coregistration [Habboush 1996, Hutton 2002].

For a given imaging modality, accuracy was defined as the difference in translation (in mm) or rotation (in degree) obtained by a given observer during a given session from the average translation or rotation calculated from the coregistration performed by all observers for the same imaging modality. The accuracy was expressed by two standard deviations (2 SD) of its distribution among the various observers. Alternately, the accuracy was also assessed from the Euclidean vectors, which express the total displacement (in mm) resulting from combining the translations and the rotations of a given point in x, y and z directions [Kapouleas 1991, West 1997]. The point that was chosen was the most distant from the image center, thus resulting in the « worst » assessment of accuracy.

Reproducibility was assessed by the intra- and interobserver variations. The intra- and interobserver variations were calculated from the distribution of the translations obtained from the coregistration (in reference to the CT_{ref}) of a given imaging modality performed several times by the same observer, or once by the various observers, respectively. The reproducibility was expressed by the variance of the intra- and interobserver variations. The difference between the total variance and the intra- and interobserver variance was called the residual variance. It gave a good estimate of the uncontrolled factors involved in the coregistration reproducibility. For the phantom object, only coregistrations from the resliced CT volumes were used to assess the reproducibility.

Consistency was assessed by the comparison of the accuracy calculated in patients imaged by MRI with T1- and T2-weighed sequences, as the same referential was used for the two data sets. The consistency was expressed by the average difference in accuracy between T1- and T2- weighed sequences in all three directions. Consistency could not be evaluated between transmission and emission PET because of potential setup error [Gilbeau 2001] since the mask was removed between both acquisitions.

6.2.5. Statistical analysis

All statistical analyzes were performed using SPSS® (version 9.0). Differences in accuracy and reproducibility for the various imaging modalities were tested using a UNIANOVA test. The level of significance for the alpha error was set at 0.05.

6.3. Results

6.3.1. Accuracy

For the phantom object, overall, the coregistration accuracy for translations in the x, y and z directions was in the order of one to four mm, except for PET after postreconstruction smoothing [Table 2]. For all three directions, a more accurate coregistration was observed with CT. For both MRI and PET, the accuracy in the z direction was always worse. Also, for PET, a slightly worse accuracy was observed after postprocessing smoothing of the data. In comparison with the unsmoothed data, this difference, however, did not reach a level of significance ($P > 0.1$). With respect to the rotational displacements, the accuracy of coregistration was within 2.2° without substantial differences between the various imaging modalities. For the patient studies, due to the use of an immobilization device limiting the rotational displacements, the observers found that applying a rotation on the image sets did not result in a better matching. Consequently, the coregistration accuracy was only evaluated for the translations [Table 3]. From the Euclidean vector analysis, on average, 50 % of the coregistrations were performed within 2.1 mm and 95 % within 5.8 mm. No difference in accuracy was observed between the various imaging modalities, except for the transmission PET, which was better than the emission PET ($P < 0.001$). When the three directions were analyzed separately, as already observed with the phantom object, the overall accuracy was worse in the z direction. These differences reached a level of significance for CT, T1- weighed MRI, and emission PET ($P < 0.03$). It was hypothesized that the worse coregistration accuracy in the z direction could be a direct consequence of the slice thickness. Indeed for the phantom object, a significant correlation ($P < 0.001$) was observed between the accuracy for the translation in all three directions and the image resolution assessed by the FWHM [Fig. 11]. The higher the image resolution, the better the coregistration. For patients, there was only a non-significant trend ($P = 0.2$) between these two variables [Fig. 12]. It is noteworthy to mention that for both the phantom object and the patients, the coregistration accuracy was always better than the image resolution assessed by the FWHM.

Table 2 : coregistration precision for various imaging modalities in the phantom object

Imaging modality	Translation (2 SD, mm)			Rotation (2SD, °)			Mean Euclidean vector (mm)
	« x »	« y »	« z »	« x »	« y »	« z »	
CT[1]	0.8	1.1	1.1	0.3	0.4	1.3	1.1 (0.0-3.7)[2]
MRI (T1)	1.6	1.6	2.7	0.7	0.5	1.0	1.3 (0.4-2.8)
FDG-PET (no smoothing)	2.9	3.3	3.7	2.1	1.4	1.5	2.9 (1.4-5.3)
FDG-PET (smoothing of 6 mm)	4.2	2.7	6.2	1.5	0.1	2.2	3.3 (0.6-10.4)

[1] data from the CT rotated and tilted pooled together
[2] 95 % probability interval

Table 3 : coregistration precision (2 SD in mm) for various imaging modalities in patients

	CT	MRI	MRI	Transmission PET		Emission PET	
	(mid-treatment)	T1	T2	No smoothing	Smoothing at 6 mm	No smoothing	Smoothing at 6 mm
Translation in "x" (mm)[1]	1.2	1.9	2.1	1.9	1.9	1.9	2.1
Translation in "y" (mm)	1.3	2.3	2.5	2.1	1.9	3.0	2.6
Translation in "z" (mm)	2.4	2.7	3.5	3.0	2.6	4.3	4.6
Mean Euclidean vector (mm)	1.1	1.5	2.0	1.4	1.2	2.1	2.1
	(0.3-3.8) [2]	(0.5-4.7)	(0.7-5.8)	(0.4-4.7)	(0.3-5.6)	(0.7-5.3)	(0.6-5.6)

[1] 2 SD
[2] 95 % probability interval

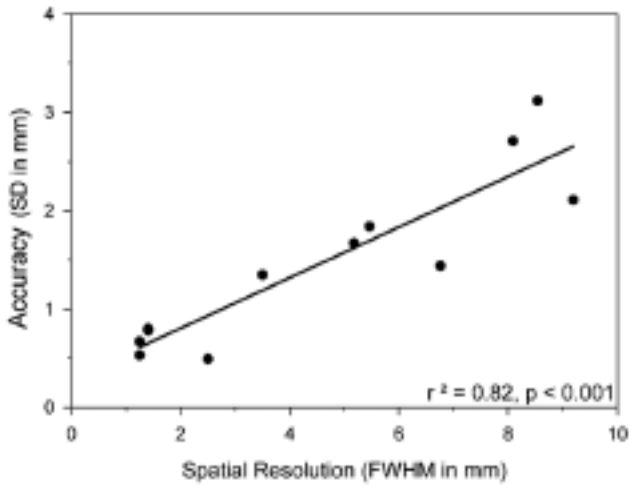

Figure 11 : Relationship between the coregistration accuracy for translations in the x, y and z directions and the image resolution assessed by the full width at half-maximum (FWHM) for the phantom object. Data for all imaging modalities have been pooled together.

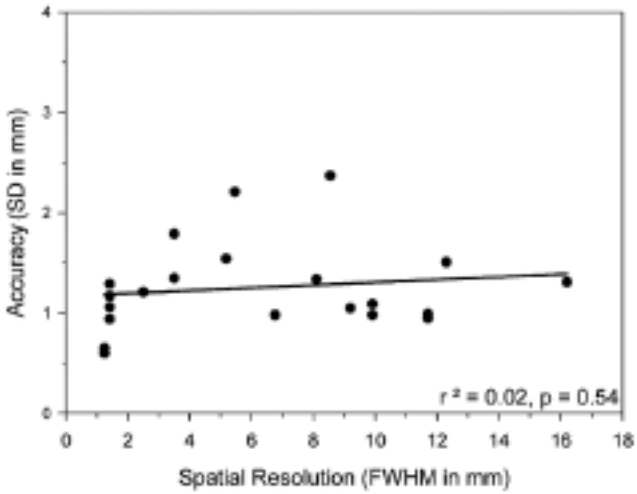

Figure 12 : Relationship between the coregistration accuracy for translations in the x, y and z directions and the image resolution assessed by the full width at half-maximum (FWHM) for the patients. Data for all imaging modalities have been pooled together.

6.3.2. Reproducibility

For the phantom object, intra- and interobserver variations were assessed from the coregistration between the five resliced CT volumes and the CT_{ref}. In all three directions, and for both the translations and the rotations, the intra- and interobserver variations were very small; the variance was always calculated below 0.09 mm^2 (data not shown).

For the patient studies, the intra- and interobserver variations were calculated from the coregistration of CT_{boost}, MRI and PET images [Table 4]. Overall, for all imaging modalities, the intra- and interobserver variations were below 0.25 mm^2, which was by far lower than the residual variance.

Table 4 : intra- and interobserver variance and residual variance in the coregistration precision (translation only) for various imaging modalities in patients.

Variance	Direction	CT	MRI	MRI	Transmission PET		Emission PET	
		(mid-treatment)	T1	T2	No smoothing	Smoothing at 6 mm	No smoothing	Smoothing at 6 mm
Intraobserver	x	0.00	0.01	0.06	0.09	0.02	0.00	0.00
	y	0.00	0.00	0.13	0.06	0.10	0.00	0.00
	z	0.00	0.01	0.06	0.09	0.02	0.00	0.00
Interobserver	x	0.00	0.00	0.13	0.06	0.10	0.00	0.00
	y	0.00	0.00	0.00	0.00	0.00	0.00	0.25
	z	0.00	0.00	0.00	0.00	0.00	0.00	0.25
Residual	x	0.39	0.86	0.99	0.82	0.99	0.89	1.20
	y	0.45	1.43	1.38	1.12	0.76	2.29	1.81
	z	1.54	1.75	3.40	2.33	1.85	4.20	3.99

6.3.3. Consistency

Consistency was assessed from the comparison of the T1- and T2-weighed MRI images [Table 5]. There was a perfect consistency in the coregistration of the two sets of images, but in the y direction where a significant (P = 0.003) difference was observed.

Table 5 : consistency in the coregistration (translation only) for the MRI volumes.

Imaging modality	Consistency (mm)		
	"x"	"y"	"z"
MRI (T1 vs T2)	-0.2	0.6*	-0.4

* *P < 0.01*

6.4. Discussion

In this section, we report a thorough evaluation of an interactive rigid coregistration method based on an interactive surface segmentation for coregistration of CT, MRI and PET images from patients with head and neck tumors.

Overall, both on a phantom object and on patients, the accuracy of the procedure was excellent with a mean vectorial displacement in the order of one to two mm for CT and MRI, and slightly worse for emission PET [Tables 2 & 3]. For the rotations, the variation was less than two degrees, which is likely a consequence of the care with which the phantom object was positioned on the table top of the various imagers [Table 2]. For patients, the coregistration accuracy for rotation could not be assessed as the observers did not find it useful to apply a rotation to get a perfect matching. This could be explained by the use of an immobilization mask, which from our experience limited considerably the rotational setup uncertainties [Gilbeau 2001]. For translations, the significant difference in the z direction between the transmission and the emission PET was relevant. It is likely that when coregistration of the segmented reference CT over the emission PET was performed using the highly saturated cerebellum for visual matching, a systematic displacement in the cranio-caudal direction was introduced due to the overestimate of the cerebellum volume. As a practical consequence, it was suggested to perform the coregistration between the reference CT and the transmission PET and then apply the coordinates obtained from the transformer to the emission PET.

Of particular interest, was the significant correlation between the coregistration accuracy and the resolution of the phantom images, which was identified as a limiting factor [Fig. 11]. The coregistration accuracy was always better than the spatial resolution of the different imaging modalities, emphasizing the utmost importance of using images with optimal resolution for coregistration purposes. For CT, slice thickness of 2.5 mm was used in this study, but higher resolution images with slice thickness around one mm could be routinely obtained without increasing the scan duration, in particular using the recently designed spiral CT with multiple rows of detectors [Flohr 2002]. For MRI, the spatial resolution was slightly worse in the z direction because of the thickness of the sections, which was a compromise between the overall duration of the examination and the necessity to accumulate enough signal. Taking into account that standard MRI examinations in the head and neck area should at least include pre- and post-contrast T1- weighed and T2-weighed images, the only reasonable way to increase the spatial resolution without increasing the examination duration is to use a head and neck coil. In the experimental setting used in our study, i.e. a flat tabletop and an immobilization mask, regular coils could not be fitted around the head and neck, and no dedicated customized coil was available. For PET, the intrinsic lower spatial resolution (FWHM ≥ 6.0 mm), in particular when post-processing smoothing of the data was applied, needs to be taken into consideration in routine clinical use. It is likely that future tomography integrating smaller and more sensitive crystal detectors (e.g. lutetium oxyorthosilicate-LSO) and optimized reconstruction algorithms will partly solve this limitation [Doshi 2000, Leahy 2000]. Spatial resolution of dedicated PET cameras for brain or small animals is already in the range of one to two mm [Chatziioannou 1999].

Surprisingly, the dependence of the coregistration accuracy on the image resolution was lost with the patient data [Fig. 12]. It is likely that this dependency was hidden by various confounding factors among which the presence of similarities between the two sets of images has been well documented. It was reported that even with low resolution SPECT images, coregistration between two sets of SPECT images was much better than between SPECT and MRI [Habboush 1996].

Similarly, coregistration between PET studies was more accurate when a similar tracer was used (e.g. FDG) than with different tracers (e.g. FDG versus L-DOPA) [Pietzryk 1994]. The image contrast is another confounding factor that cannot be minimized, images with low signal-to-noise ratio (e.g. SPECT)

being much more difficult to accurately coregister than highly contrasted image (e.g. MRI) [Habboush 1996]. Last, the intrinsic amount of information depicted in the image and the setup quality are other factors that could be listed as confounding factors. In our study, the latter can be considered minimal due to the use of an immobilization mask. Despite the presence of these confounding factors, even for patients, the importance of spatial resolution cannot be ignored. Indeed, it has been reported that the coregistration precision with FDG-PET was 10 % lower with eight mm thick slices than with the native four mm thick slices [Uematsu 1998].

Comparison between our data on accuracy and studies previously reported is not easy for several reasons. Almost all studies involved coregistration of brain images using, for the majority of them, MRI as the reference modality [Kapouleas 1991, Turkington 1993, West 1997]. The image resolution was usually expressed in voxel size and not in FWHM. Furthermore, no study specifically looked at coregistration in the head and neck area, which inherently has a much higher probability of imprecision owing to the various anatomical structures involved and the complex movements of the neck. In summary, studies have reported maximum values of translational displacements between 2.8 and 13.0 mm [West 1997]. Interestingly, as described in our study, larger displacements in the z direction have also been observed [Pietzryk 1994, Cai 1999]. Altogether, our data appear to compare well with these previously published studies, maximum displacements in patients reaching absolute values of 4.2, 4.9, 7.1, 7.1, 4.4, 5.4 and 6.1 mm for CT, T1-weighed MRI, T2-weighed MRI, unsmoothed transmission PET, smoothed transmission PET, unsmoothed emission PET and smoothed PET, respectively.

The consistency study, though limited, showed that images with T1- and T2-weighed sequences tended to be coregistered on the same way. The only significant difference which was observed in the y direction could be theoretically explained by the ‘water-to-fat shift’ (WFS) [Hood 1999]. However, WFS is usually observed for much faster sequences (e.g. spin echo) and for larger field of view. These conditions were not encountered in our study, and the WFS is thus unlikely to play a role to explain the difference observed in our study.

The coregistration procedure was also evaluated by its reproducibility, which assessed the importance of the variable ‘observer’ in the overall accuracy [Table 4]. Typically, intra- and interobserver variances were very low and by far below the residual variances, which result from the various confounding factors

discussed above (e.g. image similarity, image contrast). It practically means that even if coregistration procedures were to be performed by several clinicians, who might not be equally talented to visually match the segmented reference CT over MRI or PET, this would not have a strong influence on the total accuracy.

In conclusion, we have reported that, providing an adequate setup is used, accurate coregistration of CT, MRI and FDG-PET images can be obtained in the head and neck area. Coregistration was consistent and highly reproducible among observers.

7. SEGMENTATION OF POSITRON EMISSION TOMOGRAPHY IMAGES

[Published as : Daisne, et al. Radiother Oncol 2003;69:247-250]

7.1. Specific introduction

Determination of a volume from functional imaging is a critical step, which is usually performed by thresholding i.e. by segmenting a lesion of interest on the basis of a given level of radioactivity. Automatic thresholding method has been developed for SPECT studies and further extended and validated for FDG-PET in patients with lung tumors [Erdi 1995, Erdi 1997]. Studies on phantom were conducted to derive the relationship between the true volume and the threshold to be applied on the PET images. Such threshold varied according to the signal-to-background (S/B) ratios, being typically higher for less contrasted images. Such method however suffers from serious shortcomings, at least when functional imaging is to be used for radiotherapy treatment planning purpose. First, such automatic segmentation requires an *a priori* estimate of the volume of the lesion of interest from CT slices or other anatomical images. In absence of an *a priori* knowledge of the volume, it has been shown that a fixed threshold value between 36 % and 44 % of the maximal activity predicts well the true volume, but only for lesions larger than four cc. Second, for lesions smaller than four cc as usually observed in head and neck tumors, or for poorly contrasted lesions (S/B below 5.5), such thresholding method could lead to substantial overestimate of the true volume, even with the knowledge of the *a priori* volume. As the main challenge of introducing functional imaging in radiotherapy treatment planning is to potentially resize the target volume or refine its shape relative to the anatomical information, the use of a CT volume as a gold standard from which a given threshold of activity will be selected, appears as a circular reasoning.

In this section, we describe an automatic segmentation method based on automatic thresholding of isoactivity independent of the *a priori* knowledge of the lesion of interest and valid for small and/or poorly contrasted lesions. This method, which has been developed on a phantom with various size objects (from 0.55 to 17.15 cc) and various radioactivity levels, is based on the relationship between the optimum threshold to fit the volume of a given object and the measured source-to-background ratio. Such relationship has been established for various reconstruction algorithms. From this fit, for a given S/B ratio, the optimum threshold was then used to calculate the volume of the object of interest.

7.2. Specific materials and methods

7.2.1. Phantom object

A cylindrical plexiglas phantom (Canberra-Packard®, Zellik, Belgium) filled with six spheres ranging from 0.55 to 17.15 cc was used. Two 10 min transmission scans were performed using external rotating rods of ^{68}Ge. After each sphere was filled with 74-111 kBq (2-3 µCi) of ^{18}F and the phantom was filled with « cold » water, two 10 min 3D emission scans were performed. The background was then filled with increasing activity of ^{18}F to get source-to-background ratios (S/B) of 8.7, 6.5, 4.7, 3.0, 2.1, and 1.5. These values are within the range observed in head and neck tumors. Emission scans with phantom accurately repositioned on table top were performed for each S/B.

Acquired data were reconstructed using the four previously described algorithms.

7.2.2. Source-to-background ratio and volume delineation

Source-to-background ratios (S/B) were measured from the different combinations between the sphere and the background activities using the sets of images reconstructed with the four different algorithms. Background activity was calculated from the average activity in regions of interest (ROI) of approximately 100 cc delineated in the phantom outside the spheres planes. To avoid the partial volume effect for the sphere having a small volume relative to the scanner resolution, source activity was calculated in the spheres having a volume ≥ 1.0 cc, i.e. with a diameter superior to the largest value of FWHM. Practically, this means that the smallest sphere of 0.55 cc with a diameter of 10.2 mm was excluded from analysis.

From the sets of images reconstructed with the different algorithms, the volume of each sphere was successively calculated using increasing thresholds of radioactivity. The thresholds were determined as a percentage of the maximal activity in the spheres; the maximal activity was defined as the average activity of the nine voxels surrounding the hottest voxel. The best threshold was selected when the least square difference between the true volume and the calculated volume was reached.

7.2.3. Statistical analysis

Statistical analyzes were performed using SPSS® (version 9.0). Regression analyzes were used to evaluate difference between calculated and true volumes of the spheres. Alpha level of significance was 0.05.

7.3. Results

The relationship between the best threshold of activity to accurately measure the true volume of the spheres and the measured S/B ratio were determined for the four reconstruction algorithms [Fig. 13]. As explained in the Materials and Methods section, the smallest sphere of 0.55 cc (10.2 mm of diameter) was excluded from the plots to avoid any partial effect in the object reconstruction. The plots were fitted using an inverse function (y = a + b*1/x) because providing the best regression parameters. These relationships indicated that for less contrasted objects (low S/B ratio), a higher threshold of activity had to be applied to adequately measure the actual volume of the spheres. Also, for a given S/B ratio, the threshold to be applied depended on the reconstruction algorithm, i.e. being slightly lower for high resolution reconstruction (e.g. FBP and OSEM) compared to low resolution reconstruction (e.g. OSEM8). For example, for a S/B value of three, the thresholds to be applied reached 51.4, 48.4, 53.2 and 54.8 % for FBP, OSEM, OSEM6 and OSEM8, respectively.

To verify the validity of the above established relationships, the volumes of the spheres were calculated by applying the threshold of activity determined as a function of the measured S/B ratio [Fig. 14]. Typically, for all reconstruction algorithms, the volume of the largest spheres was slightly underestimated whereas the smallest spheres were overestimated. These effects were more pronounced for OSEM8, although the difference between the different reconstruction algorithms was not significant ($P = 0.8$). For OSEM8, the 17.15 cc sphere was underestimated by 13 % whereas the 1 cc sphere was overestimated by 67 %. Corresponding values for FBP reached 7 % and 14 %, respectively.

7.4. Discussion

In the present study, we have developed a method to calculate spherical volumes from FDG-PET images based on the actual measurement of the S/B ratio [Fig. 13]. This method which has been validated for volumes in the range of one to 17 cc is independent of the *a priori* knowledge of the volume of interest.

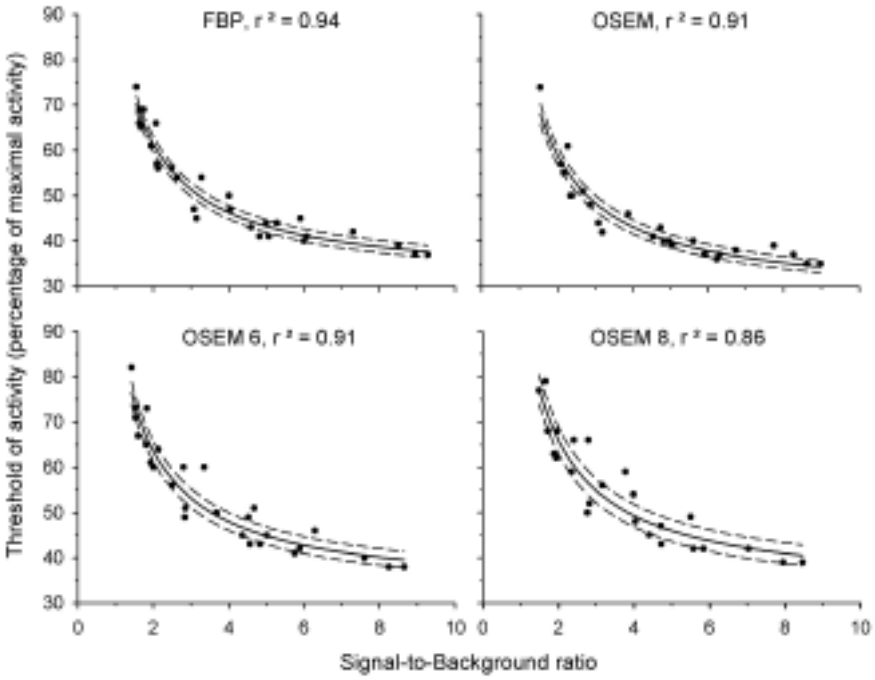

Figure 13 : Relationship between the signal-to-background ratio and the threshold to be applied to fit spheres of various volumes between 1.02 and 17.15 cc. Four different reconstruction algorithms have been used, Filtered Back Projection (FBP), Fourier rebinning combined with an Ordered Subsets Expectation-Maximization without post-smoothing (OSEM) or with Gaussian post-smoothing of 6 mm (OSEM6) or 8 mm (OSEM8). The data have been fitted through an inverse function. Ninety-five percent prediction intervals on the fit are drawn in dotted lines.

Our results also showed that the threshold to be applied to get the most accurate size measurement varied with the reconstruction algorithm, being typically lower for FPB and OSEM without Gaussian smoothing than for OSEM with Gaussian smoothing. Moreover, there was a trend for an underestimate of the size of the large spheres using lower resolution reconstruction algorithms (OSEM6 and OSEM8), compared to FBP and OSEM [Fig. 14].

The use of functional imaging for radiotherapy treatment planning requires a 3-D assessment of the volumes of interest independently of any other imaging modalities. The key feature of the method described in this study was that the volumetric assessment did not require any *a priori* knowledge of the volume of the object of interest, as opposed to previous works in the field [Erdi 1997]. Our method only required the measurement of the source-to-background ratio. This is an advantage not only because volumetric assessment can be performed in absence of anatomical information of the object of interest, but also because it does not link the two imaging modalities, thus permitting to reveal potential

intrinsic differences between functional and anatomic evaluations of the same object.

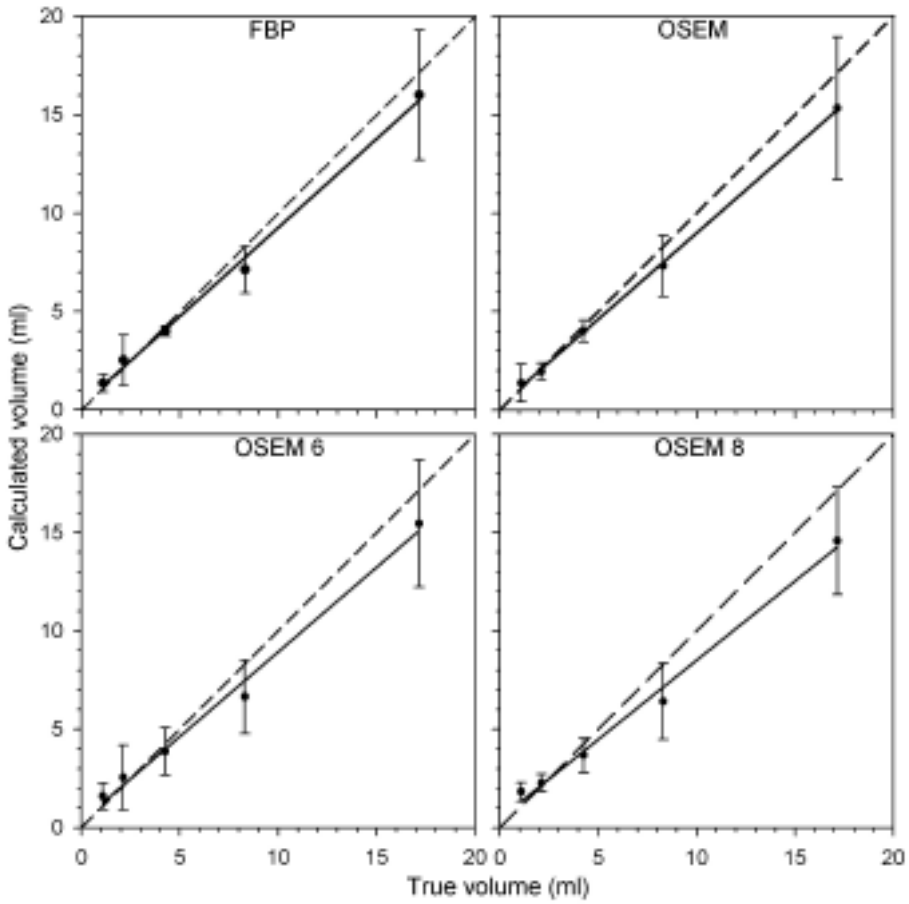

Figure 14 : Relationship between the true volume and the calculated volume of spheres. The volumes of the spheres were calculated by applying a threshold of activity as a function of the measured signal-to-background ratios (see Fig. 13). Four different reconstruction algorithms have been used, Filtered Back Projection (FBP), Fourier rebinning combined with an Ordered Subsets Expectation-Maximization without post-smoothing (OSEM) or with Gaussian post-smoothing of 6 mm (OSEM6) or 8 mm (OSEM8). Data points are average ± 2 SD. The data have been fitted through a linear regression. The dotted lines represent the perfect correlation between the true and the calculated volumes.

In the present study, adequate estimate of the volume was observed for spheres between 2.12 and 17.15 cc [Fig. 14]. There was a trend for a more accurate estimate within the whole range of spheres sizes using images reconstructed with FBP and OSEM without smoothing, which resulted in images with a better spatial resolution than the smoothed iterative reconstruction algorithms OSEM6 or OSEM8. This was particularly striking for volumes smaller than two cc, where an overestimate up to 67 % was observed with OSEM8.

However, such an apparent large overestimate in volume only represented an overestimate in diameter of 0.3 mm. Overall, using the method described in the present study, adequate estimate was observed for objects having at least a diameter between once and twice the FWHM. For objects smaller than the FWHM, as the determination of the volume is likely to be influenced by the partial volume effect, the method reported in the present study does not hold anymore [Aston 2002]. As discussed in section 6.4., the use of future PET camera integrating more sensitive crystal detectors (e.g. lutetium oxyorthosilicate –LSO) and optimized reconstruction algorithms will improve the spatial resolution and thus will enable more accurate assessment of smaller objects.

One limitation of our phantom study is that it did not address the issue of objects with complex shape usually observed in clinical situations. As a matter of fact, this study was only designed to look at the relationship between the S/B ratio and the best threshold of radioactivity to apply for an accurate estimation of tumor volumes, so as to derive mathematical plots that could be used for *in vivo* imaging. The next step was to validate this concept in patients with head and neck tumors, using the surgical specimen as the gold standard, which will be developed in the next section.

8. COMPARISON BETWEEN COMPUTER ASSISTED TOMOGRAPHY, MAGNETIC RESONANCE IMAGING AND ^{18}FLUORO-DEOXY-GLUCOSE POSITRON EMISSION TOMOGRAPHY FOR TARGET VOLUME DELINEATION

[Published as : Daisne, et al. Radiology 2004;233:93-100]

8.1. Specific introduction

The purpose of this section is to compare CT, MRI, and FDG-PET for the delineation of the tumor volume in pharyngolaryngeal squamous cell carcinoma, and to validate these imaging modalities with, whenever available, the macroscopic surgical specimen.

8.2. Specific materials and methods

8.2.1. Patient population and imaging

The 29 patients previously described (§ 5.1) were all included in this prospective analysis. Image acquisition (CT, MRI and FDG-PET reconstructed with FBP algorithm) and their coregistration were performed as previously described.

8.2.2. Processing of the surgical specimen

For patients undergoing total laryngectomy, a procedure was developed allowing a three-dimensional coregistration of the macroscopic specimen with presurgical imaging modalities. Briefly, the fresh surgical specimen was collected « en bloc » in the operating room, and placed in a polystyrene cast containing three longitudinal wood rods (diameter of three mm) equally spaced in the axial plane of the specimen. The cast was filled with a 16 % gelatine solution (UCB®, Belgium), and put at -20 °C for 48 hours, thereafter to -80 °C for at least 72 hours. Using pig jaws, we observed that in comparison with other fixation procedures (e.g. formalin), the freezing method induced very little or no tissue retraction. In our patient material, the lack of tissue retraction was assessed in five patients on the volume of the thyroid gland and on the distance between the posterior edges of the thyroid cartilage. The comparison was performed with the CT images. The frozen specimen containing cast was then cut in the axial plane with a carpenter band saw (Elu®, Germany) to generate parallel and contiguous slices. It was shown during the validation of the procedure on wood

blocks and animal specimens that the material lost due to the thickness of the saw was similar to the slice thickness. Consequently, for each laryngeal specimen, the slice thickness was calculated by dividing the length of the cast by twice the number of obtained axial slices. Typically, slice thickness ranged from 1.7 to 2.0 mm. Each slice was digitized on both faces using a Snapscan 1236s flat-bed scanner (Agfa®, Germany) and saved in a TIFF format with a resolution of 150x150 dpi. Digitized slices were aligned using the wood rods as fiducial markers with the Zeiss® KS 400 software (courtesy of Pathology Dept.). The volume of the surgical specimen was finally reconstructed using home made software by interpolating the slices to their thickness, and saved in the Interfile format. This file format was chosen because being supported by our coregistration software. This allowed us to coregister the macroscopic volume to conventional imaging modalities [Fig. 15].

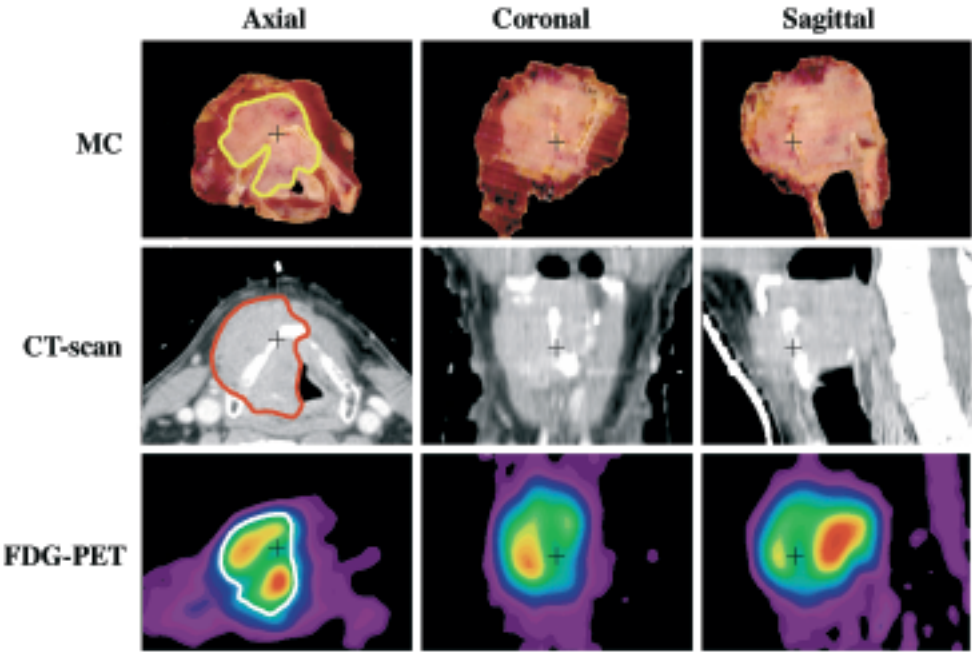

Figure 15 : Illustration of a coregistration between the macroscopic specimen (MC), the CT and the FDG-PET images. Volumes are displayed on axial, coronal and sagittal planes. The small cross represents a same point in space in each of the modalities. Infiltration of the parathyroid muscles on the left side is clearly visualized on the macroscopic slices.

8.2.3. Tumor volume delineation

The gross tumor volumes (GTV) were retrospectively delineated blindly on axial slices by the same operator successively on the different modalities using the so-called VolQuant home-made software (PET Lab, Louvain-la-Neuve, Belgium). To avoid possible biases, at least two weeks separated the delineation of each volume for a particular patient. Image based GTVs were always compared with the clinical information from palpation and/or endoscopic evaluation.

CT volumes were delineated from fixed display windowing images (center = 0 HU), width = 300 HU). Consistent criteria for soft tissue infiltration (i.e. contrast enhancement, left-right asymmetry, fatty space infiltration), and for cartilage and/or bone infiltration (i.e. cortex erosion or frank lysis, increased density, and soft tissue infiltration on both sides of a bone/cartilage) were used [Becker 1995].

MRI volumes were initially delineated on the T2-weighted images, but with comparison to the pre- and postcontrast T1-weighted images when necessary. Criteria for malignancy on the T2-weighted images were : unilateral change in anatomy when compared to the normal contralateral side, mass effect, nodular or infiltrative abnormal tissue, fat replacement, and usually hyposignal intensity. Rare necrotic areas had high signal intensity. Neoplastic areas displayed low signal intensity on the T1-weighted contrasting with the fatty surrounding tissue, and moderate enhancement contrasting with intense enhancement of inflammatory margins. Blurring movement artifacts of the base of the tongue and larynx were corrected for air cavities using the CT images as template. All contours were reviewed blindly by a trained (13 years of experience in H&N radiology) Head & Neck radiologist to check the consistency of the delineation with the criteria defined above.

PET volumes were automatically delineated using a segmentation algorithm based on the measured signal-to-noise ratio as previously described. Due to the longer range of the positron in air cavities, a slight overestimate of the PET volume could occur at the interface with air. Consequently, correction for air cavities was also applied on the PET images using the CT images as template.
MC volumes were delineated from visualization of gross tumor infiltration with the help of an experienced (five years of experience in HN pathology) Head and Neck pathologist. The delineation was performed without any knowledge of the imaging data. On macroscopic tumor section, the main criteria for delineation was the « fish meat » color of the structure.

8.2.4. Statistical analysis

The GTVs obtained from CT, MRI, PET and MC images were analyzed pairwise quantitatively and qualitatively. For the imaging modalities, the whole series of 29 patients were analyzed. For the comparison with the surgical specimens, nine patients were analyzed. Due to possible site-dependent differences among the various imaging modalities (e.g. more susceptibility of MRI to movement artifacts in laryngeal tumors), a distinction was made between oropharyngeal tumors on the one hand and hypopharyngolaryngeal tumors on the other hand. Quantitative analysis included calculation of the absolute volume and relative estimate of the volume matching using Boolean analysis. For example, the mismatch between CT and MRI (mismatch CT/MRI) was defined as the volume defined only by CT expressed as a percentage of the total volume assessed by MRI [Fig. 16]. The effect of the imaging modality on tumor volume assessment was estimated using linear mixed-effect models. Multiple comparisons were performed to determine the significance of different imaging modality pairs. Adjustments for multiple comparisons were made with the Bonferroni method or with the Sidak method when the gold standard MC was

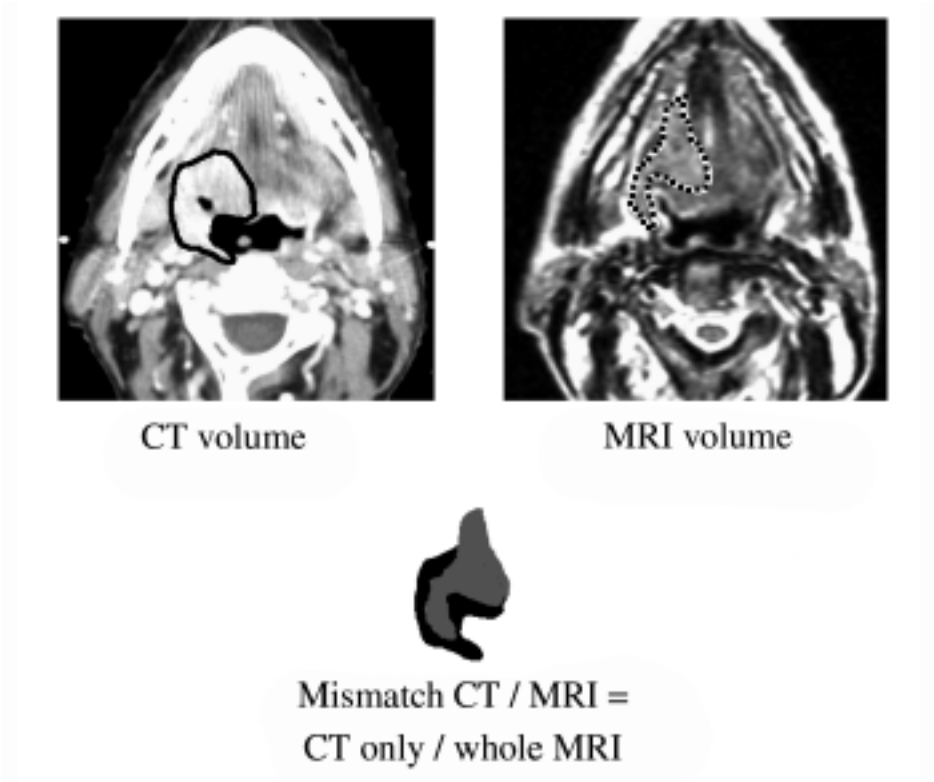

Figure 16 : Illustration of a Boolean analysis. The mismatch of CT over MRI is calculated by dividing the volume visualized only with CT by the whole volume delineated with MRI. The results express the fraction of the MRI volume which would be additionally delineated by the use of CT.

available. All the statistical calculations were performed with SPSS 12.0. Alpha level of significance was set at 0.05. Qualitative analysis of GTV was also performed on all imaging modalities and on the MC to try to understand the reasons of the discrepancies (under- and/or overestimate of the target volumes) between the images. This analysis was essentially based on assessment of anatomic variation between modalities. For PET images, since no anatomic information was available, interpretation was performed after fusion between the functional images and either CT, MRI or MC. In the five patients for whom measurements of thyroid volumes and mean distance between posterior edges of thyroid cartilage were available on CT and MC images, statistical comparisons were performed with a Wilcoxon rank test (SPSS 9.0) using an alpha level of significance of 0.05.

8.3. Results

8.3.1. Oropharyngeal tumors

The imaging modality factor was found to be significant for the GTV measurement ($F = 5.98$, $P = 0.02$). No significant difference ($P = 1.0$) was observed between the average of the GTVs delineated with CT (32.0 cc) or MRI (27.9 cc) [Table 6]. In contrast, the average of the GTVs delineated from FDG-PET images (20.3 cc) was smaller than GTVs delineated with CT ($P = 0.02$) or MRI ($P = 0.10$). Although smaller, the GTVs contoured with PET were not totally

Table 6 : Gross Tumor Volumes in patients with oropharyngeal tumors (+ one synchrone oral tumor).

Patient #	Tumor site[1]	T stage	Gross Tumor Volume (cc)		
			CT	MRI	FDG-PET
1	BoT	T3	34.6	29.9	22.1
2	TF	T4	14.2	16.9	13.1
3	TF	T2	21.9	19.8	13.3
4	GTS	T2	7.7	5.5	8.1
5	BoT	T2	10.4	11.2	9.7
	MT	T2	8.8	6.4	9.1
6	PPW	T4	52.0	65.4	28.5
7	PPW	T0	137.7	92.8	88.96
8	BoT	T2	5.1	0.0	5.1
9	BoT	T2	41.4	34.4	17.9
10	TF	T3	18.0	24.0	7.8
Mean			32.0	27.9	20.3*

[1] BoT: base of tongue; TF: tonsillar fossa; GTS: glossotonsillar sulcus; MT: mobile tongue; PPW: posterior pharyngeal wall;
* $P \leq 0.10$

encompassed by the GTVs delineated from the two other modalities [Table 7]. On average, a volume corresponding to 14 % of the GTVs contoured from CT images was only delineated by FDG-PET (mismatch PET/CT). Also, on average, a volume corresponding to 20 % of the GTVs contoured from MRI images was only delineated by FDG-PET (mismatch PET/MRI). On the contrary, GTVs contoured from CT or MRI exceeded the GTVs delineated from FDG-PET by a large extent. Using CT images, on average, an additional volume corresponding to 73 % of the GTVs contoured from FDG-PET images was delineated (mismatch CT/FDG-PET). Using MRI images, on average, an additional volume corresponding to 64 % of the GTVs contoured from FDG-PET images was delineated (mismatch MRI/FDG-PET). Last, the comparison between CT and MRI indicated that although quantitatively very similar, these volumes did not totally overlap with mismatches of 28 % and 42 %.

Table 7 : Average mismatch of oropharyngeal Gross Tumor Volumes for various imaging modalities (10 patients).

	Imaging modality		
	CT	MRI	FDG-PET
CT / x	-	42%	73%
MRI / x	28%	-	64%
FDG-PET / x	14%	20%	-

From a descriptive point of view, areas only visualized by CT concerned enhanced peritumoral soft tissues for which distinction between tumor infiltration, inflammation or fibrosis was difficult. MRI showed exquisite sensitivity to assess possible infiltration of muscles and parapharyngeal space. MRI was also very helpful in those patients with teeth filling artifacts on CT scan slices.

8.3.2. Laryngeal and hypopharyngeal tumors

In the 19 patients with laryngeal or hypopharyngeal tumors, results similar to those observed with oropharyngeal tumors were found. The imaging modality factor was also found to be significant for the GTV measurement ($F = 11.33$, $P = 0.003$). Although patients with similar tumor stage were included, overall, smaller GTVs were delineated compared to oropharyngeal tumors [Table 8]. No significant difference ($P = 1.0$) was observed between the average of the GTVs delineated with CT (21.4. cc) or MRI (21.4 cc) [Table 8]. In contrast, the average of the GTVs delineated from FDG-PET images (13.4 cc) was significantly smaller than GTVs delineated with CT ($P < 0.01$) or MRI ($P < 0.01$).

Table 8 : Gross Tumor Volumes in patients with laryngeal or hypopharyngeal tumors

Patient #	Tumor site[1]	T stage	Gross Tumor Volume (cc)			
			CT	MRI	FDG-PET	MC
1	PS	T4	47.7	36.3	19.3	-
2	GL	T3	18.0	9.9	6.0	-
3	GL	T3	41.1	30.2	9.2	-
4	RC	T3	7.1	10.6	7.3	-
5	PS	T2	4.1	9.1	2.3	-
6	SGL	T2	3.7	1.4	1.2	-
7	SubGL	T3	5.8	7.0	3.2	-
8	PS	T3	17.3	17.6	12.6	-
9	PS	T4	13.1	30.7	11.4	-
10	PS	T4	55.6	53.4	34.2	-
11	SubGL	T2	1.9	2.4	3.4	2.2
12	GL	T4	6.2	9.8	8.5	5.1
13	LAR	T4	41.0	58.4	30.2	30.9
14	LAR	T4	11.1	6.6	8.0	4.1
15	LAR	T4	14.6	22.0	10.2	5.6
16	LAR	T4	18.4	22.0	11.4	8.6
17	LAR	T4	28.1	32.3	26.6	17.3
18	LAR	T4	25.0	23.5	20.0	15.4
19	LAR	T4	40.4	37.3	28.7	24.3
Mean[2]			21.4	21.4	13.4*	-
Mean[3]			20.8	23.8	16.3*	12.6*

[1] PS: piriform sinus; RC: retrocricoid area; SGL: supraglottic larynx; GL: glottic larynx; Sub GL: subglottic larynx; LAR: larynx without other specification.
[2] including all 19 tumors
[3] including only patients where the surgical specimen was obtained
* $P \leq 0.05$

As for oropharyngeal tumors, the PET GTVs were not totally encompassed by GTVs delineated from CT or MRI [Table 9]. On average, a volume corresponding to 13 % of the GTVs contoured from CT or MRI images was only delineated by FDG-PET (mismatch FDG-PET/CT and FDG-PET/MRI). On the contrary, GTVs contoured from CT or MRI exceeded the GTVs delineated from FDG-PET by a large extent. Using CT or MRI images, on average, an additional volume corresponding to 80 % of the GTVs contoured from FDG-PET images was delineated (mismatch CT/FDG-PET and MRI/FDG-PET). Last, the comparison between CT and MRI indicated that although quantitatively very similar, these volumes did not totally overlap with mismatches of 37 %.

Table 9 : Average mismatch of laryngeal or hypopharyngeal Gross Tumor Volumes for various imaging modalities (19 patients)

	Imaging modality		
	CT	MRI	FDG-PET
CT / x	-	37%	80%
MRI / x	37%	-	80%
FDG-PET / x	13%	13%	-

From a descriptive point of view, CT depicted tumor extension at the level of the lateral and posterior pharyngeal wall that was not observed with MRI. On the contrary, MRI exhibited exquisite sensitivity to detect possible cartilage infiltration, and contralateral side or extralaryngeal extension.

8.3.3. Validation with the macroscopic specimen

Regarding volumes of the thyroid lobes, no significant difference ($P = 0.06$) was observed between thyroid volumes delineated from the CT (mean [range] of 14.4 cc [5.5-25.9]) and the MC (mean [range] of 16.1 cc [6.9-29.6]). In the same patients, no significant difference ($P = 0.9$) was observed in the mean distance between the posterior edges of the thyroid cartilage between the CT (mean [range] of 42.6 mm [36.7-55.5]) and the MC (mean [range] of 42.7 mm [38.5-54.3]).

In the group of nine patients who underwent a total laryngectomy, the average of the GTVs delineated from the surgical specimen reached a volume of 12.6 cc [table 8]. This volume was smaller than the average of the GTVs contoured from FDG-PET (16.3 cc; $P = 0.06$), from CT (20.8 cc; $P = 0.003$) or from MRI (23.8 cc; $P = 0.001$). Although much smaller, the GTVs delineated from the

MC were not totally encompassed by the imaging modalities, even by CT and MRI [Table 10]. On average, 10 %, 9 % and 13 % of the GTVs contoured from CT, MRI and FDG-PET images, respectively, were only delineated from the macroscopic surgical specimen. Thorough examination of the delineated GTVs indicated that all three imaging modalities underevaluated superficial tumor extension in the mucosa of the contralateral larynx or the subglottis, as well as extralaryngeal extension. The lack of specificity of the imaging modalities illustrated by the mismatch between CT, MRI, PET and MC, mainly concerned overestimate of cartilage, extralaryngeal, preepiglottic space and thyroid gland infiltration.

Table 10 : Average mismatch of laryngeal Gross Tumor Volumes for various imaging modalities and the surgical specimen (9 patients)

	Imaging modality			
	CT	MRI	FDG-PET	MC
CT / x	-	26%	48%	81%
MRI / x	45%	-	67%	107%
PET /x	17%	15%	-	46%
MC / x	10%	9%	13%	-

8.4. Discussion

The present study showed that GTVs in the pharyngolaryngeal area were differently contoured by CT, MRI and FDG-PET images. Consistently, in both groups of tumors, no significant difference was observed between GTVs delineated from CT and MRI, whereas, GTVs assessed from FDG-PET were smaller with difference close to 40 %. Of interest, none of these GTVs totally overlapped with each other, even when FDG-PET was used. Up to 20 % of the GTV assessed from anatomic imaging was only observed with FDG-PET. The key finding of our study was that in comparison with the surgical specimen taken as the reference, all the imaging modalities tended to overestimate the tumor extension. For anatomic imaging, average GTVs were up to 107 % larger, whereas for functional imaging, still a 50 % overestimate was observed. Despite this finding, all three imaging modalities failed to visualize a small fraction of the macroscopic tumor extension, thereby revealing their insufficient spatial resolution.

The validity of the analysis relies to a large extent on the accuracy of the overall methodology used to compare the various imaging modalities. In particular it relies on the 3D reconstruction of the surgical specimen generating the reference GTV, and on the precision of the image coregistration, which directly impacts on the assessment of the matching between the various modalities. Regarding the reconstruction of the surgical specimen, the present study has shown that macroscopic tissue distortion associated with the procedure was negligible, at least for the two landmarks that were analyzed. Regarding the coregistration, analysis performed on the same set of patients have documented that the mean precision as assessed from the Euclidean vectors was in the order of 1.1 to 2.4 mm. More specifically, coregistration of transmission PET and T2-weighed MRI images with CT images was performed on average within 1.4 and 2.0 mm, respectively. The method used in this study was thus robust and differences in GTVs could not be attributable to procedural inaccuracy or weakness.

A major finding of our study, which could have tremendous impact for the radiotherapy treatment planning of patients with HNSCC, is that the GTVs delineated from FDG-PET were by far the closest to the reference volume assessed from the surgical specimens. Also, one has found in our series of patients that FDG-PET scan by itself was more specific than CT or MRI. This is in contradiction with a previous study, which concluded that FDG-PET scan could improve the staging accuracy of oral cavity, oropharyngeal and laryngeal squamous cell carcinomas, but when used in addition to CT or MRI [Wong 1996]. In this study of Wong et al., the accuracy of the various imaging modalities was assessed by visual comparison of few landmarks individualized on the surgical specimen without any use of 3D registration or systematic procedure for PET image analysis. Another important characteristic of our study was that the PET derived volumes were automatically delineated, which substantially reduced the duration of the contouring procedure in comparison with the use of CT or MRI, and annihilated any inter- or intraobserver variability.

Although closer, the volumes delineated from FDG-PET were still larger than those delineated from the surgical specimens. This finding may result from the method used for the automatic delineation and/or from the spatial resolution of the PET. The automatic delineation procedure was validated in spheres, i.e. symmetrical volumes with homogeneous activity and sharp demarcation from the background noise. Tumors are more complex in shape with convex and concave contours, and may display heterogeneous distribution of radioactivity.

Automated delineation processing may have missed such subtle discontinuities in tumor volume. More discriminative analysis such as clustering based segmentation may be required for a better separation between the background noise and the true signal radioactivity [Anzai 1999]. Reanalysis of our data using such method is in progress. Moreover, FDG-PET suffers limited spatial resolution with large voxels (FWHM of 7.7 x 6.9 x 7.9 mm^3) averaging regions of discontinuation in the radioactivity. This limitation may explain the lack of sensitivity of FDG-PET for assessing the superficial mucosal tumor extension. It may also explain the lack of specificity resulting in a slight overestimate of the tumor volume. We want to stress again that the use of the next generation PET camera integrating more sensitive crystal detectors (e.g. lutetium oxyorthosilicate –LSO) together with optimized reconstruction algorithms will likely increase the spatial resolution of the technique resulting in more accurate assessment of smaller objects of more complex shape [Doshi 2000, Leahy 2000]. Small Field of View PET cameras dedicated to brain or small animal examination have a spatial resolution in the range of one to two mm [Chatziioannou 1999]. Conversely, PET examination using positron emitters with higher energies than ^{18}F (e.g. ^{15}O or ^{82}Rb) will do worse since higher energy results in decreased spatial resolution.

In our study, CT and MRI had unexpected low specificity with a subsequent large overestimate of the GTVs. In addition, in the subset of patients for whom surgical specimen was available they both missed a significant percentage of the tumor volume below the detection thresholds. For CT, specificity of 95 %, and 85-95 % has been reported for oropharyngeal, and laryngeal and hypopharyngeal tumors, respectively [Grandjean 1993, Becker 1995, Kazkayasi 1995, Zbären 1996, Jones 1997, Crecco 1999, Bomanji 2000, Lenz 2000]. For MRI, specificity ranging between 75 % for bone invasion to 90-95 % for muscle invasion has been reported; for laryngeal and hypopharyngeal tumors, average figures of 75-85 % have been reported [Grandjean 1993, Becker 1995, Kazkayasi 1995, Zbären 1996, Lenz 2000]. In these later locations, nonspecific nonmalignant changes in signal intensity of the cartilage account for specificity values as low as 55 % [Becker 1995, Zbären 1996, Lenz 2000]. In our series too, examination of the surgical specimen often failed to confirm the infiltration of the thyroid cartilage, which was suspected on MRI images.

Potential limitations in our study however need to be addressed. Analysis of MRI images was performed on optimized images acquired using the body coil. The need for a similar repositioning in the three modalities required the use

of an immobilization device, which precluded the use of dedicated head and neck coils. Sufficient signal-to-noise ratio of the images was however maintained by adequate changes in the pulse sequence data combining the technical constraints and the need to keep the acquisition times as short as possible. Moreover, the MRI studies were performed on a clinical 1.5 Tesla imager, ensuring the feasibility of the procedure in standard conditions. Continuing technical improvements in MRI technology led to higher image quality (higher signal-to-noise ratio, better spatial resolution through lowering the slice thickness and increasing image matrices,...). However, the relationship between the increase in image quality after a minimal threshold has been reached and the increase in diagnostic relevance still needs evaluation. Overall diagnostic accuracy is affected by improvement in image quality, but whether such improvement will impact on the sensitivity and/or the specificity of MRI is still unknown. With the setting used in our study, one option to bypass the limitation caused by the mask would be to use a tailored surface coil positioned on the mask close to the area of interest. Such option however would only allow the imaging of a smaller volume. Another option is to abandon the mask for MRI image acquisition. But this option would require the use of different coregistration algorithms allowing image deformation. Such algorithms are still under development.

Other potential limitations in our study need to be kept in mind. With one exception (T2 subglottic tumor) only patients with extended T4 tumors could be recruited for comparing the imaging modalities with the surgical specimens. Whether conclusions drawn from these large tumors would still hold for smaller tumors is questionable. No data suggest that the sensitivity or the specificity of CT and MRI are different for smaller tumors, with the exception of those smaller than the spatial resolution of the cameras. And undetectable macroscopic extensions may also exist at the margins of large T4 tumors. For FDG-PET, this limitation is more critical since small volumes can be underestimated due to the partial volume effect, though this effect is considered negligible for volumes larger than twice the FWHM, i.e. a sphere diameter larger than 15 mm for the currently available cameras [Miller 1990]. But from a clinical point of view, one has to admit that the relative contribution of imaging modalities for small tumors (e.g. T1 tumors) is less critical in comparison with the clinical examination.

Another potential limitation of our study is that the comparative analysis with the surgical specimen could only be performed in laryngeal carcinomas as a result

of methodological difficulties related to image coregistration. The validity of the conclusions drawn from this site to others may be uncertain but our study highlighted intrinsic factors for discrepancies between modalities, mainly the lack of specificity of muscle, cartilage or bone infiltration. It is likely that these factors are similar in head and neck sites other than the larynx, which reinforce the extrapolation of our conclusions from laryngeal tumors to those in other sites.

A major finding of our study was that compared to surgical specimen all three imaging modalities suffered insufficient spatial resolution to detect superficial tumor extension. It is likely that no imaging modality could ever reach the ultimate goal of detecting microscopic extension. The need for adding a security margin to the GTV, which covers the predictable microscopic extension of the tumor seems thereby warranted, resulting in the Clinical Target Volume or CTV. The impact of the use of various imaging modalities on delineation of the CTV is thus a key issue that still needs to be addressed in our series. As a last endpoint, the impact of the use of the various imaging modalities on the dose distribution after 3D-CRT or IMRT planning also needs to be addressed. These two issues will be developed in the next sections.

In conclusion, the present study has demonstrated a potential role of FDG-PET imaging for the delineation of the GTV in HNSCC, providing a proper methodology is used.

9. COMPARISON BETWEEN ^{18}FLUORO-DEOXY-GLUCOSE- AND METHIONINE-POSITRON EMISSION TOMOGRAPHY FOR TARGET VOLUME DELINEATION

[Published as : Geets, et al. Radioter Oncol 2004;71:267-273]

9.1. Specific introduction

Besides FDG-PET, MET-PET has also been used for characterization of HNSCC. The uptake of MET has been shown to reflect amino acid increased transport, transmethylation rate and protein synthesis within malignant tissues [Weber Wolfgang 1999]. Sensitivity and specificity of MET-PET for HNSCC staging are similar to FDG [Leskinen-Kallio 1994]. A relationship between MET uptake and cell proliferation of HNSCC has been shown *in vitro* and *in vivo* [Miyazawa 1993, Minn 1995, Nuutinen 1998], suggesting that MET could be more specific than FDG for measuring tumor aggressiveness. In addition, the early response to chemotherapy could be successfully assessed by MET in hypopharyngeal tumors, allowing for adapting the treatment scheme [Chesnay 2003]. It progressively appears that metabolic imaging with MET-PET and FDG could allow for targeting the tumor tissue with the highest metabolic activity, i.e. the viable part of the tumor deserving maximal treatment. However, the head and neck region is a complex region and PET imaging suffers from the lack of anatomical landmarks. Moreover, physiological FDG and MET uptake by the normal structures such as salivary glands, or by non tumor tissues such as acute inflammation (especially during radiotherapy), can hamper the accuracy of tumor volume delineation. Therefore, metabolic imaging must be carefully assessed before it is routinely introduced as a new GTV determination tool.

In this study, we evaluated MET-PET as an imaging method for GTV delineation of HNSCC, and compared it to FDG-PET and CT.

9.2. Specific materials and methods

CT, FDG- and MET-PET data available for the 23 patients who underwent complete imaging examination were used. Imaging protocols, coregistration method, volume delineation and results analysis methodology were identical to what is described in section 8.

Statistical analyses were performed with SPSS 12.0. The effect of the imaging modality on tumor volume assessment was estimated using linear mixed-effect models. Multiple comparisons were performed to determine the significance of different imaging modality pairs. Adjustments for multiple comparisons were made with the Bonferroni method. Alpha level of significance was set at 0.05.

9.3. Results

9.3.1. Oropharyngeal tumors

The mean CT volume was similar to the mean MET-PET volume, but both were larger than the mean FDG-PET volume. The difference between CT and FDG-PET was statistically significant (P = 0.02). Mean MET-PET volume was larger than mean FDG-PET volume, and this was statistically significant (P = 0.05). Detailed data are shown in Table 11. The volume mismatch of CT over MET-PET and FDG-PET reached on average 44 % and 63 %, respectively. The MET-PET/FDG-PET mismatch was on average 43 %. However, the FDG volume was not totally covered by the MET-PET volume, since we noted a FDG-PET/MET-PET mismatch of 14 % [Table 12].

Table 11 : Gross Tumor Volumes in patients with oropharyngeal tumors (+ one synchrone oral tumor).

Patient #	Tumor site[1]	T stage	Gross Tumor Volume (cc)		
			CT	FDG-PET	MET-PET
1	BoT	T3	34.6	22.1	27.7
2	TF	T4	14.2	13.1	13.9
3	TF	T2	21.9	13.3	26.4
4	GTS	T2	7.7	8.1	8.8
5	BoT	T2	10.4	9.7	14.1
	MT	T2	8.8	9.1	7.2
6	PPW	T4	52.0	28.5	29.7
7	PPW	T0	137.7	88.96	81.7
8	BoT	T2	5.1	5.1	13.5
9	BoT	T2	41.4	17.9	26.7
10	TF	T3	18.0	7.8	18.1
Mean			32.0	20.3*	24.4

[1] BoT: base of tongue; TF: tonsillar fossa; GTS: glossotonsillar sulcus; MT: mobile tongue; PPW: posterior pharyngeal wall;
* $P \leq 0.05$

From a qualitative point of view, the lateral and posterior walls were frequently included within the tumor volume on CT, although there was no evidence of tumor like metabolic activity on PET images. Compared to FDG-PET, MET-PET images were less contrasted especially at the vicinity of the tumor. The uptake of salivary glands, particularly submandibular glands, was very high, similar to the tumor uptake. Therefore, it was often difficult (i.e. in 5 patients out of 10) to differentiate the tumor from the submandibular gland on MET-PET images, particularly when the tumor was located at the base of the tongue. Even after manual removal of the salivary glands from the MET-PET volumes (when no evidence of invasion was noted on CT images), these remained larger than the FDG-PET volumes.

Table 12 : Average mismatch of oropharyngeal Gross Tumor Volumes for various imaging modalities (10 patients).

	Imaging modality		
	CT	FDG-PET	MET-PET
CT / x	-	73%	44%
FDG-PET / x	14%	-	14%
MET-PET / x	21%	43%	-

9.3.2. Laryngeal and hypopharyngeal tumors

As for oropharyngeal tumor volumes, the difference between CT and FDG-PET volumes was statistically significant ($P \leq 0.01$). In addition, the difference between the MET-PET and the FDG-PET volumes was also statistically significant ($P \leq 0.01$) [Table 13]. Except for patient # 19, all the CT volumes were bigger than FDG-PET volumes, while the MET-PET volumes were systematically bigger than FDG-PET volumes. There was a large discrepancy between CT volumes and both FDG- and MET-PET volumes, as expressed by mismatches of 80 and 46 %, respectively. The mismatch between MET- and FDG-PET volumes showed the same relation as for oropharyngeal tumors. The mismatch MET-PET/FDG-PET was 64 % and the FDG-PET/MET-PET mismatch was 9 % [Table 14]. It is also noteworthy that the discrepancies between CT and FDG- or MET-PET are higher for laryngeal/hypopharyngeal tumors than for oropharyngeal tumors.

From a qualitative point of view, we mainly noticed a very high MET uptake in laryngeal and pharyngeal mucosa.

Table 13 : Gross Tumor Volumes in patients with laryngeal or hypopharyngeal tumors

Patient #	Tumor site[1]	T stage	Gross Tumor Volume (cc)		
			CT	FDG-PET	MET-PET
1	PS	T4	47.7	19.3	-
2	GL	T3	18.0	6.0	11.9
3	GL	T3	41.1	9.2	14.2
4	RC	T3	7.1	7.3	12.1
5	PS	T2	4.1	2.3	8.7
6	SGL	T2	3.7	1.2	4.8
7	SubGL	T3	5.8	3.2	4.2
8	PS	T3	17.3	12.6	-
9	PS	T4	13.1	11.4	27.9
10	PS	T4	55.6	34.2	46
11	SubGL	T2	1.9	3.4	-
12	GL	T4	6.2	8.5	-
13	LAR	T4	41.0	30.2	35.8
14	LAR	T4	11.1	8.0	8.6
15	LAR	T4	14.6	10.2	-
16	LAR	T4	18.4	11.4	-
17	LAR	T4	28.1	26.6	43.4
18	LAR	T4	25.0	20.0	39.5
19	LAR	T4	40.4	28.7	26.7
Mean[2]			21.4	13.4*	-
Mean[3]			20.5	14.5*	21.8

[1] PS: piriform sinus; RC: retrocricoid area; SGL: supraglottic larynx; GL: glottic larynx; Sub GL: subglottic larynx; LAR: larynx without other specification.
[2] including all 19 tumors
[3] including only patients where MET-PET could be performed
* $P \leq 0.05$

Table 14 : Average mismatch of laryngeal or hypopharyngeal Gross Tumor Volumes for various imaging modalities (13 patients)

	Imaging modality		
	CT	FDG-PET	MET-PET
CT / x	-	80%	46%
FDG-PET / x	13%	-	9%
MET-PET / x	27%	64%	-

9.4. Discussion

The results of our study show that MET- and FDG-PET are not equivalent in determining the tumor volumes of HNSCC. Although the use of FDG-PET can reduce the tumor volumes by 40 % as compared to CT, MET-PET volumes are not statistically different from the CT volumes. Moreover, MET-PET volumes are significantly larger than FDG-PET volumes. The larger MET-PET volumes compared to the FDG-PET volumes are probably the consequence of the high physiologic MET uptake by tumor surrounding tissues like the submandibular gland, the mucosa or the bone marrow [Lindholm 1993, Leskinen-Kallio 1994], resulting in the fact that normal organs are considered as tumor. Therefore a manual correction of the tumor volume was needed in five tumors located at the base of the tongue, close to salivary glands. Furthermore, we noticed that the major cause of volume overestimation with MET was indeed the mucosa physiologic uptake of the tracer. This is an important observation because our patients were scanned before any radiation therapy. Since radiation would further increase the mucosa uptake of MET because of the intense inflammation, we believe that MET-PET would become totally unreliable for tumor volume measurement and radiation fields adaptation during therapy. In contrast, the physiologic FDG uptake by salivary glands was lower than the MET uptake and did not impair the tumor delineation.

Besides significant differences in absolute volumes, we also observed interesting results in terms of mismatch between modalities. The high mismatch of MET- over FDG-PET volumes, reaching 43 % and 64 %, mainly reflects the difference between the two absolute volumes but also the fact that structures included in the MET volumes are not considered as part of the tumor on FDG-PET images, suggesting that FDG could be more specific for tumor delineation than MET in the head and neck region. On the contrary, the small mismatch of FDG- over MET-PET means that FDG-PET volumes were almost totally included in the MET-PET volumes. The mismatch measures of 9 % and 14 % partially can be attributed to the small though present inaccuracy of the coregistration step. Actually, because the mismatch is based on volumetric measures, a small translation gap can result in a larger mismatch. Our results suggest that for HNSCC tumor volume delineation, FDG- is superior to MET-PET. Therefore, the specificity of MET uptake in head and neck region has to be questioned. In a micro-autoradiographic comparison between MET and FDG in an animal model, it was suggested [Kubota 1995] that MET could be more accurate than FDG for tumor assessment since MET was mainly taken up by viable cancer cells, while FDG concentrated

preferentially in macrophages and granulation tissues. Nevertheless, such results must be carefully interpreted when it comes to *in vivo* application. Indeed, lack of specificity must be interpreted here in terms of poor tissue discrimination of MET, i.e. its poor ability to differentiate the tumor from its direct environment. In other words, the same study conducted in patients with lung cancer might lead to totally different results since no uptake in normal structures is expected to hamper tumor delineation with MET-PET. As used in our study, MET-PET does not allow to accurately differentiating the tumor from its environment because of similar uptakes 30 min after injection. It is possible that more complex approaches could overcome this difficulty. For example, the 3D principal components analysis (PCA) using dynamic PET acquisitions is being evaluated. The PCA technique is based on the cluster analysis of pixels displaying the same dynamic uptake of the tracer. This method could allow for differentiating normal tissue from inflammation and tumor, and thus improve the tissue characterization. PCA has already been used successfully in head and neck cancer for differentiating tumor from postradiation changes with FDG-PET [Anzai 1999]. Further studies are needed to establish the additional value of dynamic cluster analysis for the assessment of tumor volumes with PET.

In conclusion, despite a better tumor specificity supported by several *in vitro* and *in vivo* models, MET-PET does not appear to be useful for the delineation of the tumor volume in patients with HNSCC. The high uptake of MET by salivary glands and oral and pharyngeal mucosa limits the accuracy of tumor delineation. This results in overall tumor volumes that are not different from the CT volumes. On the contrary, FDG-PET still seems more promising and its use would result in a 40 % reduction of the target volume. Our study stresses the point that metabolic imaging must be carefully validated in every clinical situation before applying it as a routine tool for radiation treatment planning.

10. SELECTION AND DELINEATION OF CLINICAL TARGET VOLUME FOR PRIMARY PHARYNGO-LARYNGEAL SQUAMOUS CELL CARCINOMA : GUIDELINES BASED ON ANATOMY AND PATHOLOGY LITERATURE

10.1. Specific introduction

The selection of the CTV is the next critical step in view of an accurate treatment, particularly in 3D-CRT and even more in IMRT because they generate steep dose gradients potentially leading to geographical miss if CTV is not correctly delineated. As one knows, local extension of a tumor is centrifugal, with a probability of finding tumor cells decreasing as one moves away from the macroscopic edges of the tumor, as was verified in lung tumors [Giraud 2000] where 95 % of microscopic extension could be found at eight mm of macroscopic edges for adenocarcinoma and at six mm for SCC. But HN anatomy is far more complex than the lung -which virtually shows no resistance to tumor extension- precluding the use of simple geometrical extensions. Indeed HN area is characterized by the presence of fascia, cartilages or bones acting as relatively strong barriers, but also of fatty spaces (parapharyngeal, preepiglottic, paraglottic) acting as « speedways » for tumor cells spread. Such a mixture of barriers and weak points implies that CTV is not limited to the simple geometrical 3D extension of GTV which must be tailored according to anatomical barriers and fatty spaces encountered [Fig. 2].

Based on this assumption, we elaborated guidelines for selection and delineation of CTV of oropharynx, larynx and hypopharynx SCC based on normal anatomy knowledge and pathology literature data on microscopic extension of these tumors.

10.2. Specific materials and methods

Normal anatomy descriptions were retrieved from two excellent textbooks [Rouvière 1972, Chevallier 1998] integrating schematic views and formal descriptions with even some anatomopathological descriptions. Literature articles were retrieved after extensive search in PubMed database using different combinations of following keywords : oropharynx, larynx, hypopharynx, cancer, microscopy, extension, margins, invasion and pathology. Among collected references, articles more specifically aiming at our goal were selected from abstracts reading. Full text articles were then retrieved from different libraries. In these articles, all references listed were thoroughly scanned to search for ref-

erences which could have been ignored by the metaanalyzer of PubMed robot. Potentially interesting full text articles were also retrieved from libraries. For articles not written in English or French, only the translation of the abstract was taken into consideration.

Common extension pathways were drawn from descriptions found in the literature and matched with normal anatomy data. When pathology data could not be found, extension pathways were drawn based only on normal anatomy knowledge. Anatomy structures and extension pathways were then delineated on CT slices acquired according to protocol described above (§ 5.2.1). This step permitted a simplification of extension pathways taking into account spatial resolution, soft tissue contrast and viewer limitations which do not often allow to visualize some anatomical details, e.g. : impossibility to discriminate preepiglottic space (PES) from paraglottic spaces (PGS); impossibility to discriminate oral tongue, floor of mouth, anterior extralaryngeal muscles or the different constrictors of the pharynx muscles; limited visualization of tiny muscles like interarytenoid ones.

After having considered the risk of structures invasion based on macroscopic tumor extension (GTV), we elaborated guidelines for the delineation of CTV in each of the subsite of larynx (subglottis, glottis and supraglottis), hypopharynx (piriform sinus, retrocricoid area, posterior pharyngeal wall) and oropharynx (base of tongue, tonsillar fossa, soft palate, posterior pharyngeal wall) SCC.

10.3. Results

10.3.1. Oropharynx

Only three publications [Halimi 1990, Jones 1997, Maroldi 1999] were found to be relevant in the literature They are sufficiently documented to provide reliable predictions on extension pathways. Missing data are extrapolated from normal anatomy knowledge [Fig. 17 & 18].

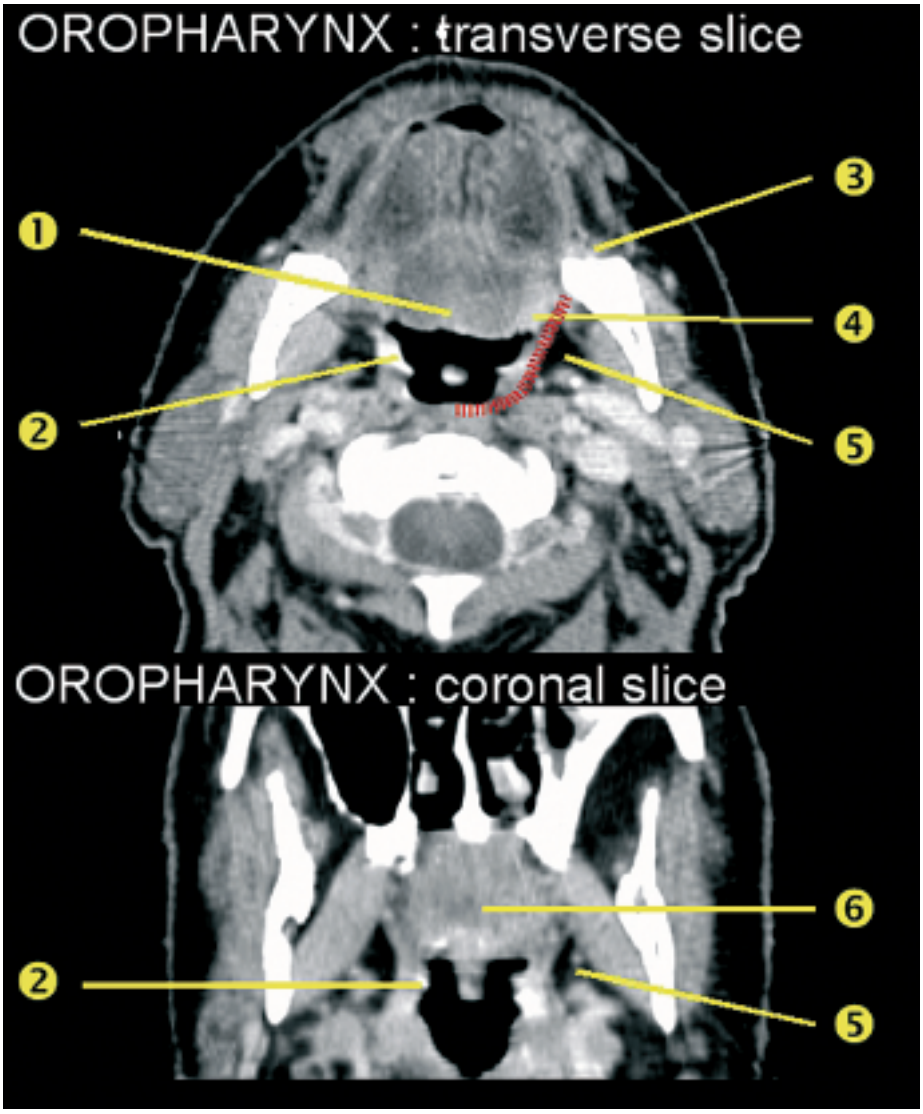

Figure 17 : Normal anatomy of the oropharynx on CT slices. (1) Base of tongue. (2) Tonsilla. The constrictor muscles located just behind tonsilla are represented by the dashed red line on the contralateral part of the slice. (3) Retromolar trigone. (4) Glossotonsillar sulcus. (5) Parapharyngeal space. (6) Soft palate.

10.3.1.1. Base of tongue

Base of tongue is constituted anteriorly of the lingual tonsil and infero-posteriorly of the two valleculae. Tumors arising in the lingual tonsil generally spread anteriorly in the mobile tongue and the floor of the mouth, posteriorly in the valleculae and laterally towards the tonsillar fossae through the glossotonsillar

sulcus (GTS). Tumors arising in the valleculae can spread anteriorly in the lingual tonsil. Inferior extension towards larynx and/or hypopharynx rarely occurs because of the existence of the hyoepiglottic membrane which is a thick fibrous structure bended between the hyoid bone and the mid-anterior face of the epiglottis. It separates valleculae from preepiglottic space (PES). It is a structure resistant to cancer cell spread. Larynx is more often invaded posteriorly via the epiglottis and hypopharynx laterally via the region of the three folds.

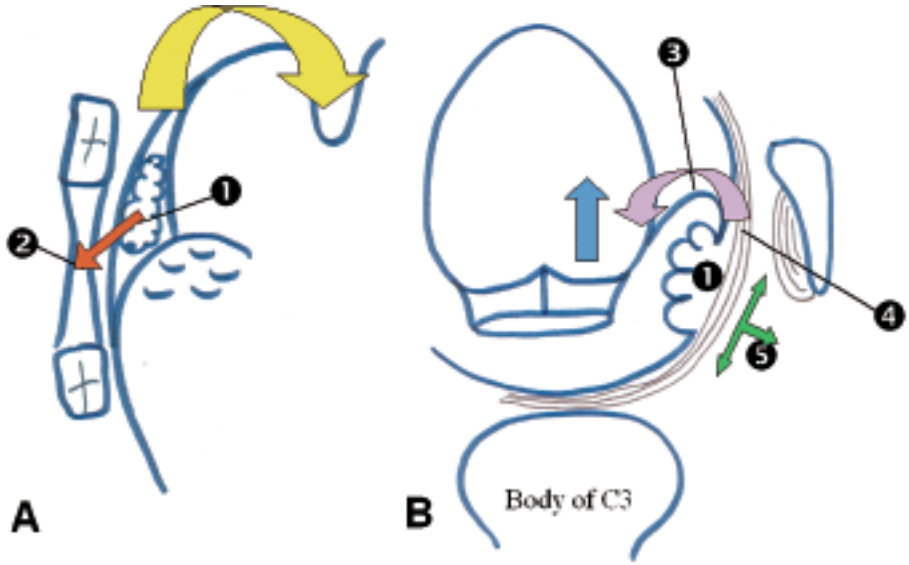

Figure 18 : (A) : anterior view of oropharynx (open mouth). Tonsillar fossa (1) tumors easily spread to the soft palate (yellow arrow) and inversely. They also easily extend through glossotonsillar sulcus towards retromolar trigone (2) from where they spread along the pterygomandibular raphe (cranially) and mylohyoid muscle (caudally). (B) : transverse slice through the body of C3. Tonsillar fossa (1) tumors also extend to constrictor muscles (4) and, after having invaded the strong pharyngobasilar raphe, to parapharyngeal space (green arrows). Glossotonsillar sulcus (3) tumors extend to base of tongue and to tonsillar fossa and vice-versa (pink arrow). Base of tongue tumors spread into mobile tongue and floor of mouth muscles (blue arrow).

10.3.1.2. Soft palate

Soft palate is directly connected to tonsillar fossae. The mucosa covering the hard palate is also an easy way of spread with virtually no barrier in the lateral and anterior directions. Laterally to the soft palate, one can find a critical structure which is called the pterygopalatine fossa. This small fatty space is roughly situated between the posterior part of the maxilla and the pterygoid plates. Once cancer cells have penetrated the pterygopalatine fossa, they can then spread through tunnels and foramina to the orbita, the infratemporal fossa and the rhinopharynx.

The soft palate has a fibrous skeleton which shape is modified thanks to the antagonist work of both tensor and levator velopalatini muscles, palatopharyngeal muscles and palatoglosse. Velopalatini muscles roughly run from the soft palate to the lateral part of the petrous bone along the lateral side of the rhinopharynx. Palatopharyngeal and palatoglosse muscles roughly run from the soft palate to the lateral part of the oropharynx where they form the skeleton of posterior and anterior pillars.

10.3.1.3. Tonsillar fossa

The easiest ways of spread for cancer located in tonsillar fossa are craniomedially in direction of soft palate and uvula and medially in direction of base of tongue through the GTS. These types of extension can be submucosal along both anterior and posterior pillars.

Tonsillar fossae are separated from cranial and mid constrictor muscles of the pharynx by the tough pharyngobasilar fascia which represents a barrier limiting for a time the extension to the muscles and to the underlying parapharyngeal space (PPS). This type of lateral penetration was thought for long to be the main extension path, which is not true [Halimi 1990]. Cancer cells rather spread laterally towards the pterygomandibular raphe. This fibrous structure is tended between the hamulus of the pterygoid bone and the mylohyoid line on the mandibula. It is the lateral point of insertion of the cranial constrictor muscle of the pharynx. It is covered by the mucosa of the retromolar trigone (RMT). This topography explains why once the raphe is reached, malignant cells spread toward the medial pterygoid muscle and then the deep spaces of the face (among which the PPS), the mandibula and finally the floor of the mouth via the mylohyoid muscle. Whatever the way of penetration into the PPS, a critical structure which can then be easily invaded is the styloglossus muscle which comes from the styloid process toward the tongue through the PPS. It thus represents a late but critical way of spread to base of skull and/or tongue.

10.3.1.4. Posterior pharyngeal wall

Posterior pharyngeal wall (PPW) is mainly constituted of a mucosal layer, the previously mentioned pharyngobasilar fascia and more deeply the overlapping layers of the three symmetrical pairs of constrictor muscles of the pharynx. Pharyngobasilar fascia being relatively resistant, cancer cells first spread isometrically in a submucosal fashion. Once the fascia is penetrated, cells enter

the muscles and then spread laterally along its fibers. Cancer cells going throughout the muscle can either try to penetrate the posterior longus capitis muscles or more probably diffuse laterally and cranio-caudally in the fatty spaces of the PPS.

10.3.1.5. Recommendations for primary Clinical Target Volume delineation [Table 15]

The following structures must always be encompassed in the CTV within a security margin arbitrarily fixed at 15 mm around the GTV if the GTV is centered on :
- base of tongue : mucosa, GTS and muscular tongue;
- soft palate : mucosa, tonsilla and pillars, pterygopalatine fossa, velopalatini muscles (roughly located on the lateral part of the oro- and rhinopharynx up to the petrous bone);
- tonsilla : mucosa, pillars, constrictor muscles, GTS and soft palate;
- PPW : mucosa and constrictor muscles, parapharyngeal space for lateral lesions.

Moreover, beyond the systematic inclusion of every other structure directly invaded (augmented by the systematic security margin), it is safe to prophylactically include defined structures if the following ones show signs of direct invasion :

- GTS : tonsilla, base of tongue and RMT;
- RMT and all perimandibular tissues (gingiva, mylohyoid muscle) : mandibula;
- mobile tongue : floor of the mouth;
- mylohoid muscle : RMT, mandibula, floor of the mouth;
- pterygopalatine fossa : posterior part of the orbita, maxilla, caudal part of the rhinopharynx, infratemporal fossa.

Examples of CTVs drawn according to these rules are reproduced at figures 19, 20, 21 & 22.

Table 15 : Guidelines for the delineation of CTV based on GTV extension in oropharyngeal tumors. The invasion of anatomical structures considered as gatekeepers to tumor extension potentially opens a «hole» in the wall mandatorily leading to consider a potential microscopic extension in more fragile surrounding structures.

Gatekeeper	Extension
Base of Tongue	• mucosa • GTS[1] • muscular tongue
Soft Palate	• mucosa • tonsilla • pillars • pterygopalatine fossa • velopalatini muscles
Tonsilla	• mucosa • constrictor muscles • GTS[1] • soft palate
Posterior Pharyngeal Wall	• mucosa • constrictor muscles • parapharyngeal space for lateral lesions
GTS[1]	• tonsilla • base of tongue • RMT[2]
RMT[2] and/or gingiva	• mandibula
Mobile tongue	• floor of the mouth
Mylohoid muscle	• RMT[2] • mandibula • floor of the mouth
Pterygopalatine fossa	• posterior part of the orbita • maxilla • caudal part of the rhinopharynx • infra-temporal fossa

[1] : GTS = Glossotonsillar sulcus; [2] : RMT = Retromolar trigone.

-

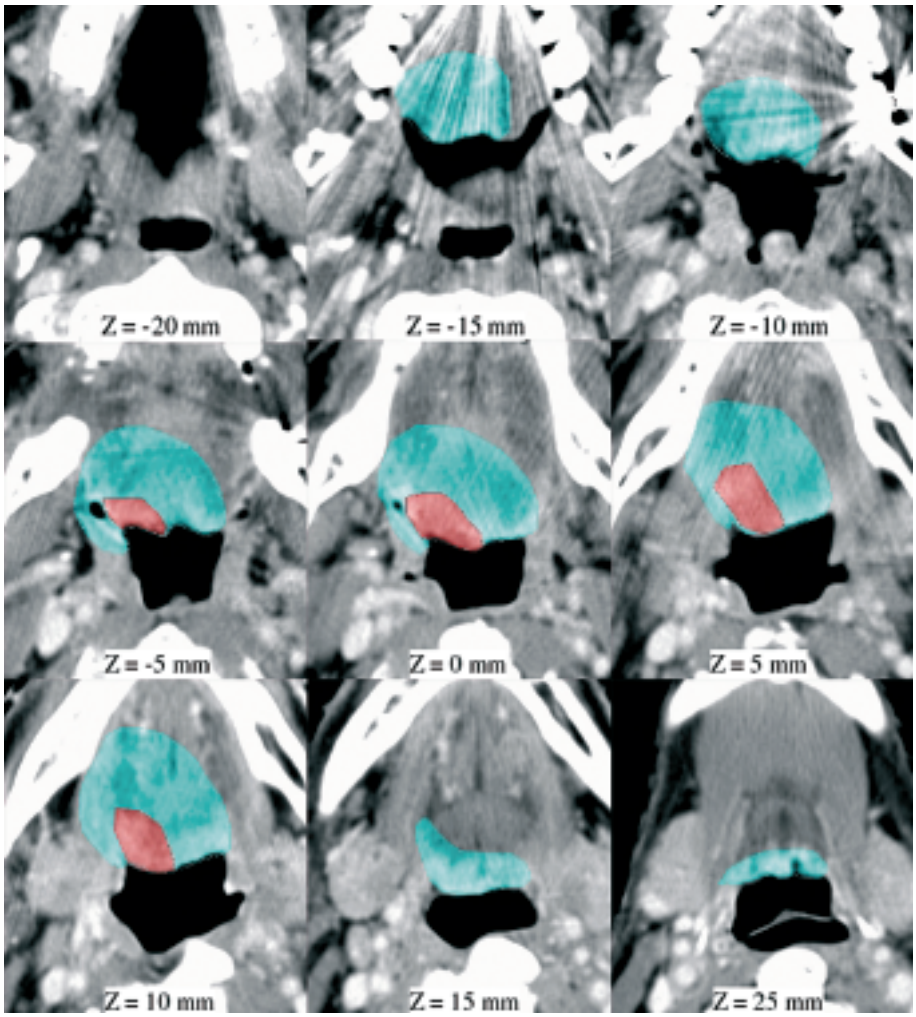

Figure 19 : Axial CT slices of a 83y male with a T2 tumor of the right part of the base of tongue (GTV in red). The CTV (in light blue) encompasses the mucosa of base of tongue, a 15 mm extension into the mobile tongue and the Glossotonsillar sulcus.

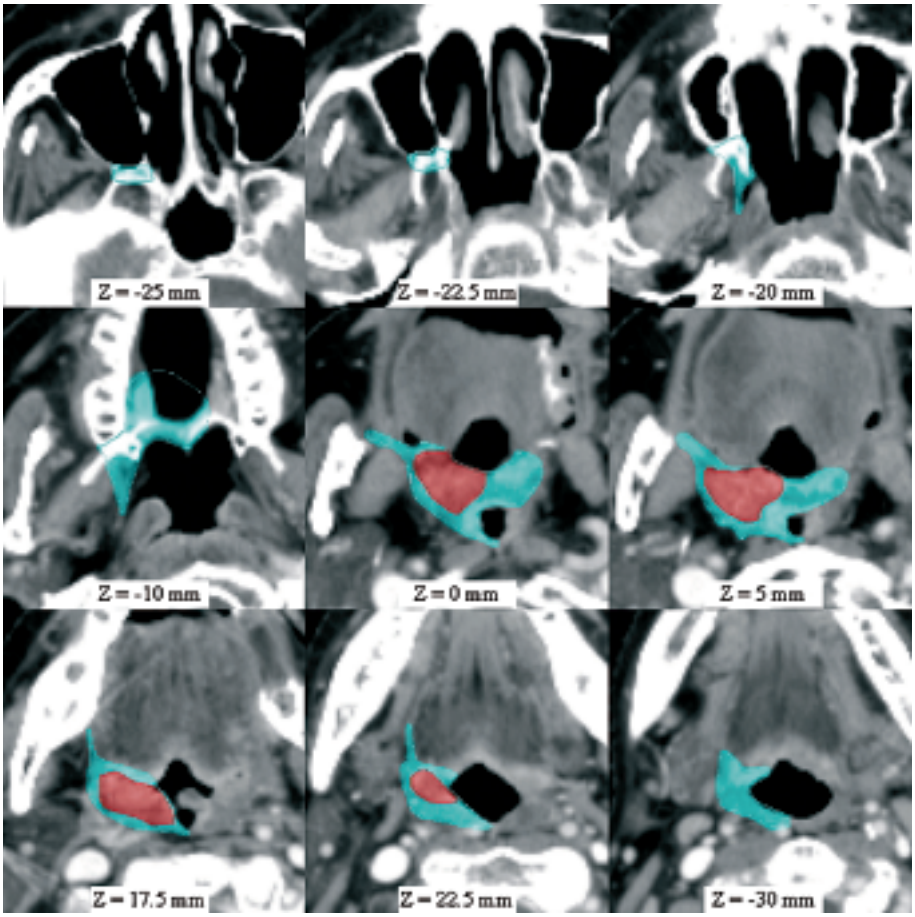

Figure 20 : Axial CT slices of a 48y female with a T2 tumor of the right tonsilla (GTV in red) extending upwards on the soft palate through the posterior pillar. The CTV (in light blue) includes the pterygopalatine fossa (slices z = -10 to -25 mm), the soft palate and the mucosa of the hard palate (not directly visualized because of partial volume effect, CTV had to be artificially extended into the air on slice z = -10 mm to compensate for this absence of visualization); the glossotonsillar sulcus and the constrictor muscles of the posterior pharyngeal wall.

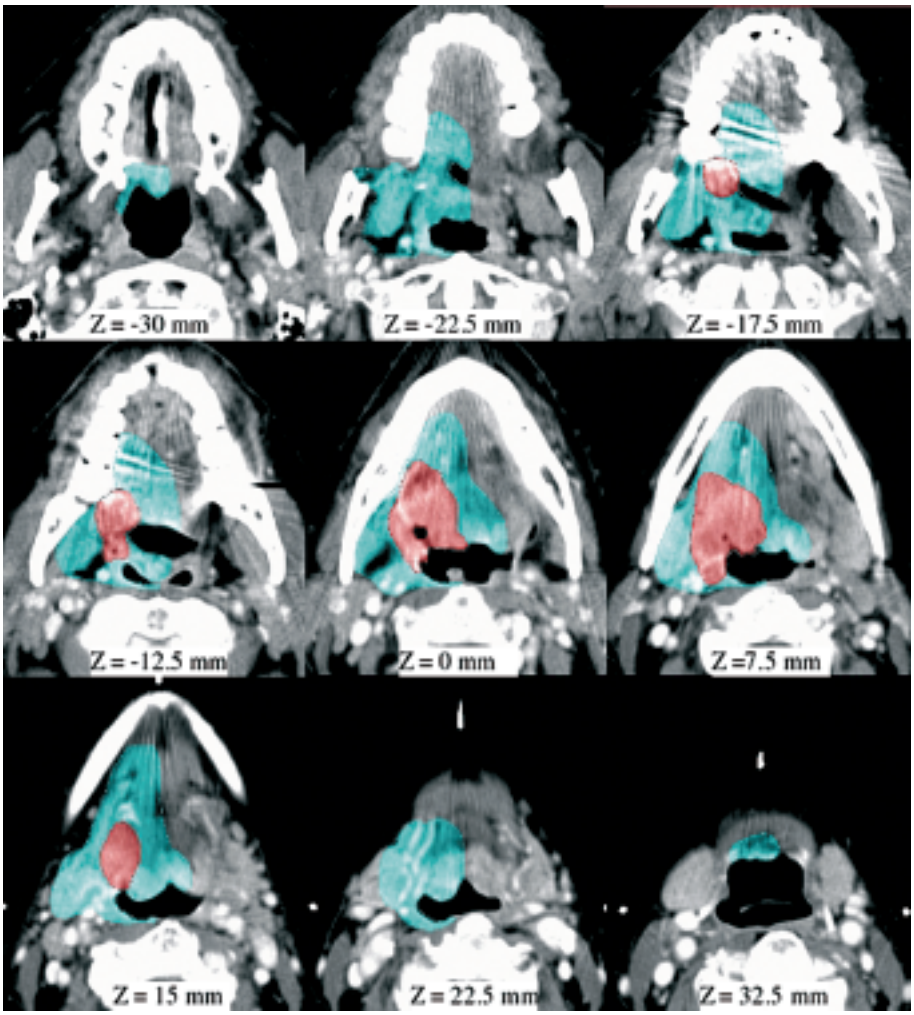

Figure 21 : Axial CT slices of a 53y female with a T4 tumor of the right tonsilla (GTV in red) extending through the glossotonsillar sulcus to the base of tongue, the mobile tongue and the floor of the mouth. It laterally extends to the parapharyngeal space through the posterior pharyngeal wall and shows an intimate contact with medial pterygoid muscle and submandibular gland. All of these structures plus the soft palate and the retromolar trigone are included in the CTV (in light blue).

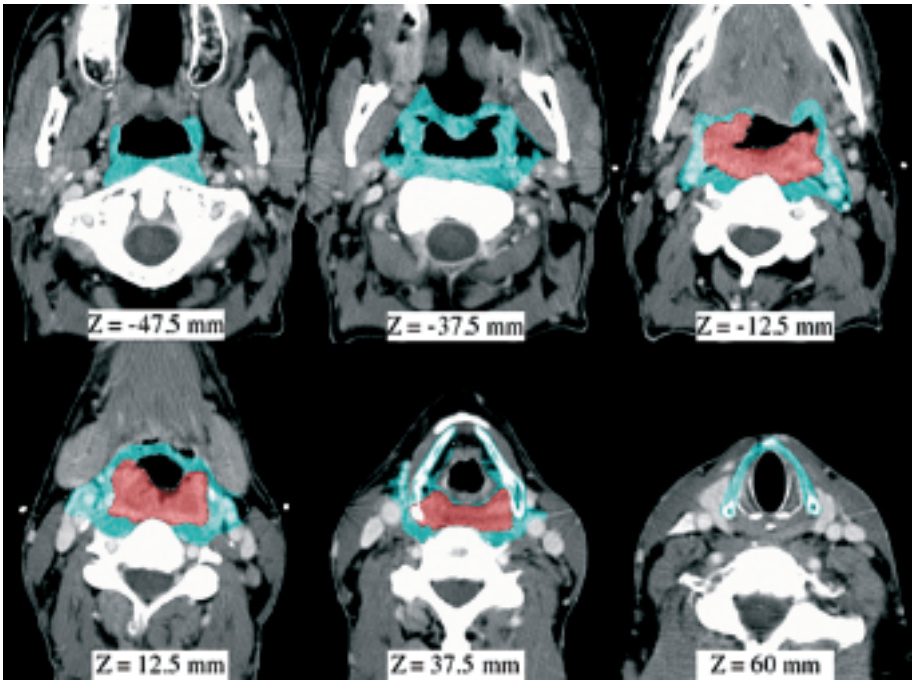

Figure 22 : Axial CT slices of a 57y male with a huge T4 tumor of the posterior pharyngeal wall (GTV in red). It extends to both lateral pharyngeal walls. Posteriorly located longus capiti muscles show clear signs of invasion and are largely included in the CTV (in light blue). Because of the lateral extension, the CTV includes cranially the soft palate, in the middle the epiglottis and caudally the thyroid cartilage and both PGS.

10.3.2. Larynx

Extensive series published since the fifties studied microscopic laryngeal tumor spread [Ogura 1955, Pressman 1960, Olofsson 1973, Olofsson 1974, Kirchner 1975, Kirchner 1975, Kirchner 1976, McDonald 1976, Micheau 1976, Olofsson 1979, van Nostrand 1982, Yeager 1982, Bagatella 1983, Lam 1983, Lam 1983, Harrison 1984, Kirchner 1987, Gilbert 1988, Welsh 1989, Gregor 1990, Sato 1993, Beitler 1994, Reidenbach 1995, Weinstein 1995, Reidenbach 1996, Durum 1997, Kirchner 1997, Reidenbach 1998, Rifai 2000]. They firmly demonstrated the natural tendency of malignant cells to spread through lesser resistant anatomical structures while avoiding stronger structures acting as barriers up to a given point [Fig. 23, 24 and 25].

10.3.2.1. Supraglottis

In the supraglottic region, the epiglottic cartilage is characterized by the presence of multiple small holes giving the cartilage its « fenestrated » characteristic. These holes act as small tunnels allowing cancer cells to directly reach the preepiglottic space (PES) in case of infrahyoepiglottic membrane location or the base of tongue in case of suprahyoepiglottic membrane tumor. It leads to PES invasion in 66 % [Olofsson 1973] to 80 % [Gregor 1990] of supraglottic tumors. As previously mentioned, the hyoepiglottic membrane is sufficiently resistant to prevent extension into the longitudinal direction, i.e. from PES to base of tongue. Anterior extralaryngeal spread is also very rare since both the hyoid bone and the thyrohyoid membrane are late resisting structures.
A particular structure which must be mentioned though not being strictly located in the supraglottic larynx is the three folds region encompassing the glossoepiglottic fold (running from base of tongue to the lateral edge of the epiglottis), the pharyngoepiglottic fold (running from the lateral face of the pharynx to the lateral edge of the epiglottis) and the aryepiglottic fold (AEF) running from the apex of the arytenoid cartilage up to the lateral edge of the epiglottis). These structures facilitate the spread of supraglottic cancers reaching the lateral edge of the epiglottis towards base of tongue, pharyngeal wall and hypopharynx, respectively.

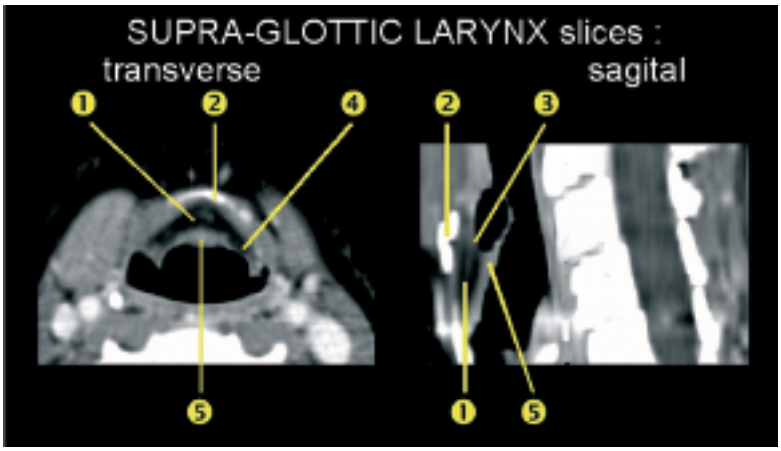

Figure 23 : Normal anatomy of the supraglottic region on CT slices. (1) Preepiglottic space. (2) Hyoid bone. (3) Hyoepiglottic membrane, separating the caudal preepiglottic space from the cranial valleculae. (4) Paraglottic space. (5) Epiglottis.

In contrast to the generally accepted ideas, ventricular folds are not critical structures for the spread beyond the glottic plane [Beitler 1994]. This descending way of extension is due to the existence of the laterally located paraglottic spaces (PGS). PGS are thin fatty spaces extending from cranial edge of hyoid bone down to cranial edge of cricoid cartilage. Being fatty spaces, they act as speedways for hidden longitudinal extension throughout the three levels of the larynx. Another common way of descendant extension is via the arytenoids [Kirchner 1997].

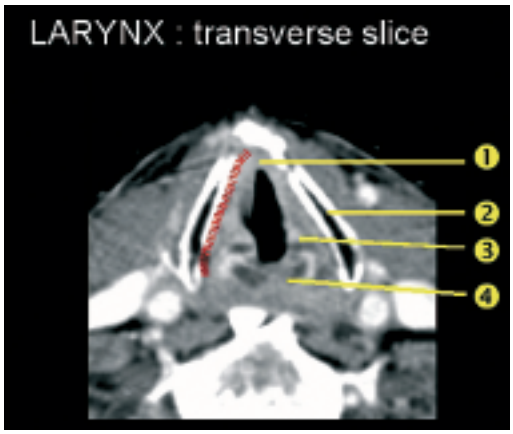

Figure 24 : Normal anatomy of the larynx at the glottic plane on a CT slice. (1) Anterior commissure. (2) Thyroid cartilage. (3) Arytenoid cartilage. (4) Cricoid cartilage. Vocal cords are bended between the anterior commissure and the arytenoids. The paraglottic space (dashed red line) is a thin fat space lying along the inner thyroid cartilage plate and the lateral border of vocal cord. The hypopharyngeal region is not opened in rest conditions and is roughly located anteriorly behind cricoid cartilage, posteriorly the vertebra and laterally the posterior edges of the thyroid cartilage.

10.3.2.2. Glottis

All laryngeal framework cartilages are particularly fragile at various membrane, ligament and muscle insertion points. For example, it is well documented [Kirchner 1975, Harrison 1984, Rifai 2000] that all T3 laryngeal tumors are at high risk of migration along the aryepiglottic muscle (vocal cord). Muscle fibers directly penetrate either the thyroid or arytenoid cartilages through their perichondrium [Yeager 1982], giving the opportunity to cancer cells to directly penetrate both cartilages. It must be added about thyroid cartilage that it was well demonstrated [Ogura 1955] that once penetrated, cancer cells can be found anywhere in it. Once the arytenoid cartilage is massively penetrated there is high risk for cricoid cartilage extension through the cricoarytenoid joint.

Extension to the hypopharynx is rarely the fact of strictly posterior spread, cancer cells being arrested in their progression by the arytenoid and the interarytenoid muscle which fibers are oriented orthogonally to spread direction. On the other hand, postero-lateral extension is not infrequent. This is the fact of

transverse extension through the PGS to the pririform sinus submucosa which shows virtually no resistance to cancer cells. Lateral thyroid cartilage and extralaryngeal extension is also frequent in this neighbourhood through the penetration of the inferior constrictor muscle of the pharynx which is laterally attached to the posterior edge of the thyroid cartilage.

Caudal infiltration towards the subglottis is possible via the submucosa.

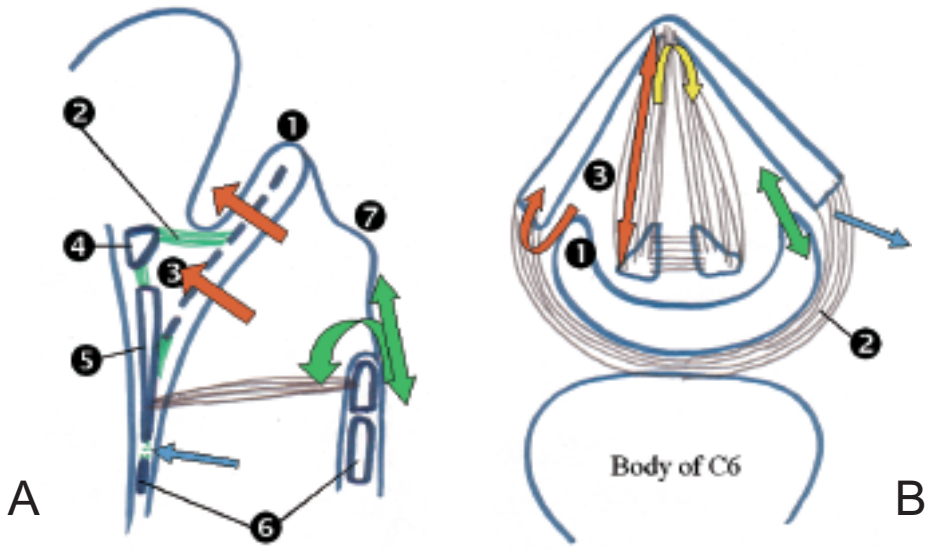

Figure 25 :
(A) : sagittal paramedial slice of the larynx and the hypopharynx. The fenestrated character of the epiglottis (1) easily leads to invasion (red arrows) of either the vallecula or the preepiglottic space (PES - 3). Other sides of PES are surrounded by strong structures (hyoepiglottic membrane -2-, hyoid bone -4- and thyroid cartilage -5) acting as solid barriers against tumor extension. Supraglottic tumors can invade hypopharynx through ary-epiglottic fold (7) and vice-versa (green arrows). The cricothyroid membrane is not a solid structure explaining the high propensity of subglottic tumors to spread outside the larynx (blue arrow).
(B) transverse slice through body of C6. Glottic tumors tend to spread horizontally by following vocal muscle fibres (red double arrow). They then infiltrate cartilages at muscle insertion points where perichondrium is lacking. They also spread to the contralateral cord through anterior commissure (yellow arrow). Paraglottic space (3) is a fatty space extending from cranial border of hyoid bone down to the cranial border of cricoid cartilage. It thus allows vertical extensions but also horizontal spread to piriform sinus (1 - green arrow) and constrictor muscles (2). From there, cancer spreads to thyroid cartilage (curved red arrow) and to paralaryngeal tissues (blue arrow).

10.3.2.3. Subglottis

In the subglottic region, the cricothyroid membrane is not strictly continuous [Kirchner 1997]. This is why anterior lesions early tend to spread outside the laryngeal framework.

Cricoid and thyroid cartilage invasion is frequent due to the early invasion of cricothyroid membrane which, like muscle fibers, directly penetrates the cartilages through the perichondrium [Yeager 1982].

Cranial extension via the submucosa is frequent, but it is more frequent through the PGS for tumors located above the cranial edge of the cricoid cartilage. Indeed, at this level, the PGS is located directly under the mucosa.

Posterior and lateral extension to the hypopharynx is a late event because of the presence of the larger part of the cricoid cartilage and the posterior cricoarytenoid muscle. However, this does not preclude PPW extension through the cricothyroid space which is located at the postero-caudal part of the thyroid cartilage. At this place, the cricothyroid membrane is missing, favoring spread of cancer cells outside the laryngeal framework.

For unknown reasons, caudal extension to the trachea is exceptional, though no clear anatomical barrier could be highlighted.

10.3.2.4. Recommendations for primary Clinical Target Volume delineation [Table 16]

The following structures must always be encompassed in the CTV within a security margin arbitrarily fixed at 15 mm around the GTV if the GTV is centered on :
- supraglottis : mucosa down to ventricles, epiglottis, preepiglottic space, paraglottic space (ipsilateral for lateral lesions, bilateral for medial lesions), aryepiglottic fold, vallecula (suprahyoid tumor);
- glottis (except T1 tumors) : mucosa from caudal border of AEF down to caudal limit of cricoid cartilage, PGS, anterior commissure (AC), vocal cord (bilateral or ipsilateral whether AC is directly involved or not), thyroid cartilage and arytenoid cartilage if ≥ T3 ;

Table 16 : Guidelines for the delineation of CTV based on GTV extension in laryngeal tumors. The invasion of anatomical structures considered as gatekeepers to tumor extension potentially opens a «hole» in the wall mandatorily leading to consider a potential microscopic extension in more fragile surrounding structures.

Gatekeeper	Extension
Supraglottis	· mucosa down to ventricles
	· epiglottis
	· PES[1]
	· PGS[2]
	· AEF[3]
	· vallecula for suprahyoid tumors
Glottis	· mucosa (AEF[3] to cricoid cartilage)
	· PGS[2]
	· AC[4]
	· vocal cord(s)
	· arytenoid and cricoid cartilages IF at least T3 lesion
Subglottis	· mucosa
	· cricoid cartilage
	· vocal cord(s)
	· anterior lesions : thyroid cartilage, prelaryngeal fat and/or muscles
PES[1]	· hyoid bone
	· thyroid cartialge
	· valleculae
Posterior Pharyngeal Wall	· paralaryngeal and -pharyngeal fatty spaces
AEF[3]	· piriform sinus
PGS[2] (posterior part)	· posterior pharyngeal wall
	· piriform sinus
Cricothyroid space	· posterior pharyngeal wall
	· piriform sinus
Arytenoid cartilage	· cricoid cartilage
	· retrocricoid region

[1] : PES = Preepiglottic space; [2] : PGS = Paraglottic space; [3] : AEF = Aryepiglottic fold; [4] : AC = Anterior commissure.
Note : for lesions located on the midline, consider bilateral extension for symetric structures (like vocal cords). For lateralized lesions, homolateral extension might be sufficient.

- subglottis : mucosa from VC down to security margin below GTV (15 mm), cricoid cartilage, vocal cord(s).

Moreover, beyond the systematic inclusion of every other structure directly invaded (augmented by the systematic security margin), it is safe to prophylactically include defined structures if the following ones show signs of direct invasion :

- PES : if fully invaded, include hyoid bone, thyroid cartilage and valleculae;
- constrictor of the pharynx muscles (PPW) : paralaryngeal(pharyngeal) fat;
- AEF : homolateral piriform sinus (PS);
- posterior part of the PGS / cricothyroid space : PPW, piriform sinus;
- arytenoid cartilage : cricoid cartilage, RC;
- anterior subglottic lesions : thyroid cartilage, prelaryngeal fat and/or muscles.

Examples of CTVs drawn according to these rules are reproduced at figures 26 & 27.

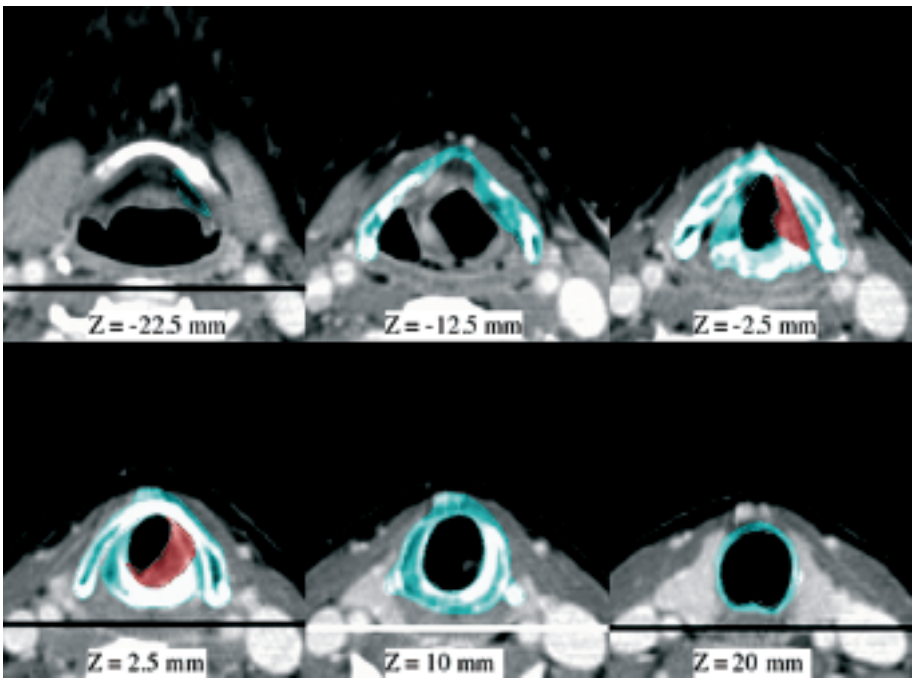

Figure 26 : Axial CT slices of a 49y female with a T3 subglottic tumor (GTV in red). Its anterior extension leads to the inclusion of the prelaryngeal fat at the level of the cricothyroid membrane. Its laterality allows to include only the homolateral paraglottic space (CTV in light blue).

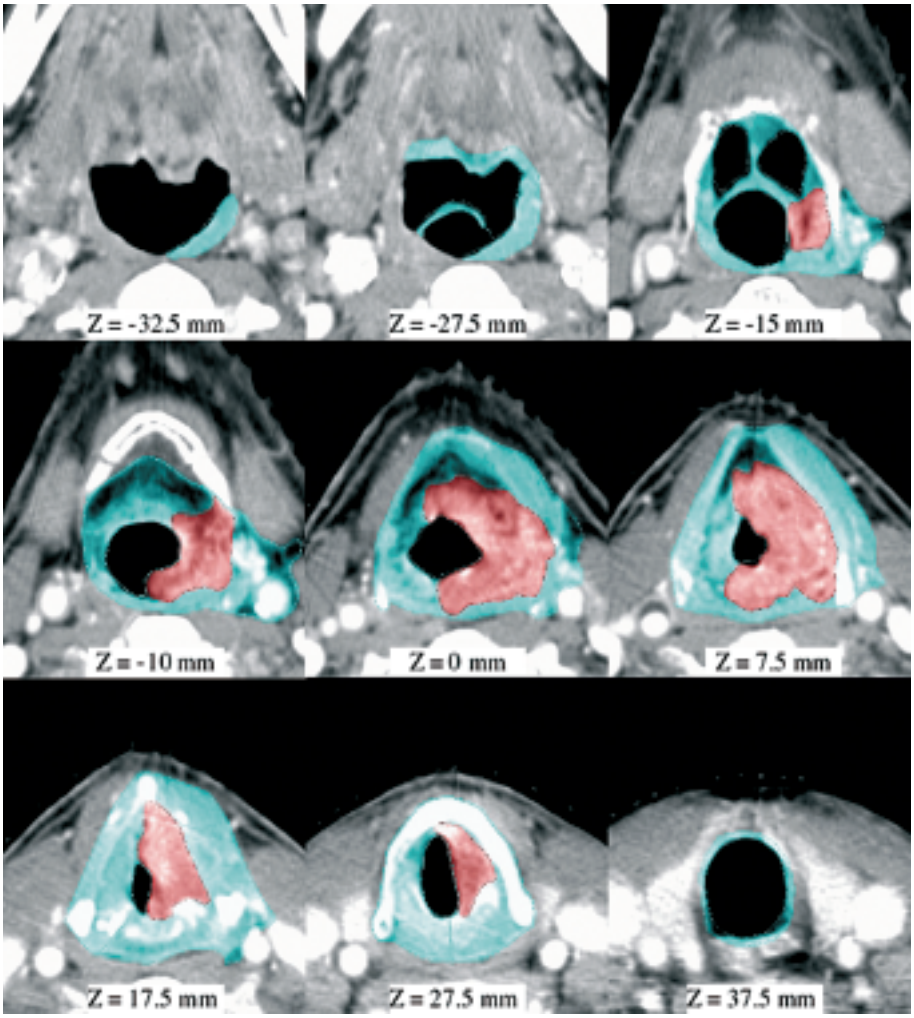

Figure 27 : Axial CT slices of a 70y male with a T3 glottic carcinoma (GTV in red) extending from the supraglottis to the subglottis. There is at least an intimate contact between the tumor and the left cricothyroid muscle (z = 0 mm) leading to its « secure » inclusion in the CTV (in light blue) from z = 0 to 17.5 mm. At z = -15mm, the tumor has reached the three folds region (through the aryepiglottic folds) making it mandatory to include valleculae and homolateral posterior pharyngeal wall constrictor muscles. Piriform sinus and retrocricoid region are included because (1) the tumor reaches the posterior border of the paraglottic space located between the posterior edge of the thyroid cartilage and the arytenoid and (2) the left aryepiglottic fold is largely invaded.

10.3.3. Hypopharynx

Compared to the work performed in the larynx, very few works have been reported about tumor spread pathways in the hypopharynx [Olofsson 1973, Kirchner 1975, Hirano 1987, Tani 1987] [Fig. 24 & 25].

10.3.3.1. Piriform sinus

Lateral lesions tend to invade the PGS anteriorly and the inferior constrictor muscle of the pharynx laterally. Cranial extension is directed towards the three folds region. Extension pathways from these structures were exposed in length in the previous sections.

Antero-medial lesions are related to the retrocricoid (RC) region and postero-medial lesions are related to the PPW.

Submucosal extensions were well documented for the hypopharynx [Ho 1997], to 37 mm away from primary lesion.

10.3.3.2. Retrocricoid region

Anterior extension could be felt as anatomically difficult because of the interposition of cricoid and arytenoid cartilages on the one hand, and of posterior cricoarytenoid and interarytenoid muscles on the other hand. But both cricoid and cricoarytenoid muscles have been reported to be invaded in about half the cases of a study [Oloffson 1973]. This could be due to the fact that hypopharyngeal cancers are often diagnosed at an advanced stage.

Laterally, extension is performed submucosally.
Cranial extension up to the cranial part of the arytenoid cartilages gives the opportunity for cancer cells to spread laterally on the aryepiglottic fold and anteriorly in the supraglottis.
Caudal extension is submucosal towards the esophagus.

10.3.3.3. Posterior Pharyngeal Wall

Please refer to section § 10.3.1.4.

10.3.3.4. Recommendations for primary Clinical Target Volume delineation [Table 17]

Table 17 : Guidelines for the delineation of CTV based on GTV extension in hypopharyngeal tumors. The invasion of anatomical structures considered as gatekeepers to tumor extension potentially opens a «hole» in the wall mandatorily leading to consider a potential microscopic extension in more fragile surrounding structures.

Gatekeeper	Extension
Piriform sinus	· mucosa (37 mm) · PGS[1] · AEF[2] · posterior pharyngeal wall
Retrocricoid region	· mucosa (37 mm) · AEF[2] · interarytenoid muscles
Posterior Pharyngeal Wall	· mucosa (37 mm) · constrictor muscles · parapharyngeal fatty space for lateral lesions
Arytenoid cartilage	· cricoid cartilage · vocal cord
Cricoid cartilage	· arytenoid cartilage
PGS[1]	· thyroid cartilage · vocal cord

[1] : PGS = Paraglottic space; [2] : AEF = Aryepiglottic fold.
Note : for lesions located on the midline, consider bilateral extension for symmetric structures (like vocal cords). For lateralized lesions, homolateral extension might be sufficient.

The following structures must always be encompassed in the CTV within a security margin arbitrarily fixed at 15 mm -except for mucosa where a 37 mm margin is necessary [Ho 1997] - around the GTV if the GTV is centered on :
- PS : mucosa (with a 37 mm security margin), PGS, AEF, PPW;
- RC : mucosa (with a 37 mm security margin), AEF, interarytenoid muscle;
- PPW : mucosa (with a 37 mm security margin), constrictor muscles and parapharyngeal space for lateral lesions.

Moreover, beyond the systematic inclusion of every other structure directly invaded (augmented by the systematic security margin), it is safe to prophylactically include defined structures if the following ones show signs of direct invasion :
- arytenoid cartilage : cricoid cartilage, vocal cord;
- cricoid cartilage : arytenoid cartilage;
- lageral part of PPW : thyroid cartilage, parapharyngeal space;
- PGS : thyroid cartilage, vocal cord.

Example of a CTV drawn according to these rules is reproduced at figure 27.

10.4. Discussion

In this review we summarize main spread pathways for primary tumors located either in the oropharynx, the larynx or the hypopharynx. The rationale for these pathways descriptions is based mainly on the extensive studies performed by pathologists, particularly in the laryngeal subsites. Missing data were extrapolated from both surgeon's experience and anatomical knowledge interpreted through the application of what could be called the « speedway & barrier » paradigm, i.e. anatomical structures intrinsically facilitating the spread of cancer cells or not. Based on these descriptions, we elaborated recommendations for the selection and delineation of primary tumor CTV after the analysis of the exact location and extension of primary tumor GTV in the oropharynx, the larynx and the hypopharynx.

A capital question which up to now has not been answered is « how many millimeters are needed to cover -but not more- the possible microscopic extensio ». It was previously demonstrated in the lung [Giraud 2000] that CTV margins of six mm for SCC and eight mm for adenocarcinoma allow coverage of 95 % of the microscopic extension. Such data are lacking in the HN area, except regarding the submucosal extensions in the hypopharynx reaching 37 mm [Ho 1997]. Historically, margins of 1.5 to 2.0 cm are used and we recommend not to change them until the later question raised will be clearly solved by microscopy studies.

As discussed in section 8, the universal image allowing to accurately answer all questions raised does not exist. The best image to date for GTV delineation is FDG-PET. However, this is a functional imaging modality which does not provide anatomical details which are essential to CTV definition. Even after GTV delineation on functional images, the use of coregistered anatomical images is mandatory to predict CTV extension.

MRI images are known to be superior to CT images for the depiction of normal anatomy details, particularly for the soft tissues. However, some technical problems limit the feasibility of the technique :
–the persistent need for image coregistration with CT for proper use in RT planning;
–the long time of acquisition (around 10 minutes) which is needed to obtain high resolution images in 3D. Moreover, high resolution 3D images acquired in a reasonable time are limited to a small volume of around 15 to 20 cm height.

–the use of the thermoplastic mask which precludes the use of a specific head and neck coil leads to loss of signal which can be compensated at the price of an additional increase in the time of acquisition;
–some artifacts -among which movement and chemical shift artifacts- are at risk of leading to inaccurate location of anatomical structures.

For all these reasons, high resolution CT with well designed contrast medium injection protocol and sufficiently thin slices (two to three mm) remains the most convenient imaging modality for depiction of normal anatomy necessary to CTV delineation.

Such types of guidelines were previously proposed by Eisbruch et al. [Eisbruch 2002]. These were the first ones proposed to the radiation oncologists community and are -hopefully- not very different from the ones we propose. Some little differences though are observed and detailed hereunder.

A general remark concerns the use of the « advanced cancer » term and the subsequent rules defined for CTV delineation. The notion of « advanced » is not defined and remains thus quite vague, potentially leading to divergences for CTV extension definition. If it is hypothesized that they are T3 or T4 tumors, there exists a risk of missing some parts of the CTV due to the underevaluation of the risk of extension in a given structure. For example, a T2 tonsillar fossa tumor -which as a reminder measures not more than four cm- is eager to extend towards the constrictor muscles of the pharynx. According to Eisbruch's recommendations, PPS would not be included in the CTV while we think it should be. On the other hand, one can find a small T4 tumor potentially invading the oral cavity via the RMT. If one strictly follows Eisbruch's recommendations, one should include pterygoid muscles, PPS, adjacent nasopharynx and mandibular bone. In our approach, only the latter structure should be included since we have no anatomical reason to extend towards the base of skull and deep spaces of the face. In other words, it means that our rules are intended to provide a « tailored CTV » based on an individualized evaluation of the extension of the GTV.

Other details are divergent among which the recommendation for a systematic inclusion of buccal mucosa in tonsillar fossa cancers seems excessive to us. Indeed, oral cavity is at risk of being invaded only if gatekeepers such as GTS, RMT or soft palate are invaded, which is not systematic at the time of diagnosis. The systematic inclusion of the homolateral thyroid lobe in case of lateral

hypopharynx lesion is also not indicated unless it is showing an intimate contact with tumor or -of course- being macroscopically invaded. It was well demonstrated [Oloffson 1973] that it is quite a tough structure being invaded in more or less five percent of the cases.

In the hypopharynx, Eisbruch recommends to include PPS from base of skull down to two cm below cricoid cartilage. Such a volume measuring approximately 10 cm height seems quite excessive, particularly for its cranial extension which is very distant from the primary tumor.

The use of such guidelines allows it to be highly selective regarding volumes to be irradiated.

The safe application of such guidelines presupposes :
- a complete and meticulous clinical examination performed in optimal conditions,
- the use of good images aiming not only to accurately predict GTV extension but also to correctly visualize normal anatomy and
- a sufficient knowledge of normal anatomy for optimal interpretation of available images.

The clinical examination must encompass at least a palpation and a direct visualization of oropharyngeal tumors, and an indirect visualization with a rigid endoscope on an anesthetized patient for all types of tumors. It is aimed at precisely describing the exact location and mucosal extension of the primary tumor. Some clinical details can also be relevant because of suspicion of a deep infiltration. For example, a trismus with referred otalgia is a sensitive but not very specific sign of infiltration of the medial pterygoid muscle [Jones 1997]. Another typical example is hoarseness associated with impairment of vocal cord vibration which causes suspicion of an infiltration of the vocal cord itself, the cricoarytenoid joint, or even the laryngeal recurrent nerve [Gilbert 1988]. In other words, such guidelines do not replace -and even emphasize more than ever the need of- a good knowledge of the normal anatomy and complete clinical examination.

For patients primarily treated by neoadjuvant chemotherapy we recommend to base CTV extension on prechemotherapy GTV delineation rather than on residual tumor after treatment. Indeed, chemoresistant clones are eager to emerge anywhere in the tumor.

Finally, these recommendations are not applicable in the postoperative settings

where normal anatomy is so disturbed that cancer ways of extension are no longer predictable.

In summary, we could draw oropharyngeal, laryngeal and hypopharyngeal SCCs pathways of spread based partly on pathological data on the one hand, and -when missing- on anatomical data and surgeons experience on the other hand. Based on these pathways, we elaborated recommendations for the delineation of CTV in patients undergoing a radiation treatment with 3D-CRT or IMRT. The validity of these guidelines still needs to be checked through long term follow-up of patients for whom they will be used.

11. IMPACT OF THE IMAGING MODALITY ON CLINICAL AND PLANNING TARGET VOLUMES DELINEATION AND ON DOSE DISTRIBUTION

11.1. Specific introduction

We could well establish that FDG-PET offers a clear advantage over CT for the delineation of the GTV : it is fast and reproducible since it is based on an automatic delineation algorithm. It is also structurally more accurate since it is more specific than CT while equivalently lacking of sensitivity for superficial tumor extensions. Whether a significant difference in terms of GTV could still impact on CTV and subsequent PTV delineation remains to be determined.

Comparative 3D-CRT planning was then performed on the different delineated PTVs to determine to which extent such differences could impact on dose distribution to both the PTV itself and the OARs.

11.2. Specific materials and methods

◆ Previously defined CTV recommendations were used to draw CTVs on CT, FDG-PET and MC images. MRI and MET-PET CTVs were not drawn since it was demonstrated that these imaging modalities were not useful to CT based GTV delineation. $CTV_{FDG\text{-}PET}$ were drawn after $GTV_{FDG\text{-}PET}$ had been transfered on corresponding coregistered CT slices because of the lack of anatomical informations on FDG-PET slices.

◆ After the CTVs were drawn, a four mm margin was then applied to get the final PTVs.

◆ Comparative 3D planning of all determined PTVs was performed with Nucletron Helax® 6.1 Treatment Planning System (TPS) on corresponding patient CT volume on which external contour, spinal cord and both parotid glands were drawn.

◆ Results of interest were :
–the comparative measurement of the CTVs and subsequent PTVs obtained for the different modalities tested;
–the total volume encompassed by the 50 % isodose (V_{50}) and the 95 % isodose (V_{95});
–the dosimetry observed at the different OARs, i.e. the maximal dose (D_{max}) at the spinal cord, the total mean dose (D_{mean}) to both parotids glands in the

laryngohypopharyngeal tumors and the individual mean dose to either homo- or contralateral parotid gland in oropharyngeal tumors.

11.3. Results

◆ Compared to CTV_{CT}, $CTV_{FDG\text{-}PET}$ remained significantly smaller, from 25 % (oropharyngeal CTVs) to 30 % (laryngohypopharyngeal ones) on average [Tables 18-20]. In the subset of operated patients, this difference was slightly less important (about 20 %) but remained significant. On the other hand, mean CTV_{MC} was not found significantly smaller than mean $CTV_{FDG\text{-}PET}$ –which was not the case for GTVs. PTV being only a geometrical extension of CTV, it is no surprise that the same trends can be observed for the comparison of the different mean PTVs [Tables 18-20].

Table 18 : mean target volumes and average dose distributions to OARs after conformal planning of oropharyngeal tumors.

	CT	PET	*P*-value
Mean GTV (cc)	32.0	20.3	0.01
Mean CTV (cc)	120.6	90.9	0.01
Mean PTV (cc)	213.6	164.2	0.01
Homolateral parotid average D_{mean} (%)	61.3	54.7	0.07
Heterolateral parotid average D_{mean} (%)	19.1	16.3	0.05
Spinal cord D_{max} (%)	39.4	36.6	0.77

◆ Compared to PTV_{CT} based planning, the use of FDG-PET images allowed the decrease of V_{50} and V_{95} by 13 % and 25 % respectively in oropharyngeal tumors and by about 20 % in laryngohypopharyngeal tumors [Tables 18-20].

◆ Concerning average dose distribution to OARs [Tables 18-20], significant dose reduction could be observed in D_{mean} to parotid glands except to the homolateral gland in the oropharyngeal tumors group when planning was based on FDG-PET images compared to CT ones. On the other hand, the difference between D_{max} to spinal cord was never significantly modified. Compared to $PTV_{FDG\text{-}PET}$ based planning, the use of PTV_{MC} volumes did not introduce any significant difference in dose distribution to these two OARs.

Table 19 : mean target volumes and average dose distributions to OARs after conformal planning of laryngeal and hypopharyngeal tumors.

	CT	PET	*P*-value
Mean GTV (cc)	21.4	13.4	0.01
Mean CTV (cc)	74.8	54.6	0.04
Mean PTV (cc)	147.2	114.9	0.04
Parotids average D_{mean} (%)	12.8	6.4	0.006
Spinal cord D_{max} (%)	31.3	27.8	0.09

Table 20 : mean target volumes and average dose distributions to OARs after conformal planning of surgical specimen of laryngeal tumors.

	CT	PET	MC
Mean GTV (cc)	20.8*	16.3*	12.6*
Mean CTV (cc)	80.0*	66.0	61.0
Mean PTV (cc)	151*	130.0	122.0
Parotids average D_{mean} (%)	4.9*	3.9	3.8
Spinal cord D_{max} (%)	29.4*	28.4*	27.2*

* significantly different average results ($P \leq 0.05$) when compared to two other average results.

11.4. Discussion

Differences between GTVs have a significant impact on subsequent CTV and PTV delineation. But what is more important is that it even has an impact on irradiated volume and dose to parotid glands. Though being intuitively logical for the oropharyngeal area, this result is more surprising for the laryngohypopharyngeal tumors which are encompassed in the laryngeal framework. Indeed, the laryngeal framework can be considered as a tube whose skeleton is composed of cartilages. The largest of them is the thyroid cartilage on which several fibrous membranes or muscular fibers are attached, creating as many weak points for cancer spread as there are attachment points (§ 7.1). By consequence, the thyroid cartilage is most often encompassed in the CTV, even for small tumors. Moreover, since we recommend to include it totally in the CTV,

nearly the whole pharyngolaryngeal « tube » is by consequence encompassed. It means that because of this, nearly all the CTVs could have been more or less identical, i.e. limited by the laryngeal tube, leading by consequence to non significant differences in irradiated volume. Moreover, the parotid glands being very distant from laryngohypopharyngeal structures, one could have thought that dose deposit would have been negligible, with no significant difference according to the modality used for planning. We suppose all these differences are related to extralaryngeal extensions of CTV, particularly to parapharyngeal space and anterior muscles.

On the other hand, the non significant difference of D_{max} to spinal cord is no surprise since the space separating the frequently encompassed constrictors of the pharynx and the very rarely encompassed vertebral body is nearly virtual. In other words, this underlines the fact that differences in CTVs delineation were not prominent in their posterior part.

The last practical issue that still needs to be solved is whether significant differences in terms of irradiated volume and dose distribution due to CTV modification will not be overweighed by prophylactic nodal irradiation [Grégoire 2003] which :
–in our experience largely increases total volume to be irradiated and
–is responsible of the majority of the dose delivered to parotid glands due to the intimate vicinity (overlap) of this OAR volume and level II CTV (PTV).

In conclusion, we could demonstrate that the use of different imaging modalities did not only induce significant differences for GTV-T delineation, but also that these differences impacted both on CTV-T and PTV-T delineation. The true impact on dose distribution to target as well as non target volumes still needs to be checked after inclusion in the TPS of nodal volumes irradiated at prophylactic or therapeutic dose. This work is currently in progress.

12. EXECUTIVE SUMMARY AND FUTURE PROSPECTS

12.1. Executive summary

We first established that our interactive rigid coregistration method was accurate, reproducible and consistent.

We also developed a method to calculate spherical volumes from functional images based on the actual measurement of the S/B ratio and determined that tumor volume estimation was better when higher resolution images were to be used.

Having solved these two preliminary endpoints, we demonstrated that FDG-PET could play a potential role for pharyngolaryngeal GTV delineation by providing at once significantly smaller, more specific and equivalently sensitive tumor volumes than CT, MRI and MET-PET imaging modalities.

We elaborated recommendations and guidelines for the selection and delineation of primary tumor CTV aiming at consistant CTV delineation. Using these guidelines, we could demonstrate that smaller GTV allowed the drawing of smaller CTV and subsequent PTV, which in turn significantly decreased the irradiated volume and the dose deposited to the parotid glands.

This whole work is not a finality in itself but rather a step forward to a better tumor targeting with RT. The next steps are already on their way and are described hereunder.

12.2. Future prospects

12.2.1. Automatic rigid / non rigid coregistration

The coregistration method we used was proved to be accurate, reproducible and consistent but remains time consuming for the operator. Automatic coregistration with mutual information (MI) algorithm (§ 4.2) optimized for HN purpose is currently implemented for future work. A study performed by du Bois d'Aysche et al. (unpublished data) with the images we used for the validation of our manual coregistration algorithm demonstrated that rigid MI did not impact in terms of accuracy but well in terms of computer processing time (from two to eight minutes according to modalities studied). It allowed in turn the decrease of operator processing time to software boot and final result review and approval (or not).

However, this rigid algorithm still requires the patient to be repositioned in the same and reproducible position through the use of the thermoplastic mask. It is desirable to get rid of the mask because (1) being rather uncomfortable for the patient and (2) being sometimes a limitation for some image acquisitions (e.g. : by precluding the use of specific antennas in MRI which leads to decreased signal-to-noise ratio). The coregistration of nonidentical images slowly becomes possible through the development of non rigid coregistration algorithms (§ 4.2).

12.2.2. Imaging during the treatment

Fractionated RT progressively kills cancer cells, theoretically leading after some fractions to a visible tumor shrinking. Geets et al. (unpublished data) already demonstrated that CT and MRI reimaging of the tumor around 45 Gy significantly decreases the GTV volume compared to the initial GTV. By consequence, the use of this volume for boost planning allows a decrease in the size of irradiated volumes and ultimately to decrease the irradiated volume and the dose to the OARs. Surprisingly, FDG-PET was not found to be useful, because of too low S/B ratios observed presumably related to peritumoral inflammatory reactions. A study is currently performed with CT, MRI and FDG-PET imaging sessions repeated each week during the five first weeks of the treatment. This should allow a determination of which time(s) and with which modality(ies) patients should be reimaged to modify treatment plans to take account of tumors shrinking.

12.2.3. Clustering

The problem of surrounding inflammation or surrounding physiological captation of PET tracers (like for MET-PET, § 9) is that it does not allow it to precisely define the limit between a tumor and the normal surrounding tissues. It can be overcome through the use of computerized statistical processing of successive images acquired as a function of time (dynamic imaging). The statistical analysis of the successive images allows it to isolate groups of voxels showing the same kinetic of tracer uptake. Anzai et al [1999] demonstrated that this method allowed them to make a distinction between vessels, inflammation and tumor itself. This method is currently under development and evaluation in our department.

12.2.4. Biological Image Guided Radiation Therapy and the development of new tracers

From a biological point of view, a tumor is all except homogeneous. As was reviewed in § 2.1.1, there are different biological compartments with clones being in more or less radiosensitive states. The development for PET or fMRI of specific tracers -targeting e.g. hypoxia, angiogenesis, EGFR overexpression, ...- would allow it to draw a map of this biological burden. Therapeutically speaking, this would lead to the selection of cases for which dose escalation on (sub)volumes [Ling 2000] and/or the administration of biological modifiers would be helpful. It underlines that recent developments in the knowledge of tumor biology and treatments coming from biotechnologies are not to be seen as an alternative to RT but rather as synergistic and complimentary options.

12.2.5. Correlations to histopathology

The development of all these new imaging techniques still needs confrontation to gold standard images to determine their exact validity. As was shown in § 8, we developed a method to reconstruct a total laryngectomy surgical specimen in 3D. This technique however suffers some intrinsic limitations like (1) not showing the ultimate microscopic limits of a tumor compared to its macroscopic limits and (2) not allowing the visualization of the different biological compartments of the tumor with fluoroscopic probes.

It would be ideal to coregister microscopic slices to macroscopic ones, but this is not directly possible because fixation and dehydration processing necessary to pathology diagnosis lead to non homotetic deformations. du Bois d'Aische et al. [2004] developed a computerized non rigid coregistration method overcoming this problem.

Like for previously mentioned endpoints, the present technical development still requires further developments and validation to enter into clinical practice.

REFERENCES

Ang KK, Andratschke NH, Milas L. Epidermal growth factor receptor and response of head-and-neck carcinoma to therapy. Int J Radiat Oncol Biol Phys 2004;58:959-965.

Anzai Y, Minoshima S, Wolf GT, Wahl RL. Head and neck cancer : detection of recurrence with three-dimensional principal components analysis at dynamic FDG PET. Radiology 1999;212:285-290.

Aston JA, Cunningham VJ, Asselin MC, Hammers A, Evans AC, Gunn RN. Positron Emission Tomography partial volume correction : estimation and algorithms. J Cereb Blood Flow Metab 2002;8:1019-1034.

Baba Y, Yamashita Y, Onomichi M, Murakami R, Takahashi M. Dynamic magnetic resonance imaging of head and neck lesions. Top Magn Reson Imaging 1999;10:125-129.

Bagatella F, Bernardini L. Behavior of cancer at the anterior commissure of the larynx. Laryngoscope 1983;93:353-356.

Becker M, Zbären P, Laeng H, Stoupis C, Porcellini B, Vock P. Neoplastic invasion of laryngeal cartilage : comparison of MR imaging and CT with histopathologic correlation. Radiology 1995;194:661-669.

Beitler JJ, Mahadevia PS, Silver CE, et al. New barriers to ventricular invasion in paraglottic laryngeal cancer. Cancer 1994;73:2648-2652.

Bernier J, Domenge C, Ozsahin M, et al. European Organization for Research and Treatment of Cancer Trial 22931. Postoperative irradiation with or without concomitant chemotherapy for locally advanced head and neck cancer. N Engl J Med 2004;350:1945-1952.

Bomanji JB, Costa DC, Ell PJ. Clinical role of positron emission tomography in oncology. Lancet Oncol 2001;2:157–164.

Bonner JA, Giralt J, Harari PM. Cetuximab prolongs survival in patients with locoregionally advanced squamous cell carcinoma of head and neck : a phase III study of high dose radiation therapy with or without cetuximab. Proc Am Soc Clin Oncol 2004;23:488.

Bourhis J, Syz N, Overgaard J, et al. Conventional versus modified fractionated radiotherapy : meta-analysis based on individual data of patients with head and neck squamous cell carcinoma (HNSCC). Radiother Oncol 2002;64:S25.

Cai J, Chu JC, Recine D, et al. CT and PET lung image registration and fusion in radiotherapy treatment planning using the chamfermatching method. Int J Radiat Oncol Biol Phys 1999;43:883–891.

Caldwell CB, Mah K, Ung YE, Danjoux CE, Balogh JM, Ganguli SN, Ehrlich LE. Observer variation in contouring gross tumor volume in patients with poorly defined non-small-cell lung tumors on CT : the impact of 18FDG-hybrid PET fusion. Int J Radiat Oncol Biol Phys 2001;51:923-931.

Chatziioannou AF, Cherry SR, Shao Y, et al. Performance evaluation of microPET : a high-resolution lutetium oxyorthosilicate PET scanner for animal imaging. J Nucl Med 1999;40:1164-1175.

Chesnay E, Babin E, Constans JM, et al. Early response to chemotherapy in hypopharyngeal cancer : assessment with 11C-methionine PET, correlation with morphologic response and clinical outcome. J Nucl Med 2003;44:526–532.

Chevallier JM, Bonfils P. Anatomie ORL. 1ère ed. Paris, FRANCE : Médecine-Sciences Flammarion. 1998.

Cohen EE, Lingen MW, Vokes EE. The expanding role of systemic therapy in head and neck cancer. J Clin Oncol 2004;22:1743-1752.

Cohen-Jonathan E, Bernhard EJ, McKenna WG. How does radiation kill cells? Curr Op Chem Biol 1999;3:77-83.

Collignon A, Maes F, Delaere D, Vandermeulen D, Suetens P, Marchal G. Automated multi-modality image registration based on information theory. In : Bizais Y, Barillot C, Di Paola R, Editors. Information Processing in Medical Imaging. Dordrecht, The Netherlands : Kluwer Academic Publishers. 1995;263–274.

Cooper JS, Pajak TF, Forastiere AA, et al. Radiation Therapy Oncology Group 9501/Intergroup. Postoperative concurrent radiotherapy and chemotherapy for high-risk squamous-cell carcinoma of the head and neck. N Engl J Med 2004;350:1937-1944.

Crecco M, Vidiri A, Angelone ML, Palma O, Morello R. Retromolar trigone tumors : evaluation by magnetic resonance imaging and correlation with pathological data. Eur J Radiol 1999;32:182-188.

Daisne JF, Duprez T, Weynand B, Lonneux M, Hamoir M, Reychler H, Gregoire V. Tumor volume in pharyngolaryngeal squamous cell carcinoma: comparison at CT, MR imaging, and FDG PET and validation with surgical specimen. Radiology 2004;233:93-100.

Daisne JF, Sibomana M, Bol A, Cosnard G, Lonneux M, Gregoire V. Evaluation of a multimodality image (CT, MRI and PET) coregistration procedure on phantom and head and neck cancer patients : accuracy, reproducibility and consistency. Radiother Oncol 2003;69:237-245.

Daisne JF, Sibomana M, Bol A, Doumont T, Lonneux M, Gregoire V. Tri-dimensional automatic segmentation of PET volumes based on measured source-to-background ratios : influence of reconstruction algorithms. Radiother Oncol 2003;69:247-250.

Delbeke D, Martin WH. Positron emission tomography imaging in oncology. Radiol Clin North Am 2001;39:883–917.

Doshi NK, Shao Y, Silverman RW, Cherry SR. Design and evaluation of an LSO PET detector for breast cancer imaging. Med Phys 2000;27:1535-1543.

du Bois d'Aische A, De Craene M, Geets X, Gregoire V, Macq B, Warfield SK. Efficient Multi-modal dense field non-rigid registration : alignment of histological and section images. Submitted to Med Im Anal, 2004.

Dursun G, Keser R, Aktürk T, Akiner MN, Demireller A, Sak SD. The significance of preepiglottic space invasion in supraglottic laryngeal carcinomas. Eur Arch Otorhinolaryngol 1997;254:S110-S112.

Eisbruch A, et al. Intensity-modulated radiation therapy for Head & Neck cancer : emphasis on the selection and delineation of the targets. Sem Rad Oncol 2002;12:238-249.

Eisbruch A, Ten Haken RK, Kim HM, Marsh LH, Ship JA. Dose, volume, and function relationships in parotid salivary glands following conformal and intensity-modulated irradiation of head and neck cancer. Int J Radiat Oncol Biol Phys 1999;45:577-587.

Eisbruch A. IMRT of HN Cancer : encouraging early results. Int J Radiat Oncol Biol Phys 2002;53:1-3.

Erdi YE, Mawlawi O, Larson SM, et al. Segmentation of lung lesion volume by adaptive positron emission tomography image thresholding. Cancer (Suppl) 1997;12:2505-2509.

Erdi YE, Wessels BW, Loew MH, Erdi AK. Threshold estimation in single photon emission computed tomography and planar imaging for clinical radioimmunotherapy. Cancer Res (Suppl) 1995;55:5823s-5826s.

Ferreira IH, Dutreix A, Bridier A, Chavaudra J, Svensson H. The ESTRO-QUALity assurance network (EQUAL). Radiother Oncol 2000;55:273-284.

Flohr T, Stierstorfer K, Bruder H, Simon J, Schaller S. New technical developments in multislice CT—Part 1 : approaching isotropic resolution with sub-millimeter 16-slice scanning. Fortschr Geb Rontgenstr Neuen Bildgeb Verfahr 2002;174:839–845.

Foote RL, Olsen KD, Davis DL, et al. Base of tongue carcinoma : patterns of failure and predictors of recurrence after surgery alone. HeadNeck 1993;15:300-307.

Forastiere AA, Goepfert H, Maor M, et al. Concurrent chemotherapy and radiotherapy for organ preservation in advanced laryngeal cancer. N Engl J Med 2003;349:2091-2098.

Fraass B, Doppke K, Hunt M, Kutcher G, Starkschall G, Stern R, Van Dyke J. American Association of Physicists in Medicine Radiation Therapy Committee Task Group 53 : quality assurance for clinical radiotherapy treatment planning. Med Phys 1998;25:1773-1829.

Fu KK, Pajak TF, Trotti A, et al. A Radiation Therapy Oncology Group (RTOG) phase III randomized study to compare hyperfractionation and two variants of accelerated fractionation to standard fractionation radiotherapy for head and neck squamous cell carcinomas : first report of RTOG 9003. Int J Radiat Oncol Biol Phys 2000;48:7-16.

Geets X, Daisne JF, Gregoire V, Hamoir M, Lonneux M. Role of 11-C-methionine positron emission tomography for the delineation of the tumor volume in pharyngo-laryngeal squamous cell carcinoma : comparison with FDG-PET and CT. Radiother Oncol 2004;71:267-273.

Gilbeau L, Octave-Prignot M, Loncol T, Renard L, Scalliet P, Gregoire V. Comparison of setup accuracy of three different thermoplastic masks for the treatment of brain and head and neck tumors. Radiother Oncol 2001;58:155–162.

Gilbert J, Forastiere AA. Organ preservation for cancer of the larynx : current indications and future directions. Sem Radiat Oncol 2004;14:167-177.

Gilbert RW, Lundgren JAV, van Nostrand AWP, Keane TJ. T3N0M0 glottic carcinoma - a pathologic analysis of 41 patients treated surgically following radiotherapy. Clin Otolaryngol 1988;13:467-479.

Giraud P, Antoine M, Larrouy A, et al. Evaluation of microscopic tumor extension in non-small-cell lung cancer for three-dimensional conformal radiotherapy planning. Int J Radiat Oncol Biol Phys 2000;48:1015-1024.

Giraud P, Elles S, Helfre S, et al. Conformal radiotherapy for lung cancer : different delineation of the gross tumor volume (GTV) by radiologists and radiation oncologists. Radiother Oncol 2002;62:27-36.

Glaser CM, Millesi W, Kornek GV, et al. Impact of hemoglobin level and use of recombinant erythropoietin on efficacy of preoperative chemoradiation therapy for squamous cell carcinoma of the oral cavity and oropharynx. Int J Radiat Oncol Biol Phys 2001;50:705-715.

Glatstein E. Intensity-Modulated radiation therapy : the inverse, the converse, and the perverse. Sem Rad Onc 2002;12:272-281.

Grandjean E, Debry C, Briche D, El Jerrarri A, Gentine A, Conraux C. Corrélations anatomo-scanographiques des cancers du pharyngo-larynx. A propos d'une étude prospective portant sur 35 patients. Ann Otolaryngol 1993;110:135-141.

Gregoire V, Levendag P, Ang KK, et al. CT-based delineation of lymph node levels and related CTVs in the node-negative neck : DAHANCA, EORTC, GORTEC, NCIC,RTOG consensus guidelines. Radiother Oncol 2003;69:227-236.

Gregor RT. The preepiglottic space revisited : is it significant ? Am J Otolaryngol 1990;11:161-164.

Haacke EM, Brown RW, Thompson MR, Venkatesan R. Chapter 13 : filtering and resolution in Fourier transform image reconstruction. In : Haacke EM, Brown RW, Thompson MR, Venkatesan R, editors. Magnetic resonance imaging : physical principles and sequences design. New York, New York, USA : Wiley. 1999;265–302.

Habboush IH, Mitchell KD, Mulkern RV, Barnes PD, Treves ST. Registration and alignment of three-dimensional images : an interactive visual approach. Radiology 1996;199:573–578.

Haffty BG, Son YH, Sasaki CT, et al. Mitomycin C as an adjunct to postoperative radiation therapy in squamous cell carcinoma of the head and neck : results from two randomized clinical trials. Int J Radiat Oncol Biol Phys 1993;27:241-250.

Halimi P, Bely N, Chevallier JM, Bernier P, Frija G. Radioanatomie de l'oropharynx. J Radiol 1990;80:223-232.

Harrison DFN. Significance and means by which laryngeal cancer invades thyroid cartilage. Ann Otol Rhinol Laryngol 1984;93:293-296.

Harrison LB, Chadha M, Hill RJ, Hu K, Shasha D. Impact of tumor hypoxia and anemia on radiation therapy outcomes. Oncologist 2002;7:492-508.

Hawkes DJ. Algorithms for radiological image registration and their clinical application. J Anat 1998;193:347–361.

Henke M, Laszig R, Rube C, et al. Erythropoietin to treat head and neck cancer patients with anaemia undergoing radiotherapy : randomised, double-blind, placebo-controlled trial. Lancet 2003;362:1255-1260.

Hermans R, Feron M, Bellon E, Dupont P, Van den Bogaert W, Baert AL. Laryngeal tumor volume measurements determined with CT : a study on intra- and interobserver variability. Int J Radiat Oncol Biol Phys. 1998;40:553-557.

Hirano M, Kurita S, Tanaka H. Histopathologic study of carcinoma of the hypopharynx : implications for conservation surgery. Ann Otol Rhinol Laryngol 1987;96:625-629.

Ho CM, Ng WF, Lam KH, Wei WJ, Yuen AP. Submucosal tumor extension in hypopharyngeal cancer. Arch Otolaryngol Head Neck Surg 1997;123:959-965.

Hood MN, Ho VB, Smirniotopoulos JG, Szumowski J. Chemical shift : the artifact and clinical tool revisited. RadioGraphics 1999;19:357–371.

Horsman MR, Overgaard J. The oxygen effect and tumour microenvironment. In : Steel GG, Editor. Basic Clinical Radiobiology. 3rd ed. London, UK : Arnold. 2002;158-168.

Hudson HM, Larkin RS. Accelerated image reconstruction using ordered subsets of projection data. IEEE Trans Med Imaging 1994;13:601–609.

Hutton BF, Braun, Thurfjell L, Lau DYH. Image registration : an essential tool for nuclear medicine. Eur J Nucl Med 2002;29:559-577.

ICRU report #50 : Prescribing, Recording and Reporting Photon Beam Therapy. 1993.

ICRU report #62 : Prescribing, Recording and Reporting Photon Beam Therapy (Supplement to ICRU report 50). 1999.

Intensity Modulated Radiation Therapy Collaborative Working Group. Intensity-modulated radiotherapy : current status and issues of interest. Int J Radiat Oncol Biol Phys 2001;51:880-914.

Jones AS, England J, Hamilton J, Helliwell TR, Field J, Gerlinger I, Karkanevatos T. Mandibular invasion in patients with oral and oropharyngeal squamous carcinoma. Clin Otolaryngol 1997;22:239-245.

Kaanders JH, Bussink J, van der Kogel AJ. ARCON : a novel biology-based approach in radiotherapy. Lancet Oncol 2002;3:728-737.

Kao J, Garofalo MC, Milano MT, Chmura SJ, Citron JR, Haraf DJ. Reirradiation of recurrent and second primary head and neck malignancies : a comprehensive review. Cancer Treat Rev 2003;29:21-30.

Kapouleas I, Alavi A, Alves WM, Gur RE, Weiss DW. Registration of three-dimensional MR and PET images of the human brain without markers. Radiology 1991;181:731–739.

Kazkayasi M, Önder T, Özkaptan Y, Can C, Pabusçu Y. Comparison of preoperative computed tomographic findings with postoperative histopathological findings in laryngeal carcinoma. Eur Arch Otorhinolaryngol 1995;252:325-331.

Kinahan PE, Rogers JG. Analytic 3D image reconstruction using all detected events. IEEE Trans Nucl Sci 1989;13:964-968.

Kirchner JA. Piriform sinus cancer : a clinical and laboratory study. Ann Otol 1975;84:793-803.

Kirchner JA. Two hundred laryngeal cancers : patterns of growth and spread as seen in serial section. Laryngoscope 1976;86:474-482.

Kirchner JA. Glottic-supraglottic barrier : fact or fantasy ? Ann Otol Rhinol Laryngol 1997;106:700-704.

Kirchner JA, Carter D. Intralaryngeal barriers to the spread of cancer. Acta Otolaryngol (Stockh) 1987;103:503-513.

Kirchner JA, Fisher JJ. Anterior commissure cancer – a clinical and laboratory study of 39 cases. Can J Otolaryngol 1975;4:637-643.

Kraus DH, Pfister DG, Harrison LB, et al. Larynx preservation with combined chemotherapy and radiation therapy in advanced hypopharynx cancer. Otolaryngol Head Neck Surg 1994;111:31-37.

Kubota R, Kubota K, Yamada S, et al. Methionine uptake by tumor tissue : a microautoradiographic comparison with FDG. J Nucl Med 1995;36:484–492.

Lam KH. Extralaryngeal spread of cancer of the larynx : a study with whole-organ sections. Head Neck Surg 1983;5:410-424.

Lam KH, Wong J. The preepiglottic and paraglottic spaces in relation to spread of carcinoma of the larynx. Am J Otolaryngol 1983;4:81-91.

Landuyt W, Hermans R, Bosmans H, et al. BOLD contrast functional magnetic resonance imaging of whole tumour during air or carbogen breathing : initial experience in rat rhabdomyosarcoma using echo planar imaging at 1.5 Tesla. Eur Radiol 2001;11:2332-2340.

Leahy R, Qi J. Statistical approaches in quantitative positron emission tomography. Statistics and Computing 2000;10:147-165.

Lenz M, Grees H, Baum U, Dobritz M, Kersting-Sommerhoff B. Oropharynx, oral cavity, floor of the mouth : CT and MRI. Eur J Radiol 2000;33:203-215.

Leskinen-Kallio S, Lindholm P, Lapela M, Joensuu H, Nordman E. Imaging of head and neck tumors with positron emission tomography and 11C-methionine. Int J Radiat Oncol Biol Phys 1994;30:1195–1199.

Leunens G, Menten J, Weltens C, Verstraete J, van der Schueren E. Quality assessment of medical decision making in radiation oncology : variability in target volume delineation for brain tumours. Radiother Oncol 1993;29:169-175.

Lindholm P, Leskinen-Kallio S, Minn H, et al. Comparison of FDG and C-11-methionine in head and neck cancer. J Nucl Med 1993;34:1711–1716.

Ling CC, Humm J, Larson S, Amols H, Fuks Z, Leibel S, Koutcher JA. Towards multidimensional radiotherapy (MD-CRT) : biological imaging and biological conformality. Int J Radiat Oncol Biol Phys 2000;47:551-560.

Low DA. Quality Assurance of Intensity-Modulated radiation therapy. Sem Rad Onc 2002;12:219-228.

Maes A, Weltens C, Flamen P, et al. Preservation of parotid function with uncomplicated conformal radiotherapy. Radiother Oncol 2002;63:203-211.

Marcie S, Aletti P, Lefkopoulos D, Tomsej M. Programme commun d'assurance de qualité de la radiothérapie conformationnelle avec modulation d'intensité (RCMI) des cancers de la tête et du cou : quality assurance program for intensity-modulated radiotherapy (IMRT) treatments of head and neck carcinomas. Cancer Radiother 2003;7:172-178.

Maroldi R, Battaglia G, Farina D, Maculotti P, Chiesa A. Tumours of the oropharynx and oral cavity : perineural spread and bone invasion. JBR-BTR 1999;82:294–300.

McDonald TJ, DeSanto LW, Weiland LH. Supraglottic larynx and its pathology as studied by whole laryngeal sections. Laryngoscope 1976;85:635-648.

Micheau C, Luboinski B, Sancho H, Cachin Y. Modes of invasion of cancer of the larynx. Cancer 1976;38:346-360.

Miller TR, Wallis JW, Grothe RA. Design and use of PET tomographs : the effect of slice spacing. J Nucl Med 1990;31:1732-1739.

Minn H, Clavo AC, Grenman R, Wahl RL. In vitro comparison of cell proliferation kinetics and uptake of tritiated fluorodeoxyglucose and L-methionine in squamous-cell carcinoma of the head and neck. J Nucl Med 1995;36:252–258.

Miyazawa H, Arai T, Iio M, Hara T. PET imaging of non-small-cell lung carcinoma with C-11-methionine : relationship between radioactivity uptake and flow cytometric parameters. J Nucl Med 1993;34:1886–1891.

Moon C, Oh Y, Roth JA. Current status of gene therapy for lung cancer and head and neck cancer. Clin Cancer Res 2003;9:5055-5067.

Mutic S, Dempsey JF, Bosch WR, et al. Multimodality image registration quality assurance for conformal three-dimensional treatment planning. Int J Radiat Oncol Biol Phys 2001;51:255–260.

Nuutinen J, Leskinen S, Lindholm P, et al. Use of C-11-methionine positron emission tomography to assess malignancy grade and predict survival in patients with lymphomas. Eur J Nucl Med 1998;25:729–735.

Ogura JH. Surgical pathology of cancer of larynx. Laryngoscope 1955;65:867-926.

Olofsson J. Growth and spread of laryngeal carcinoma. Can J Otolaryngol 1974;3:446-459.

Olofsson J, Sökjer H. Radiologic assessment of laryngeal carcinoma. A clinico-pathologic comparison based on whole-organ serial sections. Acta Radiol Diagn 1979;20:789-814.

Olofsson J, van Nostrand AWP. Growth and spread of laryngeal and hypopharyngeal carcinoma with reflections on the effect of preoperative irradiation; 139 cases studied by whole organ serial sectionning. Acta Otolaryngol (Stockh) 1973;S308:1-84.

Overgaard J, Hansen HS, Overgaard M, et al. A randomized double-blind phase III study of nimorazole as a hypoxic radiosensitizer of primary radiotherapy in supraglottic larynx and pharynx carcinoma. Results of the Danish Head and Neck Cancer Study (DAHANCA) Protocol 5-85. Radiother Oncol 1998;46:135-146.

Peters LJ, Goepfert H, Ang KK, et al. Evaluation of the dose for postoperative radiation therapy of head and neck cancer : first report of a prospective randomized trial. Int J Radiat Oncol Biol Phys 1993;26:3-11.

Pietzryk U, Herholz K, Fink G, et al. An interactive technique for three-dimensional image registration : validation for PET, SPECT, MRI and CT brain studies. J Nucl Med 1994;35:2011–2018.

Pignon JP, Bourhis J, Domenge C, Designe L. Chemotherapy added to locoregional treatment for head and neck squamous-cell carcinoma: three meta-analyses of updated individual data. MACH-NC Collaborative Group. Meta-Analysis of Chemotherapy on Head and Neck Cancer. Lancet 2000;355:949-955.

Pluim JP, Maintz JB, Viergever MA. Mutual-information-based registration of medical images : a survey. IEEE Trans Med Imaging 2003;22:986-1004.

Powers BE, Thames HD, Gillette SM, Smith C, Beck ER, Gillette EL. Volume effects in the irradiated canine spinal cord : do they exist when the probability of injury is low ? Radiother Oncol 1998;46:297-306.

Pressman JJ, Simon MB, Monnell C. Anatomical studies related to the dissemination of cancer of the larynx. Trans Am Acad Ophthalmol Otolaryngol 1960;64:628-638.

Rasch C, Keus R, Pameijer FA, et al. The potential impact of CT-MRI matching on tumor volume delineation in advanced head and neck cancer. Int J Radiat Oncol Biol Phys 1997;39:841–848.

Registre du Cancer. Earlier reported data are about the year 1998. These are available on internet : www.registreducancer.org.

Reidenbach MM. Normal topography of the conus elasticus. Anatomical bases for the spread of laryngeal cancer. Surg Radiol Anat 1995;17:107-111.

Reidenbach MM. The paraglottic space and transglottic cancer : anatomical considerations. Clin Anat 1996;9:244-251.

Reidenbach MM. Topographical anatomy and oncologic implications of the anterolateral surface of the arytenoid cartilage. Eur Arch Otorhinolaryngol 1998;255:140-142.

Rifai M, Khattab H. Anterior commissure cancer - histopathologic study. Am J Otolaryngol 2000;21:294-297.

Rijpkema M, Kaanders JH, Joosten FB, van der Kogel AJ, Heerschap A. Effects of breathing a hyperoxic hypercapnic gas mixture on blood oxygenation and vascularity of head-and-neck tumors as measured by magnetic resonance imaging. Int J Radiat Oncol Biol Phys 2002;53:1185-1191.

Robbins KT, Medina JE, Wolfe GT, Levine PA, Sessions RB, Pruet CW. Standardizing neck dissection terminology. Official report of the Academy's committee for head and neck surgery and oncology. Arch Otolaryngol Head Neck Surg 1991;117:601-605.

Rosenthal DI, Ang KK. Altered radiation therapy fractionation, chemoradiation, and patient selection for the treatment of head and neck squamous carcinoma. Sem Radiat Oncol 2004;14:153-166.

Rouvière H. Anatomie Humaine. Tome 1. 12ème ed. Paris, FRANCE : Masson. 1972.

Rowley HA, Grant PE, Roberts TPL. Diffusion MR imaging – theory and applications. Neuroimaging Clin N Am 1999;9:343-361.

Rubin P, Williams JP. Principles of radiation oncology and cancer radiotherapy. In : Rubin P, editor. Clinical oncology – a multidisciplinar approach for physicians and students. 8th Edition. Philadelphia, Pennsylvania, USA : W.B. Saunders. 2001;99-125.

Sartor CI. Epidermal growth factor family receptors and inhibitors : radiation response modulators. Sem Radiat Oncol 2003;13:22-30.

Sato K, Kurita S, Hirano M. Location of the preepiglottic space and its relationship to the paraglottic space. Ann Otol Rhinol Laryngol 1993;102:930-934.

Sauter ER, Nesbit M, Litwin S, Klein-Szanto AJ, Cheffetz S, Herlyn M. Antisense cyclin D1 induces apoptosis and tumor shrinkage in human squamous carcinomas. Cancer Res 1999;59:4876-4881.

Schaefer U, Micke O, Schueller P, Willich N. Recurrent head and neck cancer : retreatment of previously irradiated areas with combined chemotherapy and radiation therapy - results of a prospective study. Radiology 2000;216:371-376.

Sercarz JA, Bailet JW, Abemayor Y, Hoh CK, Lufkin RB. Computer coregistration of positron emission tomography and magnetic resonance images in head and neck cancer. Am J Otolaryngol 1998;19:130–135.

Shintani S, Kiyota A, Mihara M, Sumida T, Kayahara H, Nakashiro K, Hamakawa H. Enhancement of radiosensitivity in head and neck cancer cells by ZD1839 ('IRESSA'), a selective epidermal growth factor receptor tyrosine kinase inhibitor. Am J Clin Oncol 2003;26:e150-e156.

Sibomana M, Coppens A, Lonneux M, et al. Volumic image analysis application bundle for Unix workstations. IEEE Medical Imaging Conference, San Francisco October 21–28;1995.

Sibomana M, Daisne JF, Bol A, Lonneux M, Gregoire V, Michel C. Head and neck multimodality volume visualization methods. IEEE Medical Imaging Conference, Norfolk, November 13–16;2002.

Smith DB, Haffty BG, Sasaki CT. Molecular markers in head and neck squamous cell carcinoma : their biological function and prognostic significance. Ann Otol Rhinol Laryngol 2001;110:221-228.

Spencer SA, Harris J, Wheeler RH, et al. RTOG 96-10 : reirradiation with concurrent hydroxyurea and 5-fluorouracil in patients with squamous cell cancer of the head and neck. Int J Radiat Oncol Biol Phys 2001;51:1299-1304.

Stratford IJ, Williams KJ, Cowen RL, Jaffar M. Combining bioreductive drugs and radiation for the treatment of solid tumors. Sem Radiat Oncol 2003;13:42-52.

Tai P, Van Dyk J, Yu E, Battista J, Stitt L, Coad T. Variability of target volume delineation in cervical esophageal cancer. Int J Radiat Oncol Biol Phys 1998;42:277-288.

Takahashi S. Conformation radiotherapy : rotation techniques as applied to radiography and radiotherapy of cancer. Acta Radiol Suppl 1965;242:1-142. Cited & partly reproduced in Morita K. Keynote address – Conformal RT and Conformation RT. Int J Radiat Oncol Biol Phys 2000;48:431-434.

Tani M, Amatsu M. Discrepancies between clinical and histopathologic diagnoses in T3 piriform sinus cancer. Laryngoscope 1987;97:93-96.

Turkington TG, Jaszczak RJ, Pelizzari CA, et al. Accuracy of registration of PET, SPECT an MR images of a brain phantom. J Nucl Med 1993;34:1587–1594.

UCL Guidelines, available on internet : www.md.ucl.ac.be/ccmf/guidelines.htm.

Uematsu H, Sadato N, Yonekura Y, et al. Coregistration of FDG PET and MRI of the head and neck using normal distribution of FDG. J Nucl Med 1998;39:2121–2127.

UICC. TNM Classification of Malignant Tumors. 5Th (1997) and 6th (2002) editions.

van den Brekel MWM. Lymph node metastases : CT and MRI. Eur J Radiol 2000;33:230-238.

Van Herk M, Kooy HM. Automatic three-dimensional correlation of CT-CT, CT-MRI, and CT-SPECT using chamfer matching. Med Phys 1994;21:1163–1178.

van Nostrand AWP, Brodarec I. Laryngeal carcinoma - modifications in surgical technique based on an understanding of tumor growth characteristics. J Otolaryngol 1982;11:186-190.

Vanuytsel LJ, Vansteenkiste JF, Stroobants SG, et al. The impact of (18)F-fluoro-2-deoxy-D-glucose positron emission tomography (FDG-PET) lymph node staging on the radiation treatment volumes in patients with non-small cell lung cancer. Radiother Oncol 2000;55:317–324.

Vermeulen K, Van Bockstaele DR,Berneman, ZN. The cell cycle: a review of regulation, deregulation and therapeutic targets in cancer. Cell Prolif 2003:36;131-149.

Veteran Affairs Study Group. Induction chemotherapy plus radiation compared with surgery plus radiation in patients with advanced laryngeal cancer. The Department of Veterans Affairs Laryngeal Cancer Study Group. N Engl J Med 1991;324:1685-1690.

Viola P, Wells MW. Alignment by maximization of mutual information. In : Grimson E, Shafer S, Blake A, Sugihara K, Editors. International Conference on Computer Vision. Los Alamitos, California, USA : IEEE Computer Society Press. 1995;16–23.

Webb S. Advances in three-dimensional conformal radiation therapy physics with intensity modulation. Lancet Oncol 2000;1:30-36.

Weber Wolfgang A, Avril N, Schwaiger M. Relevance of positron emission tomography in oncology. Strahlenther Onkol 1999;175:356–373.

Weinstein GS, Laccourreye O, Brasnu D, Tucker J, Montone K. Reconsidering a paradigm : the spread of supraglottic carcinoma to the glottis. Laryngoscope 1995;105:1129-1133.

Weiss E, Richter S, Krauss T, et al. Conformal radiotherapy planning of cervix carcinoma: differences in the delineation of the clinical target volume. A comparison between gynaecologic and radiation oncologists. Radiother Oncol 2003;67:87-95.

Welsh LW, Welsh JJ, Rizzo TA. Internal anatomy of the larynx and the spread of cancer. Ann Otol Rhinol Laryngol 1989;98:228-234.

West J, Fitzpatrick JM, Wang MY, et al. Comparison and evaluation of retrospective intermodality brain image registration techniques. J Comput Assist Tomogr 1997;21:554–566.

Wienhard K, Dahlbom M, Eriksson L, et al. The ECAT EXACT HR : performance of a new high resolution positron scanner. J Comput Assist Tomogr 1997;18:110–118.

Wong WL, Hussain K, Chevretton E, et al. Validation and clinical application of computer-combined computed tomography and positron emission tomography with 2-[18F]fluoro-2-deoxy-D-glucose head and neck images. Am J Surg 1996;172:628–632.

Woods RP, Grafton ST, Holmes CJ, Cherry SR, Mazziotta JC. Automated image registration : I. General methods and intrasubject, intramodality validation. J Comput Assist Tomogr 1998;22:139–152.

Yeager VL, Archer CR. Anatomical routes for cancer invasion of laryngeal cartilages. Laryngoscope 1982;92:449-452.

Zbären P, Becker M, Läng H. Pretherapeutic staging of laryngeal carcinoma. Clinical findings, computed tomography and magnetic resonance imaging compared with histopathology. Cancer 1996;77:1263-1273.

Zbären P, Egger C. Growth patterns of piriform sinus carcinomas. Laryngoscope 1997;107:511-518.

Zelefsky MJ, Harrison LB, Fass DE, Armstrong JG, Shah JP, Strong EW. Postoperative radiation therapy for squamous cell carcinomas of the oral cavity and oropharynx : impact of therapy on patients with positive surgical margins. Int J Radiat Oncol Biol Phys 1993;25:17-21.